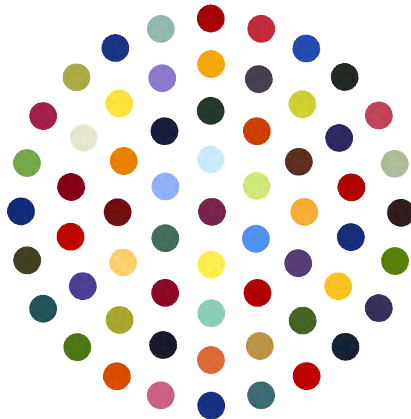


Master's thesis

Numerical computations of relative equilibria of identical vortices on the plane and on the sphere

Tobias Dirksen, s062064



Supervisors:

Hassan Aref, Mark Stremler, and Shane Ross
Department of Engineering Science and Mechanics
Virginia Polytechnic Institute and State University

Tomas Bohr
Department of Physics
Technical University of Denmark

February 17, 2012

*The front page image shows a relative equilibrium of 61 identical point vortices. The image is almost identical to the painting *Cineole* (2004) by the British artist Damien Hirst, and the vortices are coloured in the same colours as in the painting. This shows how equilibrium patterns fascinate a wide range of people.*

In memory of Hassan Aref

Abstract

This work is about relative equilibria of identical point vortices, which are vortex patterns in uniform rotation, that do not change their shape or size. We carry out a thorough study of these solutions, and discuss some of the interesting phenomena that arise in this context. One of these unexpected phenomenon is the existence of asymmetric solutions discovered by Aref & Vainchtein in 1998 [13]. Another interesting phenomena is the fact that pairs of very close relative equilibria exist, which was discovered by the author prior to this work [20].

A semi-analytical approach is used by solving the governing equations for relative equilibria in MATLAB. On the plane the equations have been solved, firstly, by random initial conditions. Both the asymmetric solutions and the close pairs of relative equilibria are found by these computations. The first close pair is found for $N = 7$, where a solution, extremely close to the centered nested equilateral triangles, exists. These two solutions cannot be distinguished by the naked eye. Secondly, the computations have been done by a continuation method. This method is done by imposing a small circulation to the different co-rotating points, that are points of relative rest, and, in small steps, increasing the circulation until all vortices have equal strength. All the intermediate solutions solve the governing equations and are thus in relative equilibrium. The initial conditions are always given by the former solution the step before. This method connects, thus, relative equilibria of N vortices with ones with $N + 1$, and I believe this is an exhaustive method to find all relative equilibria by induction.

The continuation computations have recreated all prior known solutions for $N \leq 8$, and have, moreover, revealed bifurcations in the solution paths. For a specific value of the continuation parameter two different paths are sometimes possible and, thus, one relative equilibrium together with one co-rotating point can be connected to two different solutions by continuation. This is, as far as known, not observed before. Furthermore, the close relative equilibria for N vortices have been generated, by continuation, from the same solution for $N - 1$, and can thus be explained by a bifurcation, where the bifurcation point is sufficiently close to 1. The asymmetric solutions for $N = 8$ has, moreover, been connected with a bifurcation.

On the sphere the equations for relative equilibria are solved by random initial conditions for $\frac{\Gamma}{4\pi\Omega R^2} = 1$ and $N = 2, \dots, 8$. More solutions than on the plane have been found. For $N = 7$ configurations exist with no symmetry axis but with a 180° rotational symmetry, and the first total asymmetric solution exist for $N = 8$. A close pair of relative equilibria appears for $N = 8$. The close solution is near the nested, centered equilateral triangles, and is, thus, similar to the one found on the plane.

We have, thus, discovered bifurcating relative equilibria, which is a new phenomenon, and this has given us more insight and knowledge about asymmetric and close pairs of solutions.

Resumé

Dette arbejde handler om relative ligevægtstilstande af identiske punkthvirvler, som er hvirvelmønstre i uniform rotation, der ikke ændrer deres form eller størrelse. Vi foretager et grundigt studium af disse løsninger og diskuterer nogle af de interessante fænomener, som forekommer i denne kontekst. Et af disse uventet fænomener er eksistensen af asymmetriske løsninger opdaget af Aref & Vainchtein i 1998 [13]. Et andet interessant fænomen er faktummet, at der eksisterer meget tætte relative ligevægtstilstande, hvilket blev opdaget af forfatteren forud for dette arbejde [20].

Der er benyttet en semi-analytisk metode ved at løse de ledende ligninger i MATLAB. I planen er ligningerne først løst med vilkårlige begyndelsesbetingelser. Både de asymmetriske løsninger og de tætte par af relative ligevægtstilstande er fundet ved disse beregninger. Det første tætte par er fundet for $N = 7$, hvor der eksisterer en løsning ekstremt tæt på de centrerede, indlejrede, ligesidede, trekanter. Disse to løsninger kan ikke skelnes med det blotte øje. Dernæst er beregningerne udført ved hjælp af en kontinuering metode. Denne metode er udført ved at påtrykke en lille cirkulation på de forskellige co-roterende punkter, som er punkter der er relativt i ro, og herefter i små step øge cirkulationen indtil alle hvirvler har samme styrke. Alle de mellemliggende løsninger løser de ledende ligninger og er derfor i relativt ækvilibrium. Begyndelsesbetingelserne er altid givet ved løsningen steppet lige før. Dette metode forbinder altså relative ligevægtstilstande med N hvirvler med dem der har $N + 1$ hvirvler, og jeg tror dette er en udtømmende metode til at finde alle relative ligevægtstilstande ved induktion.

Kontinueringsberegningerne har genskabt alle tidligere kendte løsninger, og har desuden vist bifurkationer i løsningsbanerne. For en specifik værdi af kontinueringparameteren er der to mulige baner, og én relativ ligevægtstilstand sammen med ét co-roterende punkt kan altså blive forbundet til to forskellige løsninger ved kontinuering. Dette er, så vidt vides, ikke observeret før. De tætte relative ligevægtstilstande for N hvirvler er desuden blevet genereret fra den samme løsning for $N - 1$ ved kontinuering. Den asymmetriske løsning for $N = 8$ er desuden bliver forbundet med en bifurkation.

På kuglen er ligningerne for relative ligevægtstilstande løst ved hjælp af tilfældige begyndelsesbetingelser for $\frac{\Gamma}{4\pi\Omega R^2} = 1$ og $N = 2, \dots, 8$. Der er her fundet flere løsninger end i planen. For $N = 7$ eksisterer der løsninger uden nogen symmetriakse men med en 180° rotationssymmetri, og den første fuldstændige asymmetriske løsninger forekommer for $N = 8$. Et tæt par af relative ligevægtstilstande forekommer også for $N = 8$. Den tætte løsning er tæt på de indlejrede, centrerede, ligesidede trekanter, og ligner derfor dem der blev fundet i planen.

Vi har altså opdaget bifurkerende relative ligevægtstilstande, hvilket er et nyt fænomen, og dette har givet os mere indsigt og viden om asymmetriske og tætte par af løsninger.

Preface

This thesis is submitted in partial fulfilment of the requirements for obtaining the degree of Master of Science in Engineering at the Technical University of Denmark. The work has been carried out at the Department of Engineering Science and Mechanics (ESM) at Virginia Polytechnic Institute and State University from September 2011 to January 2012 corresponding to a credit of 30 ECTS points. The project was supervised by Prof. Hassan Aref (ESM), Assoc. Prof. Mark Stremmer (ESM), Asst. Prof. Shane Ross (ESM), and Prof. Tomas Bohr (DTU Physics).

The work with vortex equilibria started for me in the Fall 2010, where I did an individual study supervised by H. Aref. This work led to the discovery of close equilibria. In the spring, the work continued, i.e. by writing the manuscript that got published in *Physics of Fluids* May 2011. After this, I went to Virginia Tech to continue my research together with H. Aref under my Thesis work. Just after 3 weeks, the 9th of September 2011, Hassan passed away suddenly and sadly. Hassan was a very inspiring supervisor and mentor, a caring person, and an extraordinary gifted scholar. I am sad that I could not finish my work with him, but first of all, I am grateful for the time I had working with him and for all the opportunities he gave me.

After this, M. Stremmer and S. Ross took over as supervisors on the same project. I would like to thank them for their willingness to this and for their good and competent supervision.

On October 12-14 I participated in the Conference of Society of Engineering Sciences in Chicago, where H. Aref was honoured with the G.I. Taylor Medal. Here, I presented my work on close equilibria. I also presented it on the Fall Fluid Mechanics Symposium at Virginia Tech, November 3, and at the APS Meeting in Baltimore, November 20-22, where the discovery of bifurcations was added to the presentation.

I would like to thank the ESM department and the Center for Fluid Dynamics, DTU, for supporting my stay at Virginia Tech and Tomas Bohr for his support and interest, as well.

Finally, I would like to thank my friends and family for their support during my stay at Virginia Tech.

Contents

Abstract	v
Resumé	vii
Preface	ix
1 Introduction	1
1.1 Motivation	2
1.2 Outline of the thesis	4
1.3 Publications	4
1.4 Presentations	4
2 Theory of point vortex dynamics and statics on the plane	5
2.1 The dynamical equations of a point vortex system	5
2.2 The equations for relative equilibria	8
2.3 Energy calculations	9
2.4 Stability analysis	10
3 Computations of vortex crystals	15
3.1 Analytical solutions	15
3.2 Asymmetric solutions	15
3.3 Close pairs of solutions	16
4 Computation of vortex crystals by a continuation method	21
4.1 Computation of co-rotating points	21
4.1.1 Analytical solutions	22
4.1.2 Numerical computations	24
4.2 Continuation of relative equilibria using co-rotating points	25
4.3 Convergence problems	26
4.4 All relative equilibria by induction	27
5 Results of the continuations	29
5.1 Examples of continuations	29
5.2 Cusps in the solution paths	31

5.3	Close pairs of solutions	33
5.4	Bifurcations in the solution paths	34
6	Relative equilibria on a sphere	43
6.1	Introduction	43
6.2	The dynamical equations of a point vortex system	44
6.3	The equation for relative equilibria	45
6.4	Numerical computations	46
6.5	Results	47
7	Conclusion and outlook	53
A	Figures of vortex crystals	55
A.1	$N = 2$	55
A.2	$N = 3$	55
A.3	$N = 4$	56
A.4	$N = 5$	56
A.5	$N = 6$	57
A.6	$N = 7$	57
A.7	$N = 8$	59
B	Figures of co-rotating points in the plane	61
B.1	Co-rotating points for $N = 2$	61
B.2	Co-rotating points for $N = 3$	62
B.3	Co-rotating points for $N = 4$	62
B.4	Co-rotating points for $N = 5$	63
B.5	Co-rotating points for $N = 6$	65
B.6	Co-rotating points for $N = 7$	68
C	Figures of continuation of vortex crystals in the plane	73
C.1	Continuation from $N = 2$ to $N = 3$	74
C.2	Continuation from $N = 3$ to $N = 2$	74
C.3	Continuation from $N = 3$ to $N = 4$	74
C.4	Continuation from $N = 4$ to $N = 3$	75
C.5	Continuation from $N = 4$ to $N = 5$	76
C.6	Continuation from $N = 5$ to $N = 4$	77
C.7	Continuation from $N = 5$ to $N = 6$	80
C.8	Continuation from $N = 6$ to $N = 5$	82
C.9	Continuation from $N = 6$ to $N = 7$	86
C.10	Continuation from $N = 7$ to $N = 6$	91
C.11	Continuation from $N = 7$ to $N = 8$	96
C.12	Continuation from $N = 8$ to $N = 7$	104
D	Relative equilibria on a sphere	113
D.1	Relative equilibria for $N = 2$	113
D.2	Relative equilibria for $N = 3$	113
D.3	Relative equilibria for $N = 4$	114
D.4	Relative equilibria for $N = 5$	115
D.5	Relative equilibria for $N = 6$	116

CONTENTS

xiii

D.6 Relative equilibria for $N = 7$ 118

D.7 Relative equilibria for $N = 8$ 121

E Letter published in Physics of Fluid 127

Bibliography 133

Introduction

This study is about patterns of vortices in equilibrium and computation of these. More precisely, relative equilibria of identical point vortices, which are patterns of identical point vortices in uniform rotation that do not change their shape or size and have thus constant inter-vortex distances. They are called relative equilibria to distinguish them from fixed or absolute equilibria in rest. Relative equilibria also go under the name *vortex crystals* [3], due to the obvious similarity with crystal patterns. The two terms will be used interchangeably.

The broad area of vortex dynamics goes back to Helmholtz (1821-1894)¹. The motion of three vortices was, e.g solved by Gröbli [4, 25] in 1877 and numerous work has been done on vortex dynamics sense. The field of vortex equilibria is part of what sometimes is called *vortex statics*, first used by Kelvin in 1875 [60]. This problem goes back to the 1870s and work by Mayer and W. Thomson, the later Lord Kelvin (see Section 1.1). A number of analytical solutions are known (see Section 3.1) and many different authors have been contributed to these solutions and to the field in general [3, 5, 43].

Several numerical explorations have been done by the author [20], as well, on relative equilibria, where the *Los Alamos Catalog* [18] from 1978 is one of the most comprehensive and early ones. The Catalog list all stable configurations for $N = 1, \dots, 30$ known up to now. Until now, no stable configurations, not included in The Catalog, have been found. The first asymmetric solutions were found numerically by Aref & Vainchtein in 1998 [13] by a continuation method similar to the one used in this work.

Prior to this work numerical explorations for $N = 4, \dots, 10$ were also done, which led to the discovery of close relative equilibria. This is pairs of relative equilibria so close that they cannot be distinguished by the naked eye, cf. Section 3.3. The present work continues the investigation and description of this phenomenon.

The goal of the work is to get a better understanding of some of these mentioned phenomena and possibly other interesting phenomena in this context. To achieve this, a method to find all relative equilibria, is wanted. Because the number of solutions generally is unknown, and because only limited analytical solutions are known, the problem is difficult.

Two methods will be used to compute equilibria. First, the governing equations will be solved numerically using random initial conditions. Secondly, a continuation method will be used to connect patterns of N vortices with patterns of $N + 1$. In the fluid points exist that are relatively at rest with respect to the vortex pattern. These are called co-rotating points. The continuation is done by imposing a small circulation to these points

¹A exposition of the history of the field is given in [43].

and slightly increase it until it has the same circulation as the other vortices. In all the intermediate steps relative equilibria are found. This method has the potential of finding all relative equilibria by induction. Namely, by knowing all relative equilibria for N vortices the continuation process will give the solutions for $N + 1$, etc. With this method, the hope is, furthermore, to gain more insight in the phenomena of asymmetric solutions [13] and close pairs of solutions [21].

This is all done on the plane. Finally, we will also start to look into relative equilibria on a sphere and compute the solutions simply using random initial conditions. A further introduction to this field is given in Chapter 6.

1.1 Motivation

The motivation for the study can be divided into two: A motivation from a standpoint of physics and one from the standpoint of mathematics.

From the standpoint of physics the problem is related to different visualisation of vortex patterns. The first one goes, as mentioned, back to work by Mayer and W. Thomson. In 1878-79 Mayer published his experiments with needle magnets placed on floating pieces of cork in an applied magnetic field, as an illustration of atomic interactions and forms [55]. The patterns are shown in Fig. 1.1. This was interpreted by W. Thomson [59], as an illustration of his theory of vortex atoms, that has long since been abandoned, where each atom was assumed to be made up of vortices in the 'ether'.

A variety of different visualisations have since been done [3, 48] and the goal of this work is, of course, to compute these patterns. Some of the experiments will be mentioned below, however, the details of the experiments will be omitted.

Yarmchuk, Gordon and Packard [61] did experiments in 1979 on vortices in superfluid ^4He , where they showed stable configurations, cf. Fig. 1.2.

Abo-Shaer *et al.* [1] made experiments of vortex lattice patterns in Bose-Einstein condensates shown in Fig. 1.3. In Fig. 1.4 a magnetized electron plasma in a so-called Malmberg-Penning trap is shown [22, 23]. The plasma displays point-vortex-like structures.

Finally, experiments using mm-sized rotating disks by Grzybowski *et al.* [27] have been done, shown in Fig. 1.5, which are some of the visualisations closest to the computed patterns.

From the standpoint of mathematics [7] the problem of relative equilibria is identical to the optimization problem of finding critical points for the product of the distances between N points in the plane given that the sum of the squares of their moduli is fixed [28].

Point vortex dynamics is also connected to many different polynomials and their solutions such as the Hermite, Laguerre, Adler-Moser polynomials and polynomials associated with the Painlevé and soliton equations [8, 19].

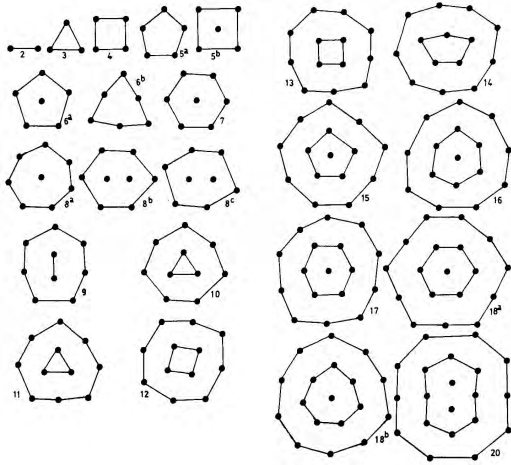


Figure 1.1: Mayer's diagrams of the patterns formed by floating magnets [55].

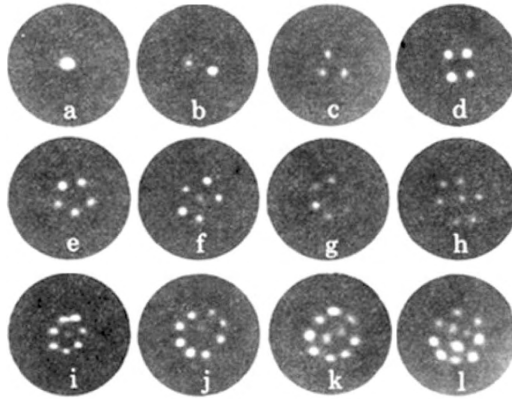


Figure 1.2: A visualisation of rotating vortex patterns in superfluid helium [61] with $1, \dots, 11$ vortices (light spots).

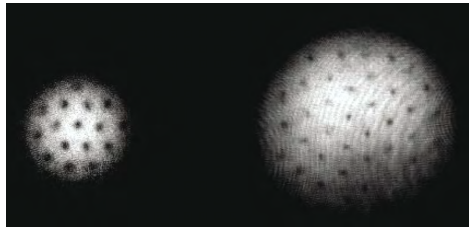


Figure 1.3: Vortex lattice patterns in Bose-Einstein condensates with 16 and 32 vortices [1].

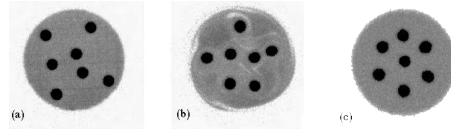


Figure 1.4: Stages in the evolution of a seven-vortex system in an electron plasma during 'cooling'. (a) Initial state (b) state after 2.5 ms (c) state at 100 ms. The state in (b) corresponds to a marginally stable equilibrium and the asymptotic state (c) is the centered hexagon. [22, 23]

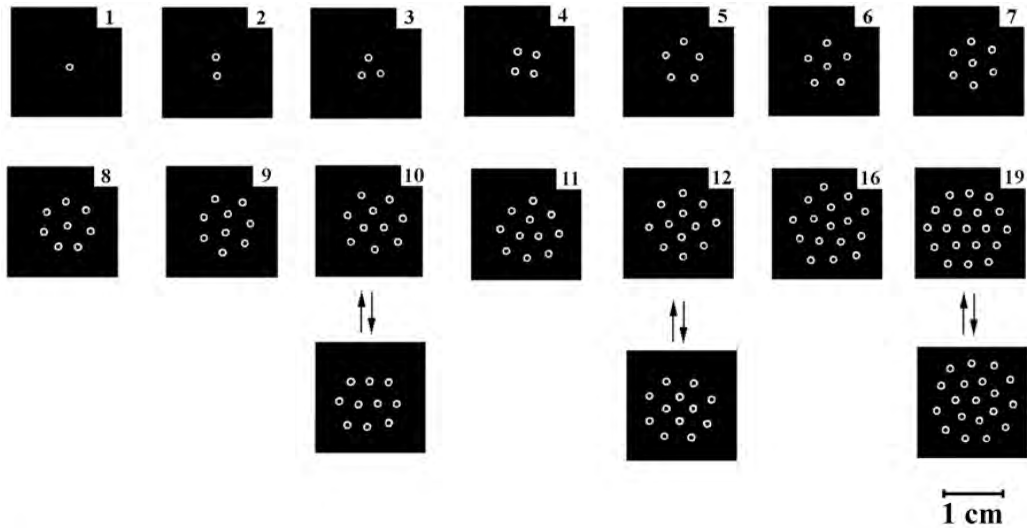


Figure 1.5: Dynamic self-assembly of spinning magnetic discs floating on a liquid-air interface from [27]. The interaction is a combination of fluid interaction produced by the spinning discs and the magnetic field. Note that there are two configurations for $N = 10, 12, 19$ and the pattern can dynamically oscillate between the two.

1.2 Outline of the thesis

The thesis consists of seven chapters, this one being the first one. The second chapter describes the theory behind the computations, and the governing equations are derived. In the third chapter some of the known analytical solutions are first given, together with a description of numerical results on asymmetric solution and close pairs of solutions. The fourth chapter focus on describing the continuation method, whereupon the results of this, are given in chapter 5. The work on relative equilibria on a sphere is given in chapter 6, and finally, is the conclusion given in chapter 7.

A large catalogue of figures of all the computations, both on the plane and on the sphere, is given in the appendices.

1.3 Publications

T. Dirksen and H. Aref

”Close pairs of relative equilibria for identical point vortices”

Physics of Fluids, Volume **23**, 051706 (2011) [21]

1.4 Presentations

T. Dirksen and H. Aref

”Close pairs of relative equilibria for identical point vortices”

48th Annual Technical Conference of Society of Engineering Sciences

October 13, 2011

T. Dirksen, H. Aref, M. Stremmer, and S. Ross

”Close pairs of relative equilibria for identical point vortices”

Fall Fluid Mechanics Symposium at Virginia Tech

November 3, 2011

T. Dirksen and H. Aref

”Close relative equilibria for identical point vortices”

64th Annual Meeting of the APS Division of Fluid Dynamics, Volume **56**, Number 18

November 21, 2011

Theory of point vortex dynamics and statics on the plane

The most important parts of the theory of point vortex dynamics and statics for this work, will be represented in this chapter. Most of it is well described in, e.g. [3, 46].

2.1 The dynamical equations of a point vortex system

We consider a system of point vortices in an incompressible, inviscid fluid. A point vortex is defined as the limit of the Rankine vortex in which the radius goes towards zero and the magnitude of the angular velocity towards infinity, in such a way that the circulation is constant. A Rankine vortex in cylindrical coordinates (r, ϕ, z) is given by [2]

$$v_\phi(r, \phi, z) = \begin{cases} \Omega r, & r \leq R \\ \frac{\Omega R^2}{r}, & r > R \end{cases} \quad (2.1a)$$

$$\omega_z = \begin{cases} 2\Omega, & r \leq R \\ 0, & r > R \end{cases} \quad (2.1b)$$

$$v_r = v_z = \omega_r = \omega_\phi = 0, \quad (2.1c)$$

where \mathbf{v} is the velocity, $\boldsymbol{\omega}$ the vorticity, R the radius of the vortex, $\Omega = \frac{\Gamma}{2\pi R^2}$ the angular velocity, and Γ the circulation¹. Taking the limits $R \rightarrow 0$, $\Omega \rightarrow \infty$ gives

$$v_\phi = \frac{\Gamma}{2\pi r}, \quad \text{for } r \neq 0 \quad (2.2a)$$

$$v_r = v_z = \omega_r = \omega_\phi = 0 \quad (2.2b)$$

$$\omega_z = \delta(r), \quad (2.2c)$$

where $\delta(x)$ is the Dirac delta function. This describes a point vortex. The point vortex approximation is analogue to the well-known point mass approximation used in gravitational problems.

¹A bold symbol \mathbf{u} always denotes a vector, u_i the components, and $u = \|\mathbf{u}\|$ the norm of the vector.

The vorticity $\boldsymbol{\omega}$ is defined by

$$\boldsymbol{\omega} = \nabla \times \mathbf{v}. \quad (2.3)$$

In a 2D flow, where $\mathbf{v} = v_x(x, y)\mathbf{e}_x + v_y(x, y)\mathbf{e}_y$, the vorticity only has a z -component

$$\boldsymbol{\omega} = \nabla \times \mathbf{v} = \omega \mathbf{e}_z = (\partial_x v_y - \partial_y v_x)\mathbf{e}_z, \quad (2.4)$$

where $\partial_a = \frac{\partial}{\partial a}$. The vorticity distribution ω with a finite amount of point vortices N , can now in 2D be described by

$$\omega(\mathbf{x}, t) = \sum_{\alpha=1}^N \frac{\Gamma_\alpha}{2\pi} \delta(\mathbf{x} - \mathbf{x}_\alpha(t)), \quad (2.5)$$

where each component has been weighted with $\frac{\Gamma_\alpha}{2\pi}$, where Γ_α is the circulation of vortex number α such that integrating the velocity around the vortex gives the circulation.

By Helmholtz decomposition theorem any vector field can be separated in a curl-free scalar potential ϕ plus a divergence-free vector potential $\boldsymbol{\psi}$

$$\mathbf{v} = \nabla \phi + \nabla \times \boldsymbol{\psi}. \quad (2.6)$$

For a divergence-free velocity $\nabla \cdot \mathbf{v} = 0$ (i.e. incompressible) the velocity can be written solely by a vector potential $\mathbf{v} = \nabla \times \boldsymbol{\psi}$. In a 2D flow this gives

$$\mathbf{v} = v_x(x, y)\mathbf{e}_x + v_y(x, y)\mathbf{e}_y = \mathbf{e}_x \partial_y \psi_z - \mathbf{e}_y \partial_x \psi_z, \quad (2.7)$$

which shows that it is sufficient to have a vector potential on the form $\boldsymbol{\psi} = \psi_z \mathbf{e}_z = \psi(x, y)\mathbf{e}_z$ where ψ is the streamfunction. Note that Eq. (2.7) automatically satisfies the incompressibility condition $\partial_x v_x + \partial_y v_y = 0$.

Inserting Eq. (2.7) in Eq. (2.3) gives

$$\nabla^2 \psi = -\omega, \quad (2.8)$$

which shows that the streamfunction satisfies a Poisson equation.

The solution for the streamfunction is now, using Green's function, given by [15]

$$\psi(\mathbf{x}) = \int G(\mathbf{x} - \mathbf{z})\omega(\mathbf{z})d\mathbf{z}, \quad (2.9)$$

where

$$G(\mathbf{x}) = -\frac{1}{2\pi} \log \|\mathbf{x}\| \quad (\text{in } \mathbb{R}^2) \quad (2.10)$$

and the velocity is then given by Eq. (2.7).

Considering now a collection of N point vortices located at $\mathbf{x}_\alpha = (x_\alpha(t), y_\alpha(t))$ where $\alpha = 1, \dots, N$, the streamfunction is, due to Eqs. (2.9) and (2.5), given by

$$\psi(x, y, t) = -\sum_{\alpha=1}^N \frac{\Gamma_\alpha}{4\pi} \iint \log \left((x - x')^2 + (y - y')^2 \right) \delta(x' - x_\alpha(t)) \delta(y' - y_\alpha(t)) dx' dy' \quad (2.11a)$$

$$= -\frac{1}{4\pi} \sum_{\alpha=1}^N \Gamma_\alpha \log \left((x - x_\alpha(t))^2 + (y - y_\alpha(t))^2 \right). \quad (2.11b)$$

The velocity induced by point vortices located at $\mathbf{x}_\alpha = (x_\alpha(t), y_\alpha(t))$ is now given by

$$\mathbf{v} = \sum_{\alpha=1}^N \nabla_{\perp} \psi_{\alpha}(x, y, t), \quad (2.12)$$

which gives the velocity components

$$v_x(x, y, t) = -\frac{1}{2\pi} \sum_{\alpha=1}^N \Gamma_{\alpha} \frac{y - y_{\alpha}(t)}{(x - x_{\alpha})^2 + (y - y_{\alpha})^2} \quad (2.13a)$$

$$v_y(x, y, t) = \frac{1}{2\pi} \sum_{\alpha=1}^N \Gamma_{\alpha} \frac{x - x_{\alpha}(t)}{(x - x_{\alpha})^2 + (y - y_{\alpha})^2}. \quad (2.13b)$$

Eq. (2.13) can also be derived from a kinematic point of view. The velocity induced by a vortex must be in the azimuthal direction and it must be inverse proportional to the length to the vortex. Finally, integrating the velocity around the vortex must give the circulation Γ . All this is seen to be fulfilled by Eq. (2.13).

In the rotating frame the velocity \mathbf{v}^R is given by [46]

$$\mathbf{v}^R = \mathbf{v} + \boldsymbol{\Omega} \times \mathbf{x}, \quad (2.14)$$

where $\boldsymbol{\Omega}$ denotes the axis of rotating and $\|\boldsymbol{\Omega}\| = \Omega$ is the angular velocity. In a 2D flow, where $\boldsymbol{\Omega} = \Omega \mathbf{e}_z$, this is

$$\mathbf{v}^R = \mathbf{v} - y\Omega \mathbf{e}_x + x\Omega \mathbf{e}_y, \quad (2.15)$$

which can easily be seen by differentiating the position remembering to differentiate the unit vectors

$$\mathbf{e}_x^R = \cos(\Omega t) \mathbf{e}_x + \sin(\Omega t) \mathbf{e}_y \quad (2.16a)$$

$$\mathbf{e}_y^R = -\sin(\Omega t) \mathbf{e}_x + \cos(\Omega t) \mathbf{e}_y. \quad (2.16b)$$

From this, the streamfunction in the rotating frame, is seen to be

$$\psi^R = \psi - \frac{1}{2} \Omega \|\mathbf{x}\|^2. \quad (2.17)$$

Now to find the equations of motion for the vortices we simply set $(x, y) = (x_{\alpha}, y_{\alpha})$ in Eqs. (2.13a) and (2.13b). This will, however, lead to a singular term, which we fortunately can remove, because the self-velocity does not contribute to the translational motion. This gives the well-known dynamical equations for a system of point vortices

$$\frac{dx_{\alpha}}{dt} = -\frac{1}{2\pi} \sum_{\beta=1}^N \Gamma_{\alpha} \frac{y_{\alpha} - y_{\beta}}{\ell_{\alpha\beta}^2}, \quad \alpha = 1, \dots, N, \quad (2.18a)$$

$$\frac{dy_{\alpha}}{dt} = \frac{1}{2\pi} \sum_{\beta=1}^N \Gamma_{\alpha} \frac{x_{\alpha} - x_{\beta}}{\ell_{\alpha\beta}^2}, \quad \alpha = 1, \dots, N, \quad (2.18b)$$

where $\ell_{\alpha\beta}^2 = (x_\alpha - x_\beta)^2 + (y_\alpha - y_\beta)^2$ and the prime indicates that $\beta \neq \alpha$.

Instead of describing the motion in the (x, y) -plane it can be done in the complex plane, which simplifies the dynamical equations to

$$\frac{dz_\alpha^*}{dt} = \frac{1}{2\pi i} \sum_{\beta=1}^N \prime \frac{\Gamma_\beta}{z_\alpha - z_\beta}, \quad \alpha = 1, \dots, N, \quad (2.19)$$

where the asterisk denotes complex conjugation and $z_\alpha \equiv x_\alpha + iy_\alpha$.

2.2 The equations for relative equilibria

Now, a situation where all the vortices have the same circulation $\Gamma_i = \Gamma$ is considered, and the goal is to find all relative equilibria where the size and the shape of a vortex pattern are unchanged, and the pattern is the uniform rotation. In other words the vortices's relative positions are unchanged. By placing the coordinate system such that the origin is coinciding with the center of rotation we have that $z_\alpha(t) = z_\alpha(0)e^{i\Omega t}$, because all vortices must stay at the same position in the co-rotating frame. Inserting this in Eq. (2.19) the dynamical equation reduces to the algebraic equation

$$\frac{2\pi\Omega}{\Gamma} z_\alpha^*(0) = \sum_{\beta=1}^N \prime \frac{1}{z_\alpha(0) - z_\beta(0)}. \quad (2.20)$$

The equation is now non-dimensionalised such that $\tilde{z} = z\sqrt{\frac{2\pi\Omega}{\Gamma}}$ or, in other words, the length is scaled such that $\frac{2\pi\Omega}{\Gamma} = 1$. This yields

$$\tilde{z}_\alpha^* = \sum_{\beta=1}^N \prime \frac{1}{\tilde{z}_\alpha - \tilde{z}_\beta}, \quad \alpha = 0 \dots N. \quad (2.21)$$

The arguments $t = 0$ have now been omitted. This corresponds to turning into a rotating frame of reference where $z_\alpha(t) = z_\alpha(0)$, which will be our frame of reference in the succeeding unless otherwise is stated. The tildes will furthermore be omitted. Eq. (2.21) is the equation of relative equilibria, which is the most important equation in this work. The equation can also be separated into real and imaginary parts yielding

$$x_\alpha = \sum_{\beta=1}^N \prime \frac{x_\alpha - x_\beta}{\ell_{\alpha\beta}^2} \quad (2.22a)$$

$$y_\alpha = \sum_{\beta=1}^N \prime \frac{y_\alpha - y_\beta}{\ell_{\alpha\beta}^2}. \quad (2.22b)$$

Finally in this section, some of the moment relations are now considered [6, 14]. From Eq. (2.21) we get that

$$\begin{aligned} N_1 \equiv \sum_{\alpha=1}^N z_\alpha &= \sum_{\alpha=1}^N \sum_{\beta=1}^N \prime \left(\frac{1}{z_\alpha - z_\beta} \right)^* = \sum_{\alpha=1}^N \sum_{\beta=1}^N \prime \frac{1}{z_\alpha^* - z_\beta^*} \\ &= \frac{1}{z_1^* - z_2^*} + \frac{1}{z_2^* - z_1^*} + \frac{1}{z_1^* - z_3^*} + \frac{1}{z_3^* - z_1^*} + \dots = 0. \end{aligned} \quad (2.23)$$

Thus the first moment vanish. Furthermore

$$\begin{aligned} M_1 &= \sum_{\alpha=1}^N |z_\alpha|^2 = \sum_{\alpha=1}^N z_\alpha \sum_{\beta=1}^N \prime \frac{1}{z_\alpha - z_\beta} = \sum_{\alpha,\beta=1}^N \prime \frac{z_\alpha}{z_\alpha - z_\beta} \\ &= \sum_{\alpha,\beta=1}^N \prime \left[\frac{\frac{1}{2}(z_\alpha - z_\beta)}{z_\alpha - z_\beta} + \frac{\frac{1}{2}(z_\alpha + z_\beta)}{z_\alpha - z_\beta} \right]. \end{aligned} \quad (2.24)$$

The second term vanishes, because it is asymmetric, i.e. interchanging α and β change the sign. Thus

$$\sum_{\alpha=1}^N |z_\alpha|^2 = \sum_{\alpha,\beta=1}^N \prime \frac{1}{2} = \frac{1}{2}N(N-1). \quad (2.25)$$

The notation $N_n = \sum_{\alpha=1}^N z_\alpha^n$ and $M_n = \sum_{\alpha=1}^N z_\alpha^n z_\alpha^*$ has been used in agreement with [14], where more relations can be found.

2.3 Energy calculations

The Hamiltonian for a point vortex system is given by [3, 5]

$$\mathcal{H} = -\frac{1}{4\pi} \sum_{\alpha,\beta}^N \prime \Gamma_\alpha \Gamma_\beta \log |z_\alpha - z_\beta|. \quad (2.26)$$

Multiplying with the area density [kg/m^2] Eq. (2.26) is seen to have the dimension of energy. This is a measure of the kinetic interaction energy and the self energy is, as seen, not included. Differentiating and utilising Eq. (2.18) gives

$$-\frac{\partial \mathcal{H}}{\partial x_\lambda} = \Gamma_\lambda \frac{dy_\lambda}{dt} \quad (2.27a)$$

$$\frac{\partial \mathcal{H}}{\partial y_\lambda} = \Gamma_\lambda \frac{dx_\lambda}{dt}. \quad (2.27b)$$

For $q_\alpha = x_\alpha, p_\alpha = \Gamma_\alpha y_\alpha$ the equations are seen to be on Hamilton's canonical form.

For $\Gamma_i = \Gamma$ instead of \mathcal{H} we tend to work with [6]

$$\theta = -\frac{8\pi}{N(N-1)\Gamma^2} \mathcal{H} = \frac{2}{N(N-1)} \sum_{\alpha,\beta=1}^N \prime \log \ell_{\alpha\beta}, \quad (2.28)$$

which is seen to be equal to

$$\theta = \langle \log \ell_{\alpha\beta}^2 \rangle, \quad (2.29)$$

where $\langle \cdot \rangle$ denotes the mean average. This quantity is thus a measure of the average logarithmic square distance and therefore not dependent on N , which makes θ preferable for comparison. This energy quantity will be used solving the problem numerically, to compare whether two solutions are different. Furthermore, the solutions are sorted with respect to decreasing energy.

If one of the vortices z_N has a circulation $\Gamma\gamma$ different from Γ the following energy is used

$$\theta = \frac{2}{N(N-1)} \left[\sum_{\alpha,\beta=1}^{N-1} \prime \log \ell_{\alpha\beta} + 2 \sum_{\alpha=1}^{N-1} \gamma \log |z_N - z_\alpha| \right]. \quad (2.30)$$

The normalisation is not that suitable here, but is kept due to comparison purposes.

The energy in the rotating frame is given by

$$\mathcal{H}^R = \mathcal{H} + \sum_{\alpha=1}^N \frac{\Gamma_\alpha \Omega}{2} |z_\alpha|^2. \quad (2.31)$$

Inserting this in Hamilton's equation (2.27) we can see that the velocities now include the corrections from going into the rotating frame, cf. Eq. (2.15). For equal circulations the normalised energy simplifies to

$$\theta^R = \frac{2}{N(N-1)} \left[\sum_{\alpha,\beta=1}^N \prime \log \ell_{\alpha\beta} + \sum_{\alpha=1}^N |z_\alpha|^2 \right] = \frac{2}{N(N-1)} \sum_{\alpha,\beta=1}^N \prime \log \ell_{\alpha\beta} + 1, \quad (2.32)$$

cf. Eq. (2.25).

2.4 Stability analysis

The stability of a regular polygon configuration was solved by J.J. Thomson in 1882 [57]. He proved the configurations to be stable if the number of vortices does not exceed six and unstable for $N \geq 8$, which is sometimes known as *Thomson's Theorem*. Further work on vortices on ring formations is done in [29] and the stability of the heptagon is treated in [32, 44]. Stability analysis for the three vortex problem is given in [9]. This analysis is extended here to the stability of a general vortex crystal. First, the full dynamical equation Eq. (2.19) is considered

$$\frac{dz_\alpha^*}{dt} = \frac{1}{2\pi i} \sum_{\beta=1}^N \prime \frac{\Gamma_\beta}{z_\alpha - z_\beta}, \quad \alpha = 1, \dots, N, \quad (2.33)$$

where $z_i \equiv z_i(0)$. For a linear stability analysis an infinitesimal perturbation η_α is imposed to the solution such that $z_\alpha^{(1)}(t) = (z_\alpha(0) + \eta_\alpha(t))e^{i\Omega t}$. Inclusion of the factor $e^{i\Omega t}$ in the perturbation is for convenience in calculation, as we shall see later. η_α is assumed to be small in the sense that all expressions will be expanded to linear order in this quantity. Doing this and subtracting out the zero'th order term Eq. (2.33) yields

$$\frac{d\eta_\alpha^*}{dt} - i\Omega\eta_\alpha^* = \frac{1}{2\pi i} \sum_{\beta=1}^N \prime \Gamma_\alpha \frac{\eta_\alpha - \eta_\beta}{(z_\alpha - z_\beta)^2}. \quad (2.34)$$

For $\Gamma_i = \Gamma$, together with a scaling such that $\frac{2\pi\Omega}{\Gamma} = 1$, the equation reads

$$\frac{d\eta_\alpha^*}{dt} = i\Omega \left(\eta_\alpha^* + \sum_{\beta=1}^N A_{\alpha\beta} \eta_\beta \right), \quad (2.35)$$

where

$$A_{\alpha\beta} = \sum_{\gamma=1}^N \frac{\delta_{\alpha\beta}}{(z_\alpha - z_\gamma)^2} - \frac{1 - \delta_{\alpha\beta}}{(z_\alpha - z_\beta)^2}, \quad (2.36)$$

where $\delta_{\alpha\beta}$ is the Kronecker delta. In vector notation Eq. (2.35) can be written as

$$\dot{\boldsymbol{\eta}}^* = i\Omega(\boldsymbol{\eta}^* + \mathbf{A}\boldsymbol{\eta}), \quad (2.37)$$

where $\boldsymbol{\eta}$ is the vector with components η_α and \mathbf{A} is the matrix with elements $A_{\alpha\beta}$. Differentiating once more and taking the complex conjugate yields

$$\ddot{\boldsymbol{\eta}} = -i\Omega(\dot{\boldsymbol{\eta}} + \mathbf{A}^*\dot{\boldsymbol{\eta}}^*) \quad (2.38)$$

and using Eq. (2.37) again gives

$$\ddot{\boldsymbol{\eta}} = -i\Omega\left(-i\Omega(\boldsymbol{\eta} + \mathbf{A}^*\boldsymbol{\eta}^*) + \mathbf{A}^*(i\Omega(\boldsymbol{\eta}^* + \mathbf{A}\boldsymbol{\eta}))\right) = \Omega^2(-1 + \mathbf{A}^*\mathbf{A})\boldsymbol{\eta}. \quad (2.39)$$

Since \mathbf{A} is symmetric, $\mathbf{A}^T = \mathbf{A}$, the Hermitian conjugate of $\mathbf{B} = \mathbf{A}^*\mathbf{A}$ can be rewritten to

$$\mathbf{B}^\dagger = (\mathbf{A}^*\mathbf{A})^\dagger = ((\mathbf{A}^*\mathbf{A})^T)^* = (\mathbf{A}^T\mathbf{A}^{*T})^* = \mathbf{A}^{*T}\mathbf{A}^T = \mathbf{A}^*\mathbf{A} = \mathbf{B}, \quad (2.40)$$

where \dagger denotes the adjoint operator. Thus, \mathbf{B} is seen to be Hermitian and can then be represented in terms of orthonormal eigenvectors having real eigenvalues.

Furthermore we have that

$$\mathbf{B}\mathbf{v}^{(k)} = \lambda_k\mathbf{v}^{(k)}, \quad (2.41)$$

where $\mathbf{v}^{(k)}$ is the k 'th eigenvector and λ_k the corresponding eigenvalue. Multiplying with $(\mathbf{v}^{(k)})^\dagger$ gives

$$(\mathbf{v}^{(k)})^\dagger \mathbf{B}\mathbf{v}^{(k)} = \lambda_k (\mathbf{v}^{(k)})^\dagger \mathbf{v}^{(k)} \quad (2.42)$$

$$(\mathbf{v}^{(k)})^\dagger \mathbf{A}^*\mathbf{A}\mathbf{v}^{(k)} = |\mathbf{A}\mathbf{v}^{(k)}|^2 = \lambda_k |\mathbf{v}^{(k)}|^2. \quad (2.43)$$

From this it is seen that the eigenvalues λ_k must moreover be non-negative, since $|\mathbf{v}^{(k)}|^2 > 0$.

Note that the vector $v_\alpha^{(0)} = 1$ is a trivial eigenvector of \mathbf{A} with the eigenvalue $\lambda_0 = 0$, since the elements of each row sum to zero. Thus, $v_\alpha^{(0)} = 1$ is also an eigenvector of \mathbf{B} . This is a translation of all the vortices at $t = 0$, which breaks the symmetry.

Consider now the vector $\mathbf{v}^{(1)}$ with components equal to the vortex positions in the relative equilibrium, $v_\alpha^{(1)} = z_\alpha$. Using Eq. (2.36) one can write

$$\left(\mathbf{A}\mathbf{v}^{(1)}\right)_\alpha = \sum_{\beta=1}^N A_{\alpha\beta}z_\beta = \sum_{\beta=1}^N \frac{z_\alpha - z_\beta}{(z_\alpha - z_\beta)^2} = \sum_{\beta=1}^N \frac{1}{z_\alpha - z_\beta} = z_\alpha^*. \quad (2.44)$$

Thus, $\mathbf{A}\mathbf{v}^{(1)} = (\mathbf{v}^{(1)})^*$. Multiplying with \mathbf{A}^* yields

$$\mathbf{B}\mathbf{v}^{(1)} = \mathbf{A}^*\mathbf{A}\mathbf{v}^{(1)} = (\mathbf{A}\mathbf{v}^{(1)})^* = \mathbf{v}^{(1)}. \quad (2.45)$$

From this we conclude that the eigenvalue $\lambda_1 = 1$ is a trivial eigenvalue of \mathbf{B} .

Expanding the perturbation in the eigenvectors $\mathbf{v}^{(k)}$

$$\boldsymbol{\eta}(t) = \sum_{k=0}^{N-1} \rho_k(t) \mathbf{v}^{(k)} \quad (2.46)$$

and inserting this in Eq. (2.38) gives

$$\frac{d^2 \rho_k}{dt^2} = \Omega^2 (\lambda_k - 1) \rho_k, \quad (2.47)$$

using that the eigenvectors are orthogonal. Finally, we can now conclude that if any eigenvalue λ_k of \mathbf{B} is larger than unity, the configuration will be unstable, because of the exponential growth. The more eigenvalues that are larger than unity the more unstable becomes the configuration. If several eigenvalues are equal to unity the configuration will be marginally stable.

Looking again at the eigenvector $v_\alpha^{(1)} = z_\alpha$ and assuming that $\boldsymbol{\eta}(0) = a \mathbf{v}^{(1)}$, we have from Eq. (2.47) that $\rho_1(t) = a + bt$. In [9] it is assumed that $\dot{\rho}(0) = 0$ and the linear term vanishes thus. This is, however, an unnecessary assumption, which we shall see. Eq. (2.37) must be fulfilled, as well, and inserting that $\boldsymbol{\eta}(t) = \rho_1(t) \mathbf{v}^{(1)}$ here yields

$$\dot{\rho}_1^*(t) |\mathbf{v}^1\rangle^* = i\Omega [\rho_1^*(t) |\mathbf{v}^1\rangle^* + \mathbf{A} \rho_1(t) |\mathbf{v}^1\rangle], \quad (2.48)$$

where Dirac's bra-ket notation is used. Multiplying with ${}^* \langle \mathbf{v}^1 |$ gives

$$\dot{\rho}_1^*(t) = i\Omega [\rho_1^*(t) + \rho_1(t) {}^* \langle \mathbf{v}^1 | \mathbf{A} | \mathbf{v}^1 \rangle]. \quad (2.49)$$

Using that $\mathbf{A} |\mathbf{v}^1\rangle = |\mathbf{v}^1\rangle^*$ yields

$$\dot{\rho}_1^*(t) = i\Omega [\rho_1^*(t) + \rho_1(t)] \quad (2.50)$$

and inserting that $\rho_1(t) = a + bt$ gives us that

$$b^* = i\Omega [a^* + b^* t + a + bt] = \begin{cases} b^* + b = 0 \Rightarrow \mathcal{R}e(b) = 0 \\ b^* = i\Omega [a^* + a] = 2i\Omega \mathcal{R}e(a). \end{cases} \quad (2.51)$$

Thus, $\mathcal{I}m(b) = -2\Omega \mathcal{R}e(a)$ and the perturbation, together with the vortex coordinates, can be written as

$$\eta_\alpha(t) = (a - 2i\Omega \mathcal{R}e(a)t) z_\alpha \quad (2.52)$$

$$z_\alpha^{(1)}(t) = (1 + a - 2i\Omega \mathcal{R}e(a)t) z_\alpha e^{i\Omega t}. \quad (2.53)$$

To linear order this can be written as

$$\begin{aligned} z_\alpha^{(1)}(t) &\approx (1 + a) (1 - 2i\Omega \mathcal{R}e(a)t) z_\alpha e^{i\Omega t} \\ &\approx (1 + a) z_\alpha e^{i\Omega(1 - 2\mathcal{R}e(a))t}. \end{aligned} \quad (2.54)$$

For an imaginary a this corresponds to a rotation, because a rotation to linear order is given by $z_\alpha \rightarrow z_\alpha e^{i\varphi} \approx (1 + i\varphi) z_\alpha$. For a being real this is a scaling of the configuration with a

corresponding change in the angular velocity. If we scale the coordinates with $(1 + \rho)$, and inserting $z_\alpha \rightarrow (1 + \rho)z_\alpha$ into Eq. (2.20) we get

$$\frac{2\pi\Omega|1 + \rho|^2}{\Gamma} z_\alpha^* = \sum_{\beta=1}^N \frac{1}{z_\alpha - z_\beta}. \quad (2.55)$$

$\Omega|1 + \rho|^2$ is, thus, invariant and the new angular velocity Ω' must fulfil that $\Omega' = \frac{\Omega}{|1 + \rho|^2} \approx \Omega(1 - 2\rho)$, which is exactly what we have in Eq. (2.54).

Finally, the equations for \mathbf{A} , considering a configuration where the circulation $\Gamma\gamma$ of the vortex at z_N is different from the others', are given by

$$A_{\alpha\beta} = -\frac{1}{(z_\alpha - z_\beta)^2}, \quad \alpha = 1, \dots, N, \beta = 1, \dots, N - 1, \alpha \neq \beta \quad (2.56a)$$

$$A_{\alpha,N} = -\frac{\gamma}{(z_\alpha - z_N)^2}, \quad \alpha = 1, \dots, N - 1 \quad (2.56b)$$

$$A_{\alpha\alpha} = \sum_{k=1}^N \frac{1}{(z_\alpha - z_k)^2} + \frac{\gamma}{(z_\alpha - z_N)^2}, \quad \alpha = 1, \dots, N - 1 \quad (2.56c)$$

$$A_{N,N} = \sum_{k=1}^N \frac{1}{(z_N - z_k)^2}. \quad (2.56d)$$

Computations of vortex crystals

In this chapter the prior known solutions to the equation for relative equilibria are described. First, the known analytical solutions are described, then the numerical explorations focusing on the asymmetric solutions and the close pairs of relative equilibria.

3.1 Analytical solutions

Many different solutions to the equations for relative equilibria (2.21) are known analytically. These will be summarised here.

Configurations with vortices at the vertices of a regular polygon are known solutions with radii $R = \sqrt{\frac{N-1}{2}}$ and, thus, the coordinates $z_\alpha = Re^{i2\pi\alpha/N}$, where $\alpha = 1, \dots, N$ [8, 10]. Polygons with no vortices at the origin are called open. Likewise, is the centered polygon, with a vortex at the origin, a solution with radius $R = \sqrt{\frac{N}{2}}$ [8, 10].

Symmetric nested polygons (s -gon), either open or centered, are also known solutions [14]. The radii R_k for the open configuration are given by [21]

$$\frac{2R_k^2 - s + 1}{R_k^s} = 2s \sum_{j=1}^p \frac{1}{R_k^s - R_j^s}, \quad (3.1)$$

where p is the number of nestings. This gives the coordinates $z_\alpha = R_k e^{i2\pi\alpha/s}$, $k = 1, \dots, p$, $\alpha = 1, \dots, s$. For the centered configuration the radii are

$$\frac{2R_k^2 - s - 1}{R_k^s} = 2s \sum_{j=1}^p \frac{1}{R_k^s - R_j^s}. \quad (3.2)$$

The co-linear solutions are known to be roots of the N th Hermite polynomial [3] and, finally, are bilinear cases, with vortices on two perpendicular lines, known solutions [11].

3.2 Asymmetric solutions

The first description of an asymmetric solution is given by Aref & Vainchtein in 1998 [13]. An asymmetric solution is understood in the sense that it has no symmetry axes. Thus, by mirroring an asymmetric solution a new solution is obtained, which cannot be obtained by rotating the former one. The configurations were found by a numerical continuation

method, similar to the one described in Chapter 4. An asymmetric solution is somewhat non-intuitive and the discovery was at that time very surprising. The two first asymmetric solutions for respectively $N = 8$ and $N = 9$ are shown in Fig. 3.1. The number of asymmetric solutions seems to grow rapidly together with the number of vortices and asymmetric solutions are expected to occur for $N \geq 8$, and to be dominant for a high number of vortices.

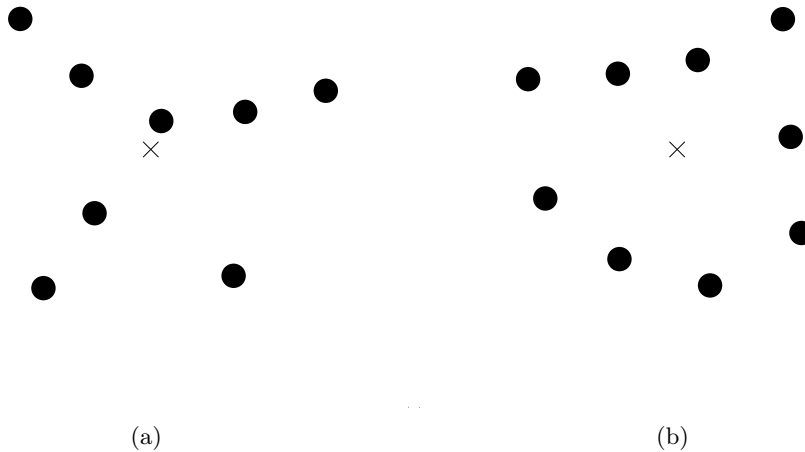


Figure 3.1: Two asymmetric solutions for (a) $N = 8$ and (b) $N = 9$ both numerically determined.

3.3 Close pairs of solutions

Even though computations including marginally stable and unstable patterns have been done before, this is done again in the hope of finding new solutions. The computations are done in MATLAB simply by solving Eq. (2.22) using random initial conditions. Different intervals for the initial conditions are used, but normally the initial conditions are between -5 and 5 , and using these initial conditions all the known solutions can be found. Double precision is used, which approximately gives 16 decimals. The solver uses a nonlinear least-squares algorithm and is called by the function `fsolve`.

The energy defined in Eq. (2.28) is used to compare the different solutions quantitatively. Thus, a solution is only saved, when its energy is different from the energies of the solutions that are already found. The program is then run until no more solutions are found. This is of course not a totally reliable method to be sure that all solutions are found, as the number of solutions is unknown. Nevertheless, the method regenerates all prior known solutions and even finds new ones.

When a solution is found it is verified explicitly that the point vortex equation (2.21) is fulfilled

$$\frac{1}{N} \sum_{\alpha=1}^N \left| \sum_{\beta=1}^N \frac{1}{z_{\alpha} - z_{\beta}} - z_{\alpha}^* \right| < \varepsilon. \quad (3.3)$$

This is the absolute sum of all the errors normalized with $\frac{1}{N}$. In our simulations we have used $\varepsilon = 10^{-12}$. Furthermore, the moment relations from Eqs. (2.23) and (2.25) are confirmed to be fulfilled.

Exhaustive investigations have been done for $N = 3, \dots, 10$, and it is believed that all solutions have been found. All the computed solutions for $N = 2, \dots, 8$ can be found in Appendix A. The solutions for $N = 9, 10$ and all vortex coordinates, together with the eigenvalues for the computed relative equilibria, can be found in [20].

The results of the computations showed some new, and until then unknown, solutions. The first one is shown in Fig. 3.2, where the black dots represent the analytical known solution, and the superimposed gray dots a new close numerically determined solution. At first sight they seemed identical, which might be why they have not been observed before, but by comparing the energies one will notice the difference and but superimposing one of the solutions they can be distinct by the naked eye. The energy in the rotating frame Eq. (2.31), between the two close solutions, is shown in Fig. 3.3. The energy for the analytical solution is at step one, and the numerical solution at step 1000. The intermediate steps comes from a simple continuation between the two solutions. The intermediate steps are thus not relative equilibria, but the vortices are simple moved simultaneously between the two solutions. From this it can be seen that the two solutions are critical points (either saddles, local minima or maxima) in the energy landscape, as they should [50].

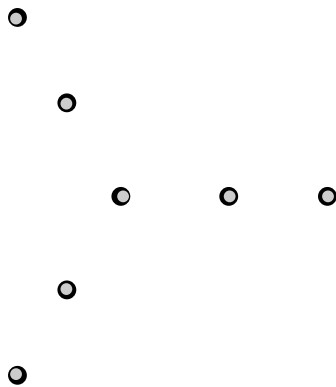


Figure 3.2: Two close solutions for $N = 7$, $s = 3$, $p = 2$. The black dots show the analytical known solutions and the gray dots the new numerically determined solutions. Both solutions are unstable.

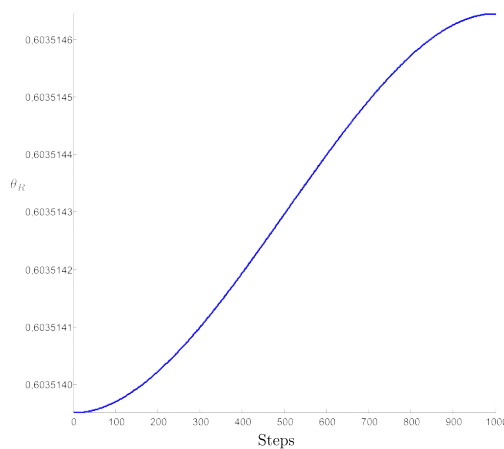


Figure 3.3: The energy in the rotating frame iterating between the two close solutions.

Two close solutions have also been found for more nestings p of triangles (s -gons), and seem to exist for an arbitrary number $p \geq 2$. In Fig. 3.4(a) it is shown for three nestings, $p = 3$ and in Fig. 3.4(b) for $p = 10$. The hypothesis is tested for $p = 2, \dots, 30$. This is in agreement with the result for equilibria of point masses under gravity, where similar (but not as close) pairs have been found [52]. However, no close pair is found for the centered equilateral triangle ($p = 1$) for vortices, which is in contrary to the result of point masses,

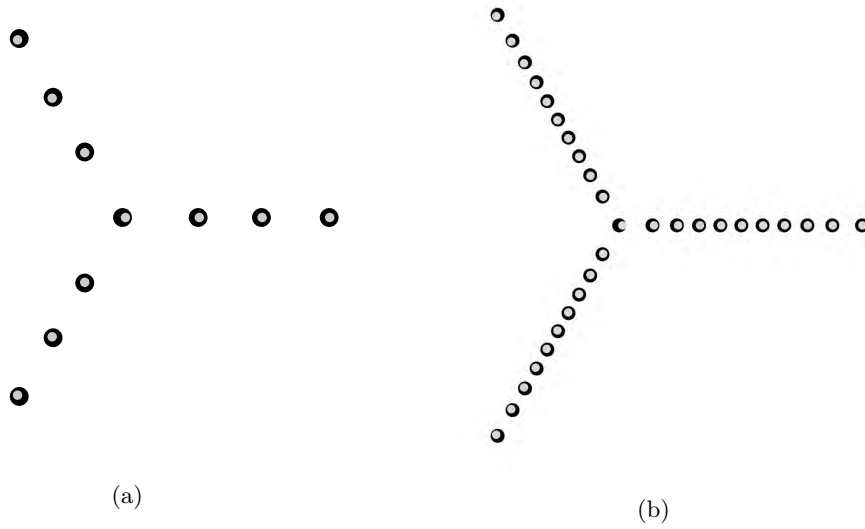


Figure 3.4: Two close solutions for (a) $N = 10$, $s = 3$, $p = 3$ and (b) $N = 31$, $s = 3$, $p = 10$. All the solutions are unstable.

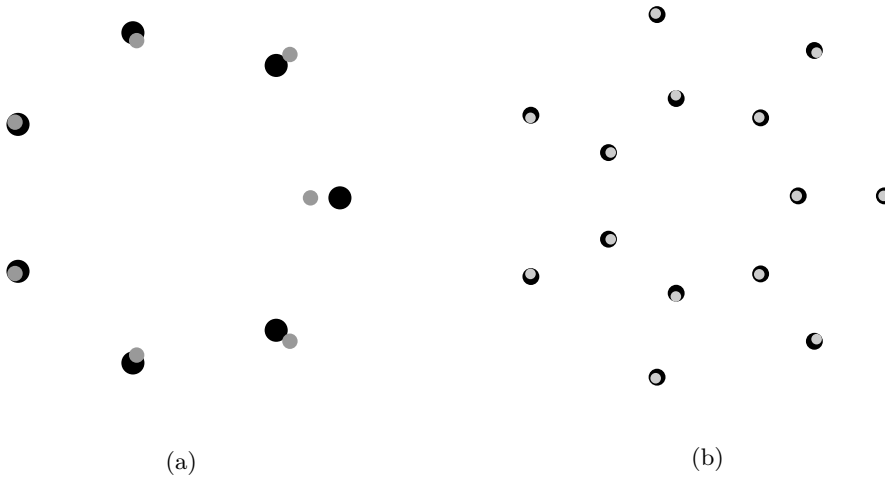


Figure 3.5: (a) Two close solutions for $N = 7$, $s = 7$, $p = 1$. The heptagon (the black solution) is marginally stable, while the gray solution is unstable. (b) Two close solutions for $N = 14$, $s = 7$, $p = 2$. Both solutions are unstable.

where a close solution near the centered triangle does exist [51].

The centered, symmetric, nested, equilateral triangles are not the only close solutions, that have been found. For $N = 7$ there is a solution quite close to the heptagon shown in Fig. 3.5(a). For two nestings $p = 2$ two close solutions again exist, cf. Fig. 3.5(b), and they are now more close than for $p = 1$. It seems to be a tendency that close pairs exist for an arbitrary number of rings here as well.

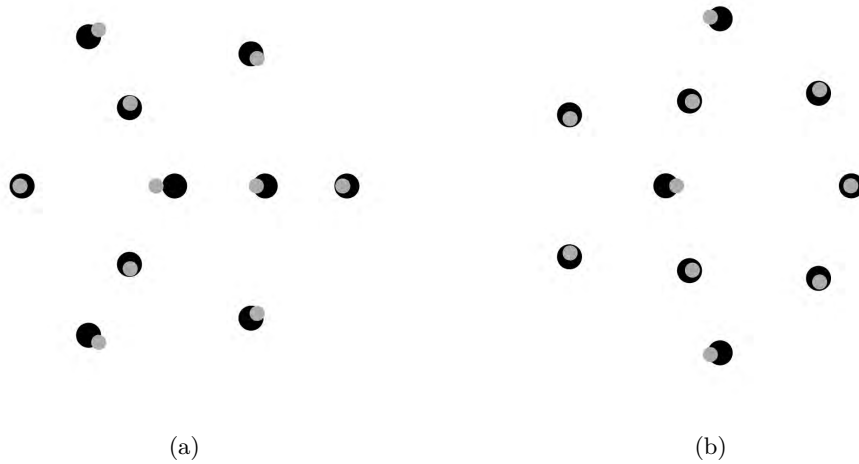


Figure 3.6: (a) Two close solutions for $N = 9$, $s = 3$, $p = 3$. Staggered configuration. Both solutions are unstable. (b) Two close solutions for $N = 10$. Both solutions are not known analytically and are unstable.

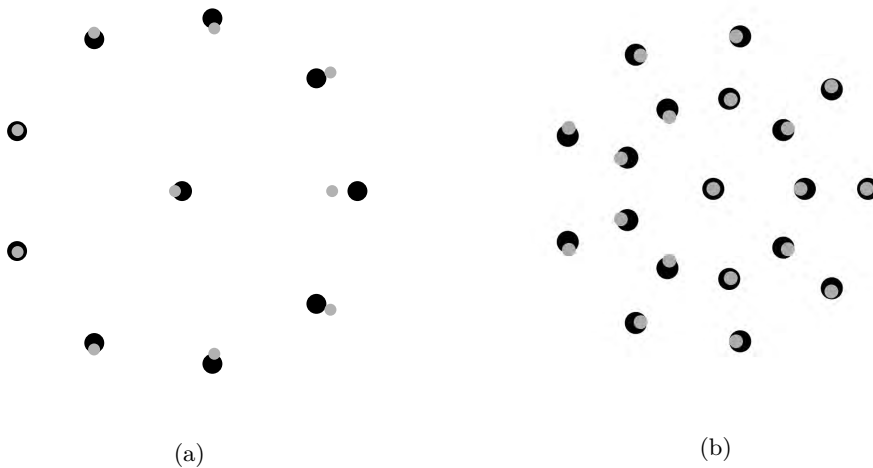


Figure 3.7: (a) Two close solutions for $N = 10$, $s = 9$, $p = 1$. The centered nonagon (in black) is marginally stable, while the grey solution is unstable. (b) Two close solutions for $N = 19$, $s = 9$, $p = 2$. Both solutions are unstable.

For $N = 10$ two other close pairs are shown in Figs. 3.6(a) and 3.6(b). Fig. 3.6(a) is interesting because this again is centered, nested, equilateral triangles, however one of the rings is now staggered or rotated. Neither of the solutions in Fig. 3.6(b) are known analytical.

Finally, there is a close solution around the centered nonagon, as shown in Fig. 3.7(a). For two rings two close solutions exist, as well, cf. Fig. 3.7(b), and, again, it seems that close pairs exist for an arbitrary number of rings.

The close pairs for $N > 10$ have been found by perturbing the analytical solutions

slightly randomly, and using this as initial conditions. The computations are done until two different solutions are found.

The above-mentioned examples are not an exhaustive list of close pairs, but the majority of the close pairs, that has been found. A few other non-analytical close pairs, as the one in Fig. 3.6(b), have been found and many other close pairs must exist for $N > 10$.

Assuming $z_\alpha^{(0)}$ and z_α are two different, but close, relative equilibria. By inserting Eq. (2.21) in $\delta z_\alpha = z_\alpha - z_\alpha^{(0)}$, this gives to linear order

$$\delta z_\alpha^* = \sum_{\beta=1}^N \frac{\delta z_\beta - \delta z_\alpha}{(z_\alpha^{(0)} - z_\beta^{(0)})^2} = \sum_{\beta=1}^N A_{\alpha\beta} \delta z_\beta, \quad (3.4)$$

where $A_{\alpha\beta}$ is the matrix arising in the stability analysis and given in Eq. (2.36). Written in vector notation Eq. (3.4) reads

$$\delta \mathbf{z}^* = \mathbf{A} \delta \mathbf{z}, \quad (3.5)$$

and using this equation twice we get

$$\delta \mathbf{z} = \mathbf{A}^* \mathbf{A} \delta \mathbf{z}. \quad (3.6)$$

This is an eigenvalue equation with the eigenvalue 1 and the eigenvector $\delta \mathbf{z}$. Thus, the matrix $\mathbf{B} = \mathbf{A}^* \mathbf{A}$ is expected to have the eigenvalue 1 if a nearby solution exist. Recalling that $\mathbf{z}^{(0)}$ is always a trivial eigenvector with the eigenvalue 1, we expect a close degeneracy of the eigenvalue 1 for $\mathbf{B} = \mathbf{A}^* \mathbf{A}$ when a close pair exists.

Unfortunately, this turns out not to be fulfilled for all the close pairs. However, the "core" configurations for the close pairs, i.e. the centered equilateral triangle, the heptagon, and the centered nonagon, do have a degeneracy of the eigenvalue 1. Looking for a degenerate eigenvalue on 1, can thus be used as a method of finding potential close pairs, and was actually the method used to find the close solution near the centered nonagon and the corresponding solution near the nested centered nonagons. Doing an analysis to second order might give a better result, however, this is left as future work.

The results in this section are published in [21] and more details can be found here.

Computation of vortex crystals by a continuation method

In this chapter a continuation procedure, that connects relative equilibria with N vortices with ones with $N + 1$ vortices, will be described. The idea is to compute co-rotating points, to be properly defined in next section, impose a circulation to one of these and, hereafter, gradually increase the circulation until it reach the value of the other vortices. All the intermediate steps solve the equations for relative equilibria. Note that this is not a dynamic continuation and neither the energy nor the impulse is conserved. The motivation for this is the possibility for finding new solutions for identical vortices, but also to investigate the intermediate solutions and phenomenon in the continuation process. Finally, the hope is to gain more insight in the two phenomenon, described in Sections 3.2 and 3.3, asymmetric solutions and close pairs of solutions.

First, the computation of co-rotating points will be described, and then the continuation process will be described. The results are given and discussed in Chapter 5.

4.1 Computation of co-rotating points

In the flow certain points rotates together with the relative equilibria of vortices. These points are either called *points of relative rest* [45], to distinguish them from stagnation points in absolute rest or *co-rotating points*, which we will use, to denote that the points rotate together with the vortex crystal.

A co-rotating point z is found by

$$z^* = \sum_{\alpha=1}^N \frac{1}{z - z_{\alpha}}. \quad (4.1)$$

This a slightly modified version of the equation for relative equilibria (2.21), where the prime in the sum is omitted, since the co-rotating points are affected by the velocity induced by all the vortices. The equation is known as *Morton's equation*.

The equation can be written using the generating polynomial, which is given by [10]

$$P(z) = \prod_{\alpha=1}^N (z - z_{\alpha}) = (z - z_1) \dots (z - z_N). \quad (4.2)$$

Differentiating this gives

$$P'(z) = P(z) \sum_{\alpha=1}^N \frac{1}{z - z_{\alpha}}. \quad (4.3)$$

Morton's equation Eq. (4.1) can, thus, be written as

$$P'(z) = z^* P(z). \quad (4.4)$$

The number of co-rotating point is, so far, unknown. However, Khavinson & Neumann [31] have shown a best upper bound on $5N - 5$ for an equation on the form $z^* = p(z)/q(z)$ and is, thus, also valid for Morton's equation.

4.1.1 Analytical solutions

In this section some of the co-rotating points will be calculated analytically to verify our numerical computations. The co-rotating points will be computed for $N = 2$, and the number of co-rotating points will be computed for polygons and centered polygons.

4.1.1.1 $N = 2$

For $N = 2$ the solution to Eq. (2.21) is $z_1 = -z_2 = \frac{1}{\sqrt{2}}$. Eq. (4.1) now becomes

$$z^* = \frac{1}{z - \frac{1}{\sqrt{2}}} + \frac{1}{z + \frac{1}{\sqrt{2}}} = \frac{2z}{z^2 - \frac{1}{2}}, \quad (4.5)$$

or

$$|z|^2 = \frac{2z^2}{z^2 - \frac{1}{2}} = \frac{2(z^2 - \frac{1}{2}) + 1}{z^2 - \frac{1}{2}} = 2 + \frac{1}{z^2 - \frac{1}{2}}. \quad (4.6)$$

This shows that z^2 must be real, i.e. z is either real or pure imaginary. For a real co-rotating point $z = x$, we have

$$x^2 - 2 = \frac{1}{x^2 - \frac{1}{2}}, \quad \Rightarrow (x^2 - 2)(x^2 - \frac{1}{2}) = 1. \quad (4.7)$$

This equation has the roots $x = 0, x = \pm\sqrt{\frac{5}{2}}$. For an imaginary co-rotating point $z = iy$, the equation reads

$$y^2 - 2 = -\frac{1}{y^2 + \frac{1}{2}}, \quad \Rightarrow (y^2 - 2)(y^2 + \frac{1}{2}) = -1, \quad (4.8)$$

with the three solutions $y = 0, y = \pm\sqrt{\frac{3}{2}}$. Thus, in total we have five co-rotating points

$$0, \pm\sqrt{\frac{5}{2}}, \pm i\sqrt{\frac{3}{2}}. \quad (4.9)$$

4.1.1.2 Polygons

For a regular N -gon of radius R the vortex positions are $P(z) = z^N - R^N$ with $R^2 = \frac{1}{2}(N-1)$. Thus, Eq. (4.4) becomes

$$z^*(z^N - R^N) = Nz^{N-1}. \quad (4.10)$$

Introducing $\zeta = z/R$ and $R^2 = \frac{1}{2}(N-1)$ gives

$$\left(\frac{1}{2}|\zeta|^2(N-1) - N\right)\zeta^N = \frac{1}{2}|\zeta|^2(N-1). \quad (4.11)$$

This shows that ζ^N must be real, and we can, thus, write $\zeta = \rho e^{i\varphi}$, where $\rho > 0$ and $\varphi = 2\pi n/N$ or $\varphi = (2n+1)\pi/N$, $n = 0, 1, \dots, N-1$. In the former case $\zeta^N = \rho^N$, in the latter $\zeta^N = -\rho^N$. Now, Eq. (4.11) gives

$$(N-1)\rho^{N+2} - 2N\rho^N \mp (N-1)\rho^2 = 0 \quad (4.12)$$

or

$$\rho^N - \frac{2N}{N-1}\rho^{N-2} = \pm 1, \quad (4.13)$$

if the zero solution $\rho = 0$ is neglected for a while. The polynomial on the left hand side P_{LH} , vanishes at $\rho = 0$ (for $N \geq 3$), is negative for small ρ , and positive for large ρ . It has a minimum at

$$\rho_m = \sqrt{2\frac{N-2}{N-1}}, \quad (4.14)$$

with the value

$$P_{LH}(\rho_m) = -\frac{4}{N-1}\rho_m^{N-2} = -2^{N/2+1}\frac{(N-2)^{N/2-1}}{(N-1)^{N/2}}. \quad (4.15)$$

For $N = 3$ this is -2 and it decreases dramatically with N . The polynomial has a unique, positive zero at

$$\rho_0 = \sqrt{2\frac{N}{N-1}}. \quad (4.16)$$

This analysis shows that Eq. (4.13) has one solutions with $+1$ on the right hand side and two solutions with -1 , cf. Fig. 4.1. Including the zero solution we obtain a total of $3N+1$ co-rotating points.

4.1.1.3 Centered polygons

For a centered, regular $(N-1)$ -gon, $N \geq 3$ the vortex positions are $P(z) = z(z^{N-1} - R^{N-1})$ with $R^2 = \frac{1}{2}N$. Now, Eq. (4.4) becomes

$$|z|^2(z^{N-1} - R^{N-1}) = Nz^{N-1} - R^{N-1}, \quad (4.17)$$

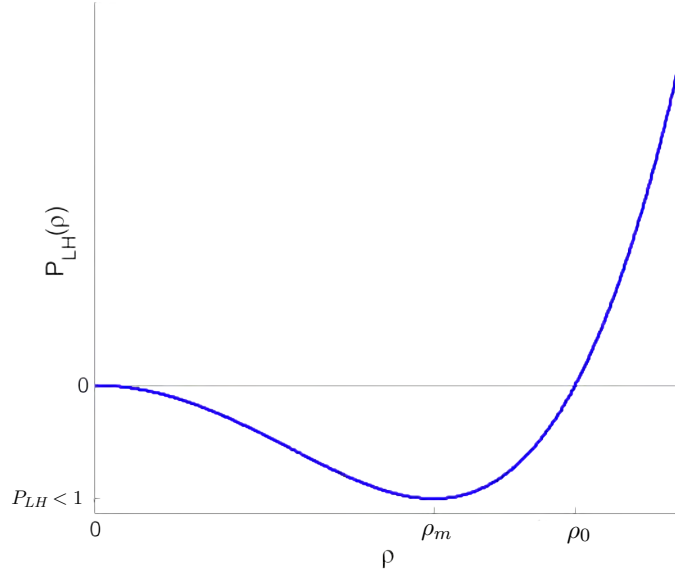


Figure 4.1: The polynomial on the left hand side of Eq. (4.13), showing that the equation has one solution with +1 on the right hand side and two solutions with -1.

and by inserting $\zeta = z/R$ again we get

$$N\left(\frac{1}{2}|\zeta|^2 - 1\right)\zeta^{N-1} = \frac{1}{2}N|\zeta|^2 - 1. \quad (4.18)$$

It follows from this equation that ζ^{N-1} is real. If we write $\zeta = \rho e^{i\varphi}$, $\rho > 0$, we have that $\varphi = 2\pi n/(N-1)$ or $\varphi = (2n+1)\pi/(N-1)$, $n = 0, 1, \dots, N-2$, and $\zeta^{N-1} = \pm\rho^{N-1}$, respectively, in the two cases. Thus, Eq. (4.18) produces two equations for ρ

$$(\rho^2 - 2)(\rho^{N-1} \mp 1) = \pm 2\frac{N-1}{N}, \quad (4.19)$$

We will focus on $N \geq 4$, because $N = 3$ is the collinear configuration of three vortices. Choosing the upper sign, the polynomial on the left hand side starts at $(0, 2)$ and has zeros at $\rho = 1$ and $\rho = \sqrt{2}$. It is positive for $0 \leq \rho < 1$ and for $\rho > \sqrt{2}$. Since the right hand side is always less than 2, we see that there are two solutions for ρ in this case, corresponding to $2(N-1)$ co-rotating points.

Choosing the lower sign, one finds that there is just one solution for $N = 4, 5, 6$ but three solutions for $N \geq 7$.

The total number of co-rotating points, then, is $3(N-1)$ for $N = 4, 5, 6$, but $5(N-1)$, the maximum allowed by Khavinson & Neumann's bound, for $N \geq 7$.

4.1.2 Numerical computations

Eq. (4.1) is implemented and solved numerically using MATLAB. As the number of co-rotating points is unknown the computations are run with random starting points until no more solutions are found. Of course, we cannot, without knowing the number of solutions, be certain that all the co-rotating points are found.

The number of co-rotating points is unknown, but we can get some insight by using Poincaré's Index Theorem [54, Theorem 8, p. 307], [46, Theorem 4.6.1]. In this context it says that the number of center point minus the number of saddle points must equal the

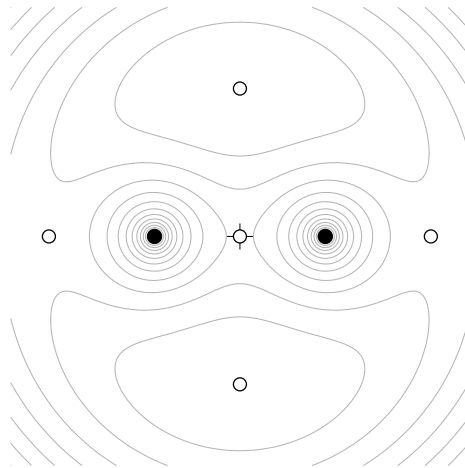


Figure 4.2: The vortex crystal for $N = 2$ shown by black dots together with the corresponding co-rotating points shown by open circles. The streamlines in the rotating frame, given in Eq. (2.17) are, furthermore, shown.

Euler-Poincaré characteristic, which for the plane is one. Whether a critical point, which is either a vortex or a co-rotating point, is a center or a saddle can be determined by looking at the streamlines [12, 56, p. 174ff]. If the streamlines close around a critical point it is a center point, otherwise it must be a saddle point. Remember that streamlines are simply level curves of the streamfunction surface. If the theorem is fulfilled it means that it is not possible to overlook just a single co-rotating point, but a saddle point must always be followed by a center point and vice versa. This gives us, furthermore, a lower bound on $N - 1$ for the number of co-rotating points, because the vortices always will be centers.

Once a solution is obtained, convergence is verified explicitly by

$$\left| z^* - \sum_{\alpha=1}^N \frac{1}{z - z_{\alpha}} \right| < \varepsilon, \quad (4.20)$$

where ε typically is set to 10^{-12} . The results, including figures with streamlines and coordinates for the co-rotating points, are given in Appendix B. Poincaré Index Theorem is used to verify that the right number of co-rotating points is found. The analytical results from Section 4.1.1 are seen to be fulfilled. The co-rotating points for $N = 2$ are shown in Fig. 4.2 by open circle. The streamlines in the rotating frame, given in Eq. (2.17) are, furthermore shown.

4.2 Continuation of relative equilibria using co-rotating points

When the co-rotating points are found, they will be used to "grow" new relative equilibria of identical point vortices. The idea is to apply a small circulation γ to one of the co-rotating

point, where $0 \leq \gamma \leq 1$. The new configuration must fulfil

$$\begin{cases} z_\alpha^* = \sum_{\beta=1}^N \frac{1}{z_\alpha - z_\beta} + \frac{\gamma}{z_\alpha - z}, & \alpha = 1, \dots, N \\ z^* = \sum_{\alpha=1}^N \frac{1}{z - z_\alpha}, \end{cases} \quad (4.21)$$

to be in relative equilibrium. z_1, \dots, z_N and z depend all on γ .

The circulation is now increased in small steps until we reach $\gamma = 1$. The intermediate configurations are all relative equilibrium and fulfil, thus, Eq. (4.21). For small γ the equations approach the relative equilibrium for N vortices and the co-rotating point, whereas they approach the relative equilibrium for $N + 1$ for large γ . This procedure is described in [13] and used to find the first asymmetric equilibrium.

In the first computation the coordinates for the vortex crystal and one of the co-rotating points are used as starting guess, whereas the solution the step before is used as starting guess hereafter. In this way relative equilibria of $N + 1$ vortices are produced from relative equilibria with N vortices, by increasing the circulation of the co-rotating point to unity. One can also come from a relative equilibrium with $N + 1$ identical vortices to one with N vortices by decreasing the circulation of one of the vortices gradually from 1 to 0. The solution paths, when this is done, turn out not necessarily to be reversible.

For each γ convergence of Eq. (4.21) is, as always, verified explicitly

$$\frac{1}{N} \left(\sum_{\alpha=1}^N \left| \sum_{\beta=1}^N \frac{1}{z_\alpha - z_\beta} + \frac{\gamma}{z_\alpha - z} - z_\alpha^* \right| + \left| \sum_{\alpha=1}^N \frac{1}{z - z_\alpha} - z^* \right| \right) < \varepsilon, \quad (4.22)$$

where ε is set to 10^{-12} . 1000 steps in γ are used in all of the computations.

One must be aware that this is not a dynamical continuation and neither the energy or the impulse are conserved in the process.

4.3 Convergence problems

Occasionally the continuations do not converge for the given value of ε . In other words, for a specific value of the continuation parameter γ the solver cannot find any solution close to the initial condition any more. Sometimes it helps to increase ε , which is then done along the way when necessary down to $\varepsilon = 10^{-8}$. This is still a fairly good precision and the final configurations with identical vortices always converge to $\varepsilon = 10^{-12}$. However, some continuations do not converge even for $\varepsilon = 10^{-2}$ and these are of cause omitted from the catalogue in Appendix C.

This is an obvious problem in terms of finding all equilibria, cf. Section 4.4, because possible new solutions and other interesting phenomena such as bifurcations, might be missed.

It is still not totally clear why some continuations do not converge. It could simple be because a continuation does not exist. Thus, at some point of the continuation parameter no solution exists close to the former solution. This could to be the case, at least for some of the cases, but this is of cause difficult to prove.

4.4 All relative equilibria by induction

The idea behind this continuation is that by knowing all relative equilibria for N vortices, which is the case for $N = 2$, by the continuation method, relative equilibria for $N + 1$ vortices can be found. Thus, all relative equilibria may be found in this way by induction. However, certain issues complicate the procedure.

First, the number of co-rotating points are not known, although there is an upper and a lower bound. The points can, however, be identified as critical points in the streamlines. This has only been done by the naked eye, but it would be possible to apply some algorithm to find critical points of the streamfunction, which would solve this problem.

Secondly, there is a possibility that there could be bifurcations on the way, such that one equilibrium together with one co-rotating point could grow into two different solutions. Thus, a method identifying these bifurcations is needed. This is studied and described in Section 5.4.

Finally, it has not been proved that solutions exist all the way down if one vortex is shrunk. Thus, for a specific value of the continuation parameter, new solutions might exist that do not exist for a slightly smaller value of the continuation parameter, which means that such a solution would not show up by our continuation method. This has, however, not been observed, and based on the computations, I believe this is not an option.

These issues might, nevertheless be solved, and the method turns out to be very efficient.

Results of the continuations

In this chapter the results from the continuation computations, described in Section 4.2, are described. The results are given as figures in Appendix C. Both the cases where the circulation is increased to unity, and the reversible cases, where the circulation is reduces to zero, are shown.

Most of the results are predictable, but some of the results surprise. Some of the initial investigations will be described first, whereafter one of the main result of this work will be described in Section 5.4

All prior known solutions have been recreated with this method, and no new solutions for identical vortices, have been found. Nevertheless, some interesting and until now unknown phenomena have been observed, which will be described in Section 5.4.

5.1 Examples of continuations

Before we turn into the more interesting discoveries some of the simple or more trivial continuations will be described. Starting with the ones from $N = 2$ to $N = 3$, we note from Section 4.1.1.1 and Fig. 4.2 that the vortex crystal has five co-rotating points, however, two pairs gives identical configurations by rotation or mirroring, which leave us with 3 configurations, that are shown in Fig. 5.1. The black dots denotes the initial vortices, the open circle the co-rotating point, and the red dots the final vortices. The lines are the solution paths arising from increasing the circulation γ of the co-rotating point. Thus, the final configurations for $N = 4$ are, as expected, the three vortices on a line or the equilateral triangle.

The reversible continuations from $N = 3$ to $N = 2$, where the circulation of one of the vortices is decreased, are shown in Fig. 5.2. It can be noticed that these continuation processes are completely reversible, and the solution paths are, thus, equal to the ones in Fig. 5.1. This is, however, not always the case.

The continuation from the equilateral triangle to the centered equilateral triangle and the reversible continuation are shown in Fig. 5.3. Notice that the continuations are not reversible, and that the final co-rotating point going from $N = 4$ to $N = 3$ is different from the initial co-rotating point going from $N = 3$ to $N = 4$. This is predictable or at least understandably, but still worth to notice. The initial and final vortex crystal for $N = 3$ is still the same. This is, however, not always the case, and turns out to be an important

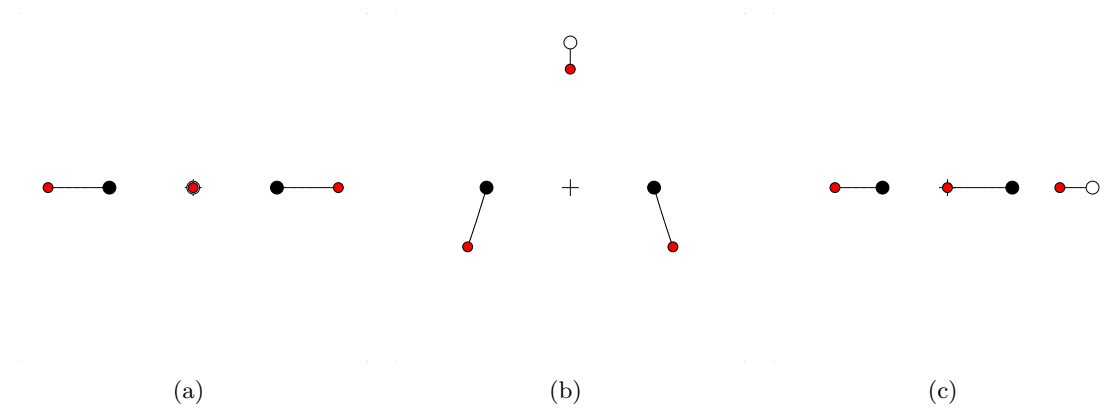


Figure 5.1: The three different continuations starting with two vortices. The black dots denotes the initial vortices, the open circle the co-rotating point, and the red dots the final vortices. The lines are the solution paths arising from increasing the circulation γ of the co-rotating point.

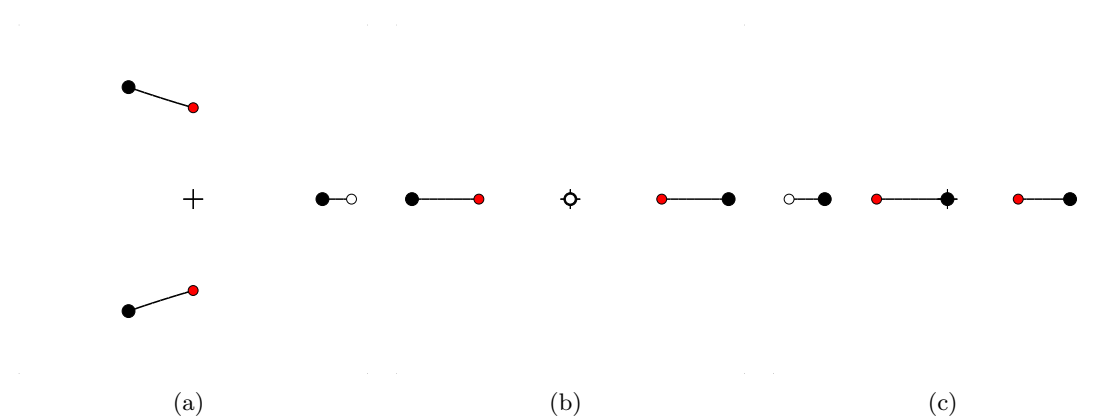


Figure 5.2: The three different continuations from $N = 3$ to $N = 2$. The black dots denotes, as always, the initial vortex position, the open circle the co-rotating point, and the red dots the final vortex positions.

characteristic, cf. Section 5.4.

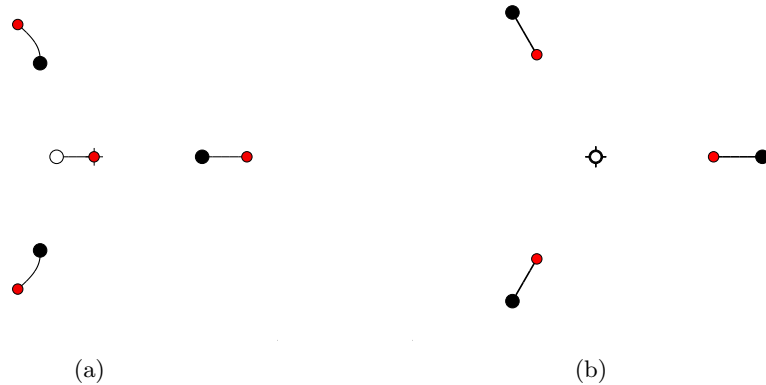


Figure 5.3: (a) A continuation from the equilateral triangle $N = 3$ to the centered equilateral triangle $N = 4$ and (b) the reversible case from $N = 4$ to $N = 3$.

5.2 Cusps in the solution paths

Initially, some of the figures showed some unexpected cusps in the solution paths. In total over 20 figures had these cusps going from N to $N + 1$ and from $N + 1$ to N . Two examples are shown in Figs. 5.4 and 5.7. This could indicate a bifurcation, which, however, turns out not to be the case.

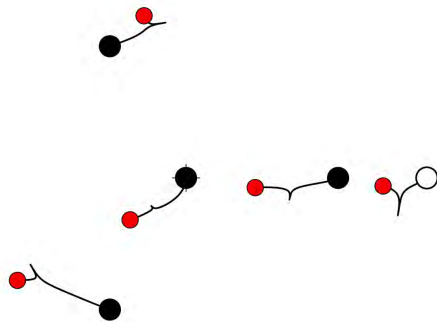


Figure 5.4: Continuation of equilibrium with $N = 4$ to $N = 5$, where the solution paths have some cusps on the way.

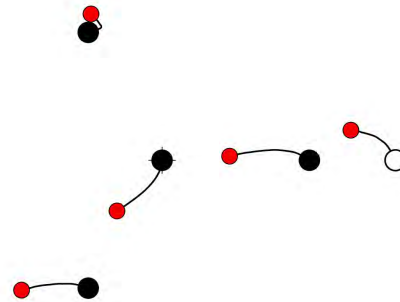


Figure 5.5: Continuation of equilibrium with $N = 4$ to $N = 5$, where the cusps in the solution paths have been removed by rotation.

The stability, in terms of the highest eigenvalue, given in Section 2.4 and Eq. (2.56), as γ is increased, is shown in Fig. 5.6 for the configuration in Fig. 5.4. There are no cusps, discontinuities, or non-differentiabilities in the stability, and nothing particular is happening at the place the cusps in the solution paths occur.

On the contrary, the cusps turned out to have a much more trivial explanation. By

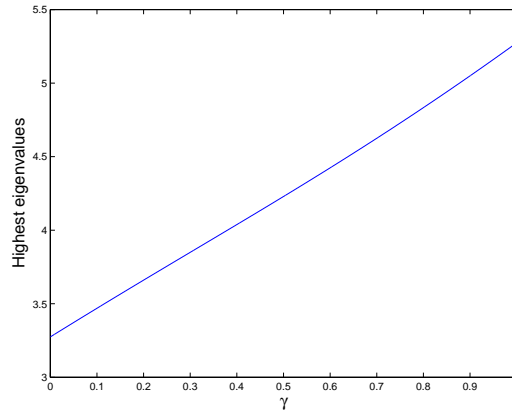


Figure 5.6: The stability in terms of the highest eigenvalue for the continuation shown in Fig. 5.4.

rotating the intermediate solutions in a specific manner, it is possible to eliminate the cusps and the solution paths become smooth, as shown in Figs. 5.5 and 5.8. The rotation is done by rotating each solution in the continuation such that the distance to the former solution becomes as small as possible. These rotations are done in the computations shown in Appendix C, whenever it is necessary. It is not clear why the numerical solver does not choose the rotation of the solution that is closest to the initial conditions (i.e. the former solution). This shows that we need to rotate the continuations in this manner, especially if something strange, like the cusps, happens.

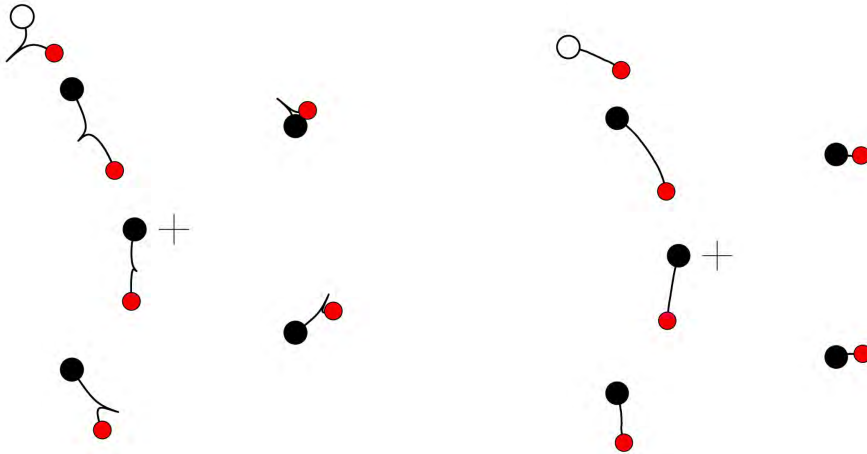


Figure 5.7: Continuation of equilibrium with $N = 5$ to $N = 6$, where the solution paths have some cusps on the way.

Figure 5.8: Continuation of equilibrium with $N = 5$ to $N = 6$, where the cusps in the solution paths have been removed by rotation.

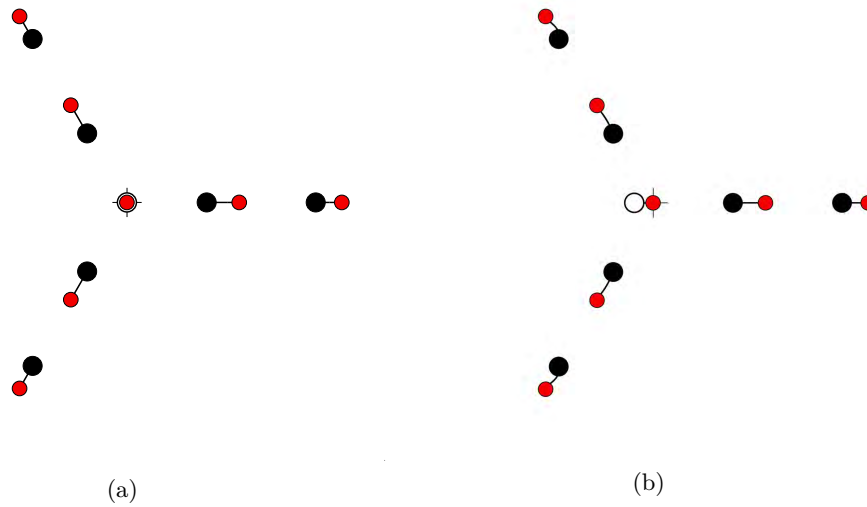


Figure 5.9: Two continuations leading to the analytically centered nested symmetric equilateral triangles.

5.3 Close pairs of solutions

As said, all known relative equilibria for $N = 3, \dots, 8$ have been recreated by the continuation method. Thus, this also applies to the close pairs of solutions. The continuations leading to the analytically known centered nested equilateral triangles are shown in Fig. 5.9. The continuations leading to the close numerical solution are shown in Fig. 5.10 and it is actually possible to see that the vortex in the middle is a bit displaced from the center of rotation. The case with a co-rotating point at the origin will be treated in Section 5.4. It is possible to recreate the other close pairs, as well. Thus, a more systematic way of finding the close pairs have been developed.

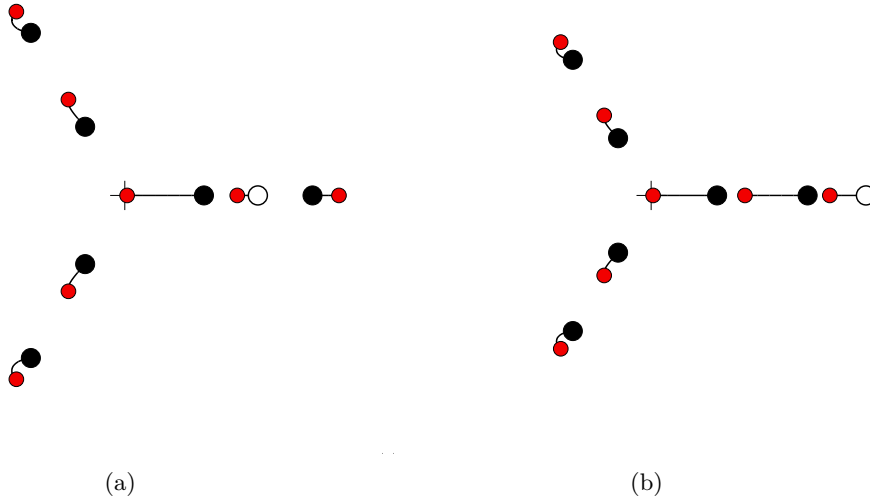


Figure 5.10: Two continuations leading to the close numerically found solutions.

5.4 Bifurcations in the solution paths

In the continuations non-differentiabilities in the solution paths sometimes occur. One example is shown in Fig. 5.11 where distinct kinks in the solution paths are seen. The kinks occur all for the same value of γ .

The stability, in terms of the highest eigenvalue, is shown in Fig. 5.12. A clear non-differentiability is seen exactly at the same point where the kinks in the solution paths occur. This suggests that another branch in the stability exists that is smooth and, thus, a bifurcation might occur at this location.

The solution paths for the remaining co-rotating points can be computed, as well, and kinks in these solution paths are of course expected. This also turns out to be the case, as illustrated in Fig. 5.13. Note that this is not all the co-rotating points, as some points will arise along the way; here one at the center of rotation.

Different approaches have been used to investigate the kinks shown in Fig. 5.11. First, instead of varying the circulation of only one vortex, several other approaches can be used where the circulation of several vortices is varied. This could show a possible bifurcation, because the system is perturbed in this way and might then be likely to choose another path if it exists. Thus, the following has been done. First, the circulation of the co-rotating point has been increased until we are just before the kink. Then the circulation of one of the vortices is decreased, whereupon the circulation of the first vortex, and finally the last vortex, is increased to unity. Many different computations of this kind, with several different values of the continuation parameters, have been made. However, none of these computations suggest any bifurcations.

Secondly, the continuation parameter has been varied back and forth from $\gamma = 0 \rightarrow 1 \rightarrow 0 \rightarrow 1$ or back and forth just slightly around the kinks, to see whether the direction matter. This is basically just a comparison of the continuations from N to $N + 1$ with the ones from $N + 1$ to N , shown, for this example, in Figs. C.48 and C.72. From this, is it

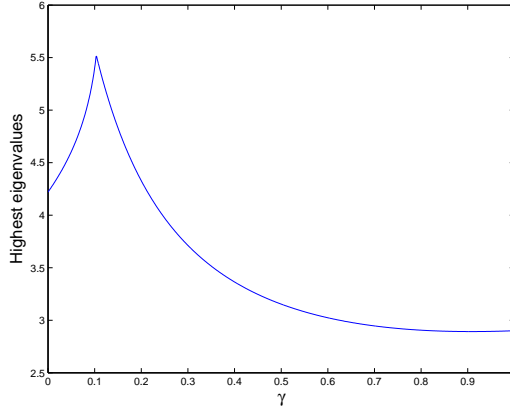
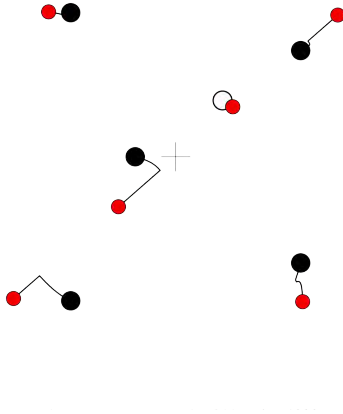


Figure 5.11: Continuation of equilibrium with $N = 5$ to $N = 6$, where the solution paths have some cusps on the way. The black dots are initial positions, red dots final positions, lines the solution paths from increasing γ gradually, and the white dot is a co-rotating point.

Figure 5.12: The stability for the configuration in Fig. 5.11 given by the highest eigenvalue with respect to the vortex strength γ .

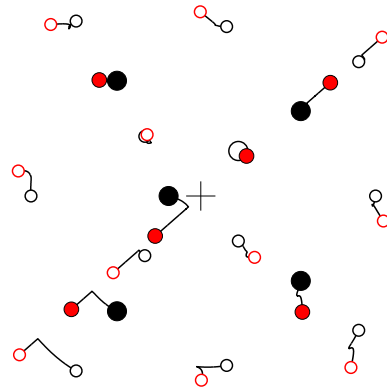


Figure 5.13: Continuation of equilibrium from $N = 5$ to $N = 6$, where the solution paths for the remaining co-rotating points are computed as well, and shown with white dots with a black (red) edge for the initial (final) positions. The final configuration does not show all co-rotating points, as the number increases along the way.

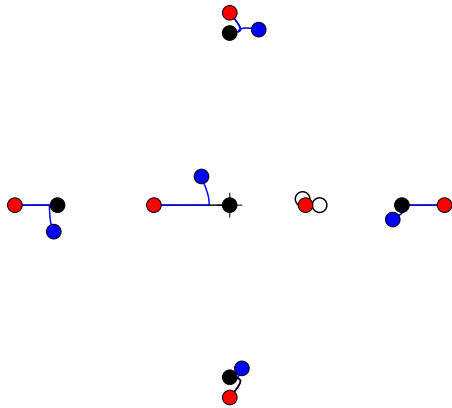


Figure 5.14: Bifurcations in the continuation. Starting with two different solutions in black and blue, one ends up with the same solution in red and the two solution paths coincide along the way.

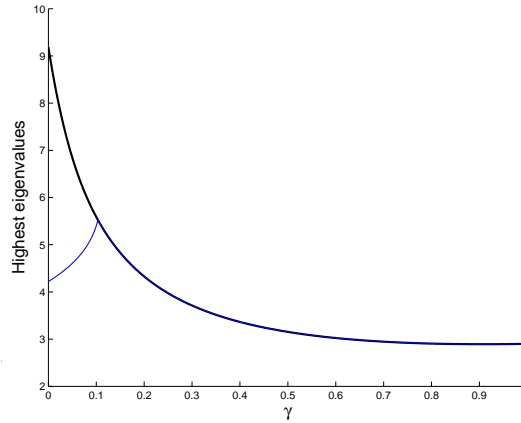


Figure 5.15: The stability for the continuation shown in Fig. 5.14. The colours correspond to the colours in Fig. 5.14.

actually possible to identify bifurcations, because this continuation process is not reversible. The bifurcation is shown in Fig. 5.14. Starting out with two different solutions the two continuations follow their individual solution paths until a certain point (around $\gamma = 0.11$), whereafter they coincide. This is, thus, a bifurcation going from $N = 6$ to $N = 5$. This explains the discontinuity in the stability in Fig. 5.12. In Fig. 5.15 the eigenvalues for both solutions are shown and now a smooth path starting with the centered square appears. Notice that the symmetry is broken after the bifurcation point for the blue solution. However, it is recovered in the end. One could also call the occurrence a trifurcation, because the blue solution path could be mirrored, leading to a third possible path. However, the stability would still only have two branches, and, therefore, we refrain from calling it a trifurcation.

Bifurcations going from N to $N + 1$ also exist. In Fig. 5.16 one from $N = 5$ to $N = 6$ is shown. This can be seen just by comparing the two continuations from $N = 6$ to $N = 5$ shown in Figs. C.66 and C.71. The stability is shown in Fig. 5.17(a) and a discontinuity is also seen here. Again, the symmetry is broken after the bifurcation point, but recovered at the end. It is here important to plot the two highest eigenvalues, because two of them cross each other. Thus, if only the highest eigenvalue was shown it would seem that there was another non-differentiability, which, however, is just a crossing. The energies for the two different continuations are very close, cf. Fig. 5.17(b). It seems that nothing particular happens at the bifurcation point, but there could, of course, be a non-noticeable non-differentiability. It turns out that no non-differentiability in the energies is observed for all bifurcations.

The hypothesis is now that the close solutions, described in Section 3.3, originate in a bifurcation. This actually turns out to be the case. This is shown in Fig. 5.18, where

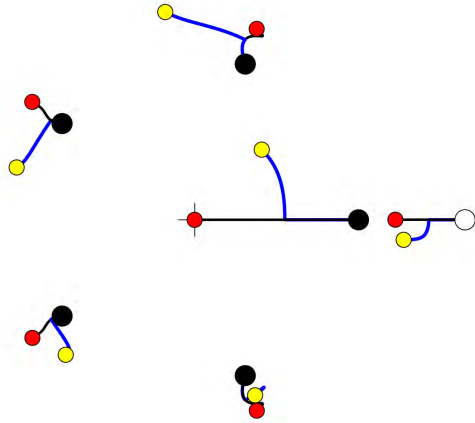
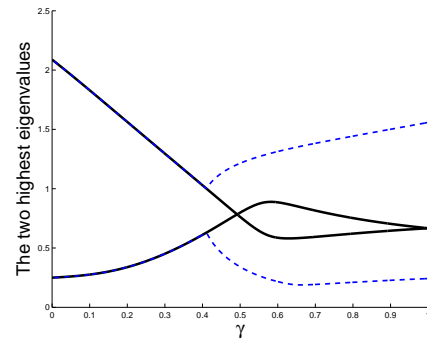
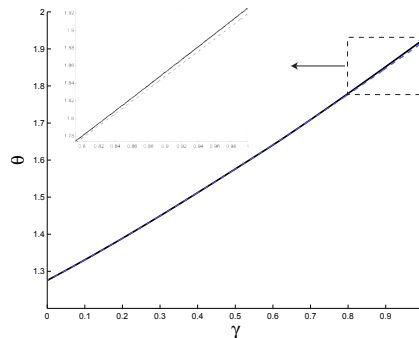


Figure 5.16: Bifurcations in the continuation. Starting with the same solution in black, the two solution paths follow each other until a certain point, where they split and go to different configurations, shown in red and yellow.



(a)



(b)

Figure 5.17: (a) The stability and (b) the energy for the continuation shown in Fig. 5.16. The colours correspond to the colours in Fig. 5.16. (a) The discontinuity on the blue lines occur at the bifurcation point.

the two continuations are placed on top of each other. The stability is shown in Fig. 5.19. It is difficult to judge whether there is any discontinuities in the derivative here, even by zooming in and dissolving further. The second highest eigenvalue seems to have a non-differentiability, whereas it is too difficult to see whether that is the case for the highest eigenvalue. The symmetry is not broken totally after the bifurcation, but the symmetry decreases, going from 3 to 1 symmetry axis. Looking at the errors of the computations in Fig. 5.20, given by Eq. (4.22), a small spike at exactly the same position as the bifurcation occur. Bifurcations exist for the configurations with more rings, as well. The other co-rotating points than the one at the center of rotation cannot be used to get a bifurcation.

Bifurcations can be found for the other close pairs, as well. First, the close pair around the heptagon is shown in Fig. 5.21. Both solutions can be made from the hexagon and the same co-rotating point. Again, a discontinuity in the stability, cf. Fig. 5.22, appears, and the symmetry is broken, but recovered in the end. Another example of close pairs is shown in Figs. 5.23 and 5.24. Here, the symmetry is broken and not recovered.

A bifurcation for the centered nested staggered equilateral triangles also exist and is shown in Figs. 5.25 and 5.26. Again, the discontinuity in the stability correspond to a

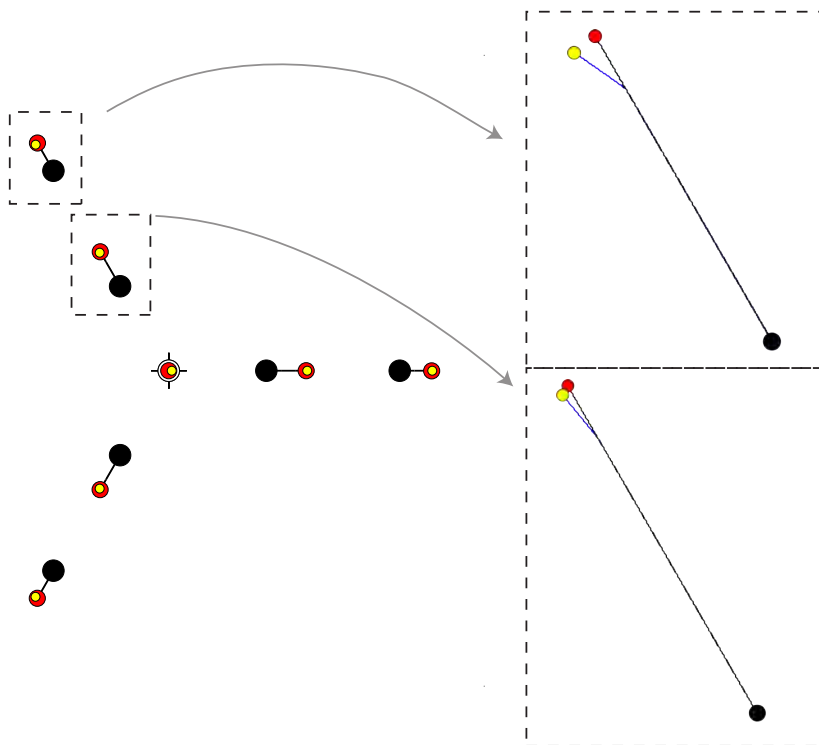


Figure 5.18: A bifurcation occur for the close pairs of solutions for the centered nested equilateral triangles. The dotted squares are shown zoomed in.

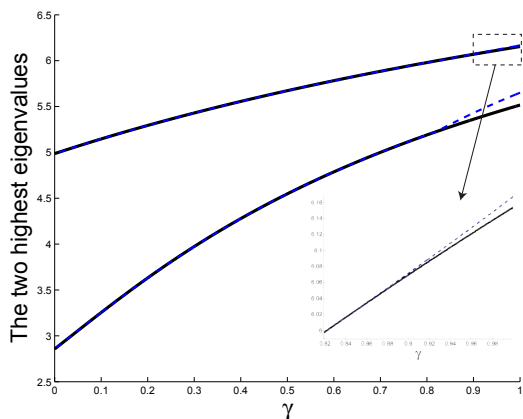
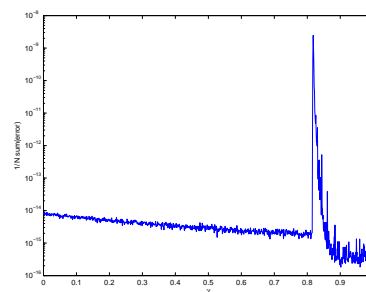
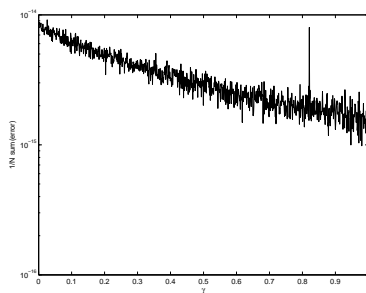


Figure 5.19: The stability for the configuration in Fig. 5.18.



(a)



(b)

Figure 5.20: The error given by Eq. (4.22) for the blue and black line in Fig. 5.18.

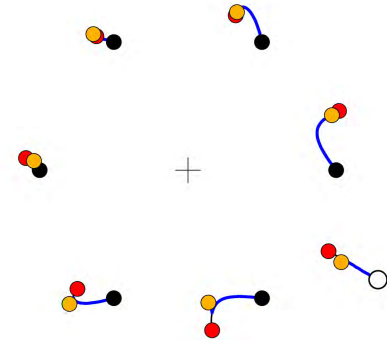


Figure 5.21: Bifurcations in the continuation from the hexagon $N = 6$ to $N = 7$.

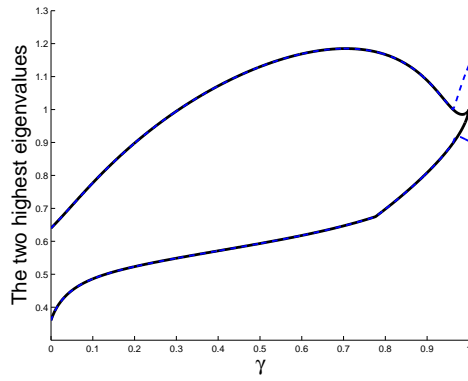


Figure 5.22: The stability for the continuation shown in Fig. 5.21.

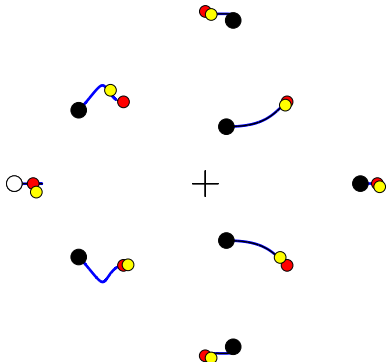


Figure 5.23: Bifurcations in the continuation from $N = 7 \rightarrow 8$.

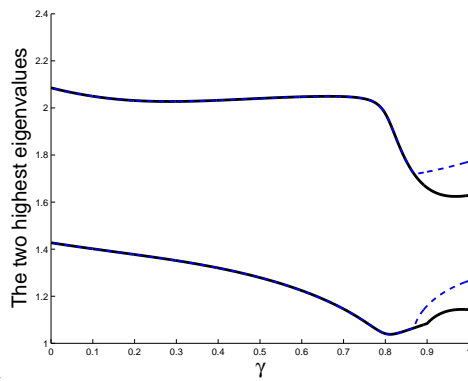


Figure 5.24: The stability for the continuation shown in Fig. 5.23.

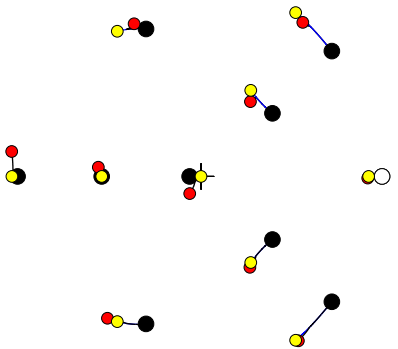


Figure 5.25: Bifurcations in the continuation from $N = 9$ to $N = 10$, where the yellow solutions is the centered staggered nested equilateral triangles.

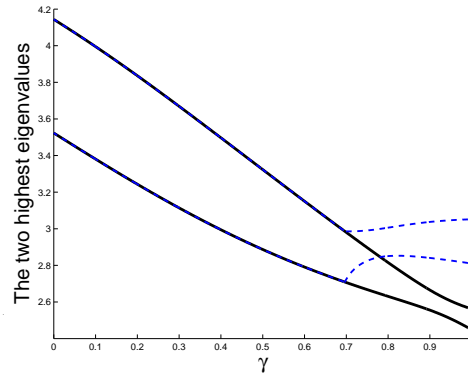


Figure 5.26: The stability for the continuation shown in Fig. 5.25.

bifurcation and a symmetry break.

A bifurcation will obviously generate close solutions close to the bifurcation point. Based on the observed bifurcations, it can be believed that all close pairs of identical vortices originate in a bifurcation, where the bifurcation point is sufficiently close to unity.

Finally, the first asymmetric solution for $N = 8$ is examined, to see whether there is any bifurcations for this configuration, as well. In Figs. 5.27 and 5.28 two different configurations for $N = 7$, both leading to the asymmetric solution for $N = 8$, are shown. Thus, the asymmetric solution is connected to a bifurcation. However, we see that both of the continuations have a discontinuity both in the solution path and in the stability, which is unexpected.

Some of the bifurcations above are found by randomly perturbing the initial conditions (between 0.5% and 5%) all the way through the continuation. If this procedure is repeated the two different solutions, and thus the bifurcations, are found. This procedure has been used for all continuations for $N = 4, \dots, 7$ running each computation 10 times. Assuming a fifty-fifty percent chance of finding each solution path, this would give a $1 - \left(\frac{1}{2}\right)^9 = 99.8\%$ probability of observing a bifurcation, if the computations are run 10 times, and it exists. This is of course a very simplified model, and a fifty-fifty percent probability is a pure guess, but it gives us some ideas about the probability of finding a bifurcation with this method.

The existence of bifurcations complicates the idea that all relative equilibria can be found by continuation, cf. Section 4.4. Even though I believe the used method to identify bifurcations is very efficient, an analytical approach is needed. Normally bifurcations can occur only when the governing system of equations becomes singular, in the sense of the Implicit function theorem [52]. Implementation of this would be important, to make sure that all bifurcations are found.

All these bifurcations have, as far as known, not been observed before and is, thus, very interesting.

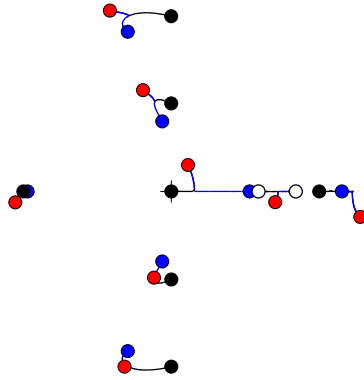


Figure 5.27: Two configurations for $N = 7$ shown in black and blue both leading to an asymmetric solution for $N = 8$ shown in red.

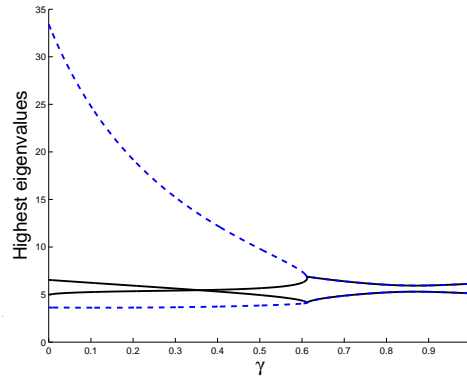


Figure 5.28: The stability for the continuation shown in Fig. 5.27.

It seems that bifurcations are always followed by a non-differentiability in the stability and vice versa. After a bifurcation the symmetry of the configuration always decreases, and, normally, the configuration becomes asymmetric. Thus, we can draw a connection between the symmetry and the smoothness of the stability. This is similar to the results in [42], where a similar continuation is done for vortex patches. Here, bifurcations are also observed and are associated with a non-differentiability in the impulse, cf. [41].

If we take a look at the specific co-rotating points causing bifurcations, both center and saddle points are revealed. Thus, no difference, whether a center or a saddle point is used in the continuation, have been found.

Finally, let's summarise the different methods to identify bifurcations.

- Bifurcations may be identified by comparing different continuations that lead to the same configuration.
- Kinks or non-differentiability in the solution paths indicate a bifurcation.
- Non-differentiability in the stability also indicate a bifurcation.
- By randomly perturbing the initial conditions along the way, and doing these computations several times, bifurcations may be identified. All discovered bifurcations have been seen in this manner.
- Spikes in the errors may suggest a bifurcation, but spikes without bifurcations and bifurcations without spikes both exist.
- It has not been possible to notice any bifurcations in the energies, cf. Fig. 5.17(b).

To summarise the results, bifurcations in the continuations have been found both for N to $N + 1$ and reverse. For the observed cases there is a symmetry breakdown after the bifurcation, and, at least, most times a non-differentiability in the stability. Finally, the

close pairs of solutions have been connected to bifurcations. Finding close pairs of solutions, becomes, thus, a part of the somewhat more general task of finding bifurcations.

Relative equilibria on a sphere

6.1 Introduction

We now turn from the plane into the sphere, which is a natural continuation. Thus, the vortex motion is now constrained to be on the sphere.

The motivation for engaging with vortex patterns on a sphere is found in geophysical fluid dynamics considering large-scale atmospheric and oceanographic flows. These computations could, thus, model concentrated regions of vorticity, such as cyclones and hurricanes like the ones shown in Figs. 6.1 and 6.2, [47].

Like on the plane, this problem is connected to other physical systems, where the charge-on-a-sphere-problem should be mentioned, where one consider the equilibrium configurations of N equal point charges confined to the surface of a sphere, repelled by their mutual Coulomb interactions [24, 58].

Vortex dynamics on the sphere has attracted much less attention then vortex dynamics on the plane, but quite some work have still been done. The field was first studies by Gromeka [26] in 1885. The derivation of the equation of motion of vortices on a sphere, however, were first done by Bogomolov [16] in 1977. The motion of three identical vortices on a sphere was also analysed by Bogomolov [17] and the general case was solved by Kidambi



Figure 6.1: The hurricane Katrina from 23 August 2005 (<http://www.nvvl.noaa.gov/> [47]).



Figure 6.2: Satellite photo of the hurricane Andrew from 16 August 1992 (<http://jpl.nasa.gov/> [47]).

and Newton in 1998 [33] 120 years after Gröbli's treatment of the planar problem.

Relative equilibria have been identified by exploitation of symmetries in [30,35–37,39,40] and relative equilibria on a great circle have been studied in [49]. However, no thorough numerical investigations are known, which motivate this work.

Relative equilibria will be computed numerically, simply using random initial conditions, as described in Section 3.3 on the plane. Stability of relative equilibria will not be examined here, but it is described in [38,53]. Neither will a continuation using co-rotating points, as described in Chapter 4 on the plane, be done, but is left as future work.

6.2 The dynamical equations of a point vortex system

A spherical coordinate system (θ, ϕ) , $0 \leq \theta \leq \pi, 0 \leq \phi \leq 2\pi$ is introduced, where the radial component r is omitted, as the motion only takes place on the surface, $r = R$, where R is the radius of the sphere. The sphere is assumed to be at rest. The Cartesian coordinates are then given by

$$x = R \sin \theta \cos \phi \quad (6.1a)$$

$$y = R \sin \theta \sin \phi \quad (6.1b)$$

$$z = R \cos \theta. \quad (6.1c)$$

The velocity at an arbitrary point \mathbf{x} induced by a vortex at \mathbf{x}_α is [46]

$$\dot{\mathbf{x}} = \frac{\Gamma_\alpha \hat{\mathbf{n}}_\alpha \times (\mathbf{x} - \mathbf{x}_\alpha)}{2\pi \|\mathbf{x} - \mathbf{x}_\alpha\|^2} = \frac{\Gamma_\alpha}{2\pi R} \frac{\mathbf{x}_\alpha \times \mathbf{x}}{\|\mathbf{x} - \mathbf{x}_\alpha\|^2}, \quad (6.2)$$

where $\hat{\mathbf{n}}_\alpha = \mathbf{x}_\alpha/R$ is the outward unit normal vector to the surface. This is seen to fulfil that the velocity is inversely proportional with the distance to the vortex and perpendicular to the direction again the vortex. Integrating around the vortex gives the circulation Γ_α and, finally, it takes into account the curvature of the surface, as the crossproduct becomes smaller with a larger curvature. Thus, the vortex interaction depends on a geodesic distance, even though a euclidean norm is used in the denominator.

The dynamical equation for the velocity for a single vortex induced by multiple vortices is now given by [46, (4.1.1)]

$$\dot{\mathbf{x}}_\alpha = \frac{1}{2\pi R} \sum_{\beta=1}^N \Gamma_\beta \frac{\mathbf{x}_\beta \times \mathbf{x}_\alpha}{\ell_{\alpha\beta}^2}, \quad (6.3)$$

where

$$\ell_{\alpha\beta}^2 = \|\mathbf{x}_\alpha - \mathbf{x}_\beta\|^2 = 2(R^2 - \mathbf{x}_\alpha \cdot \mathbf{x}_\beta), \quad (6.4)$$

which can easily be seen inserting the equation for a sphere $x^2 + y^2 + z^2 = R^2$. Eq. (6.3) can be written in spherical coordinates [16,17,34], [46, (4.1.2)-(4.1.3)]

$$\dot{\theta}_\alpha = -\frac{1}{4\pi R^2} \sum_{\beta=1}^N \Gamma_\beta \frac{\sin \theta_\alpha \sin(\phi_\alpha - \phi_\beta)}{1 - \cos \gamma_{\alpha\beta}} \quad (6.5a)$$

$$\sin \theta_\alpha \dot{\phi}_\alpha = \frac{1}{4\pi R^2} \sum_{\beta=1}^N \Gamma_\beta \frac{\sin \theta_\alpha \cos \theta_\beta - \cos \theta_\alpha \sin \theta_\beta \cos(\phi_\alpha - \phi_\beta)}{1 - \cos \gamma_{\alpha\beta}}, \quad (6.5b)$$

where

$$\cos \gamma_{\alpha\beta} = \cos \theta_{\alpha} \cos \theta_{\beta} + \sin \theta_{\alpha} \sin \theta_{\beta} \cos(\phi_{\alpha} - \phi_{\beta}).$$

The Hamiltonian for the system is given by [46]

$$\mathcal{H} = -\frac{1}{4\pi R^2} \sum_{\alpha,\beta=1}^N \Gamma_{\alpha} \Gamma_{\beta} \log(\ell_{\alpha\beta}), \quad (6.6)$$

which, again, can be normalised such that

$$\theta = \frac{2}{N(N-1)} \sum_{\alpha,\beta=1}^N \log(\ell_{\alpha\beta}) = \langle \log(\ell_{\alpha\beta}^2) \rangle. \quad (6.7)$$

6.3 The equation for relative equilibria

Without loss of generality we assume that the z -axis is the rotation axis. With this we can introduce a rotating frame (θ^R, ϕ^R)

$$\theta^R = \theta \quad (6.8a)$$

$$\phi^R = \phi - \Omega t \quad (6.8b)$$

in which the vortex positions must be at rest to have a relative equilibrium. For $\Gamma_i = \Gamma$ the equations for a relative equilibrium is seen, from Eq. (6.5), to be

$$0 = \sum_{\beta=1}^N \frac{\sin \theta_{\alpha} \sin(\phi_{\alpha} - \phi_{\beta})}{1 - \cos \gamma_{\alpha\beta}} \quad (6.9a)$$

$$\sin \theta_{\alpha} = \frac{\Gamma}{4\pi\Omega R^2} \sum_{\beta=1}^N \frac{\sin \theta_{\alpha} \cos \theta_{\beta} - \cos \theta_{\alpha} \sin \theta_{\beta} \cos(\phi_{\alpha} - \phi_{\beta})}{1 - \cos \gamma_{\alpha\beta}}. \quad (6.9b)$$

Using that $\dot{\mathbf{x}}_{\alpha} = \boldsymbol{\Omega} \times \mathbf{x}_{\alpha}$ for a rigid body rotation [15, p.19] these equations can be written in Cartesian coordinates [3], [46, (p.192)]

$$\boldsymbol{\Omega} \times \mathbf{x}_{\alpha} = \frac{\Gamma}{4\pi R} \sum_{\beta=1}^N \frac{\mathbf{x}_{\beta} \times \mathbf{x}_{\alpha}}{R^2 - \mathbf{x}_{\alpha} \cdot \mathbf{x}_{\beta}}. \quad (6.10)$$

Non-dimensionalising such that $\mathbf{x} = R\tilde{\mathbf{x}}$ and assuming that $\boldsymbol{\Omega} = \Omega\mathbf{e}_z$ the equations read

$$\tilde{y}_{\alpha} = C \sum_{\beta=1}^N \frac{\tilde{y}_{\alpha} \tilde{z}_{\beta} - \tilde{y}_{\beta} \tilde{z}_{\alpha}}{1 - \tilde{\mathbf{x}}_{\alpha} \cdot \tilde{\mathbf{x}}_{\beta}} \quad (6.11a)$$

$$\tilde{x}_{\alpha} = -C \sum_{\beta=1}^N \frac{\tilde{z}_{\alpha} \tilde{x}_{\beta} - \tilde{z}_{\beta} \tilde{x}_{\alpha}}{1 - \tilde{\mathbf{x}}_{\alpha} \cdot \tilde{\mathbf{x}}_{\beta}} \quad (6.11b)$$

$$0 = \sum_{\beta=1}^N \frac{\tilde{x}_{\alpha} \tilde{y}_{\beta} - \tilde{x}_{\beta} \tilde{y}_{\alpha}}{1 - \tilde{\mathbf{x}}_{\alpha} \cdot \tilde{\mathbf{x}}_{\beta}}, \quad (6.11c)$$

where $C = \frac{\Gamma}{4\pi\Omega R^2}$.

An upper bound of the number of relative equilibria is shown in [49] to be $\frac{(n+1)!}{2}$. However, this grows very rapidly and gives, e.g. 181440 for $N = 8$, and is, thus, very far from the actual number.

For $R \rightarrow \infty$ these equations should give the same results than on the plane. This is shown in [46, p.174] going from the equivalent equations in the stereographic projection. Theoretically it should be possible to make a continuation from $R \gg 1$, which would give solutions close to the known solutions on the plane, to any given value of R . However, it turns out to be difficult to make this continuation due to the numeric, but some computations with a large radius have still been done. The connection between the coordinates in the planar case z^{pl} and the coordinates on the sphere \mathbf{x}^{sp} is

$$(x^{sp} + iy^{sp})R \rightarrow z^{pl}, \quad \text{for } R \rightarrow \infty, \quad (6.12)$$

where $R = \frac{1}{\sqrt{2C}}$ using that $\frac{\Gamma}{2\pi\Omega} = 1$ for the solutions on the plane.

6.4 Numerical computations

Numerical computations have now been done by solving Eq. (6.11) in MATLAB with $C = 1$. The initial conditions are random between $0 \leq \theta \leq \pi$, $-\pi \leq \phi \leq \pi$ and hereafter converted to Cartesian coordinates by Eq. (6.1). In this way they are constrained to be on the sphere. Convergence is checked explicitly, as done in the plane.

The results are shown on the plane by a stereographic projection given by the polar coordinates $(r = \tan(\theta/2), \phi)$ shown in Fig. 6.3 [46]. However, if a solution has a vortex both at the North Pole and the South Pole this projection does not work, because the South Pole ($\theta = \pi$) maps to infinity. In these cases, or when a vortex is close to the South Pole, the Northern Hemisphere and the Southern Hemisphere are shown as two different projections. The Northern Hemisphere maps as above, while the Southern Hemisphere maps as $r = \cot(\theta/2)$ where the tangent plane then is placed at the South Pole. The two different plotting methods are shown in Fig. 6.4 with the same configuration for $N = 6$, for comparison. The circles display equator. The configuration is, furthermore, shown on a spherical 3D plot in Fig. 6.4(c).

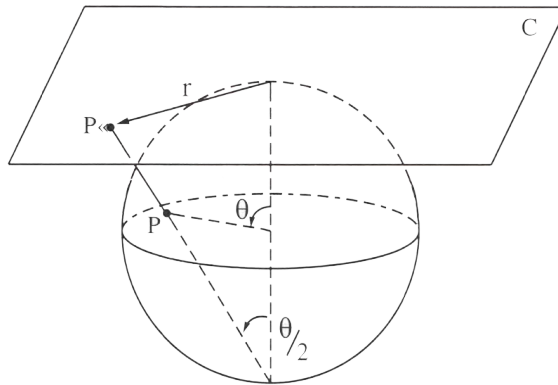


Figure 6.3: Stereographic projection of a vortex onto the plane tangent to the sphere at the North Pole. Taken from [46, Fig. 4.16].

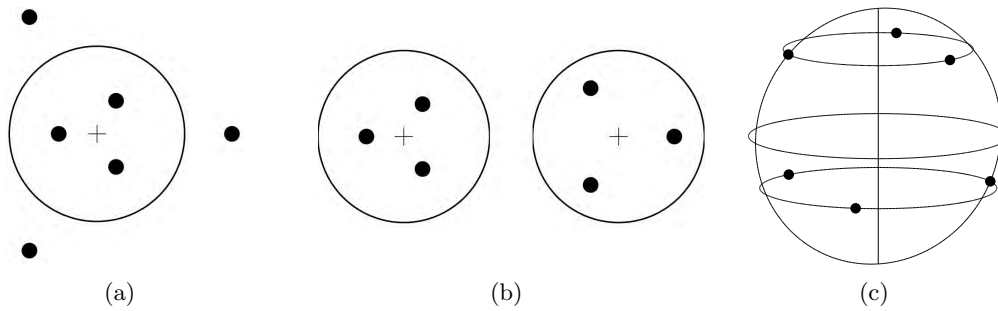


Figure 6.4: Plots of the same configuration for $N = 6$ using (a) one stereographic projection, (b) two projections showing each hemisphere separately, or (c) shown on a 3D spherical plot.

The solutions are arranged by decreasing value of the energy Eq. (6.7).

Computations with a small C have also been done with the planar solutions as initial conditions. These solutions have then again been compared with the planar solutions.

6.5 Results

The results for $C = 1$ and $N = 2, \dots, 8$ are shown in Appendix D. Keep in mind that the results are strongly dependent on the constant C . For other values other patterns might appear and some patterns might disappear.

For $N = 2$ one solution has been found, as expected. For $N = 3$ three solutions are found. Two solutions have been found with the vortices lying on a great circle and one with the vortices lying on an equilateral triangle, on the same latitude. The latter is verified using the result of Newton [46, (4.2.14)]

$$\Omega = \frac{\Gamma}{4\pi} \frac{[9\Gamma^2 R^2 - 3\Gamma^2 s^2]^{1/2}}{2\pi R s^2}, \quad (6.13)$$

which gives the desired side length $s = \sqrt{6\sqrt{2} - 6}$. The three solutions are shown in Fig. 6.5.

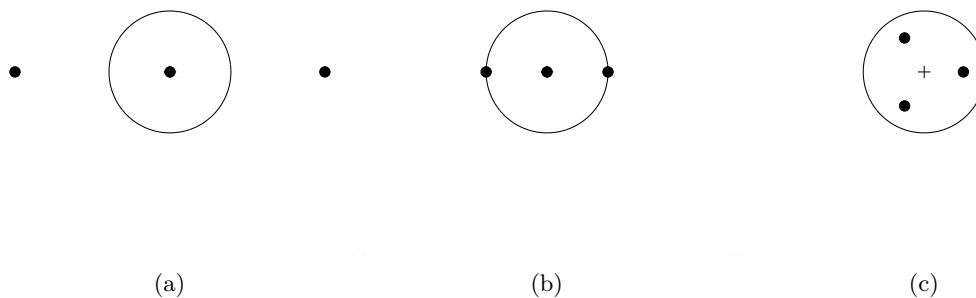


Figure 6.5: The three different relative equilibria for $N = 3$ and $C = 1$

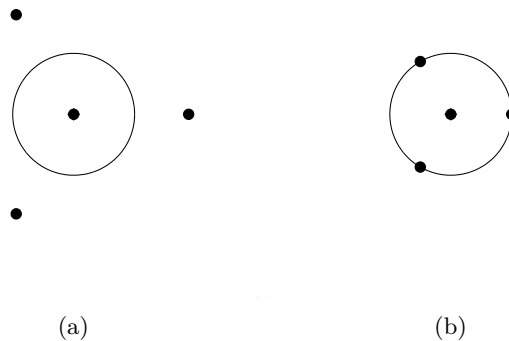


Figure 6.6: The two centered triangles for $N = 4$ with vortices on the same latitude.

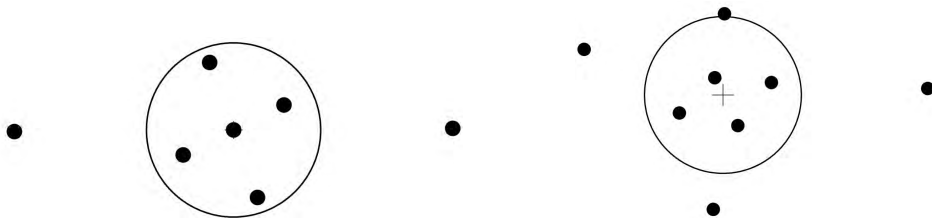


Figure 6.7: The first equilibrium on the sphere that has no symmetry axis. The configuration has, however, a 180° rotational symmetry.

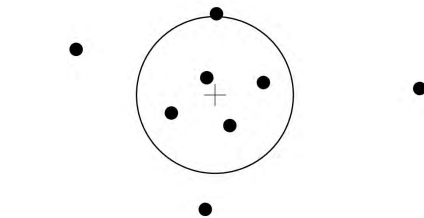


Figure 6.8: The first equilibrium on the sphere that neither has a symmetry axis nor a rotational symmetry.

For $N = 4$ 6 solutions have been found: Two centered triangles, shown in Fig. 6.6, two tetragons, and two solutions on a great circle. For $N = 5$ 10 solutions exist, thus twice as many than on the plane, and for $N = 6$ 13 solutions exist.

For $N = 7$ 27 solutions have been found, and two cases that have no symmetry axes, for the first time, appear, one shown in Fig. 6.7. However, both configurations has a 180° rotational symmetry.

For $N = 8$ 43 solutions have been found, and a total of 4 configurations have no symmetry at all, where one of them is shown in Fig. 6.8. Thus, the first total asymmetric solution appears for $N = 8$, as on the plane.

No close solutions similar to the ones on the plane have been found for $N = 7$ and $C = 1$, but they exist of course in the limit $R \rightarrow \infty$. However, close solutions for $N = 8$ and $C = 1$ exist, cf. Figs. D.91 and D.92. This is, as in the planar case, two nested equilateral triangles, but now there is a vortex at both poles. The two solutions are shown on top of each other in Fig. 6.9.

These close solutions are believed to originate in a bifurcation, as in the planar case. It is natural to investigate, whether a close pair also exists for more than two rings and whether close pairs exist for larger N . This is, however, very difficult without a analytical solution, which is not known, and, at least, it require very much computing power.

For each $N = 3, \dots, 8$ two different configurations exist that lie on a great circle, cf.

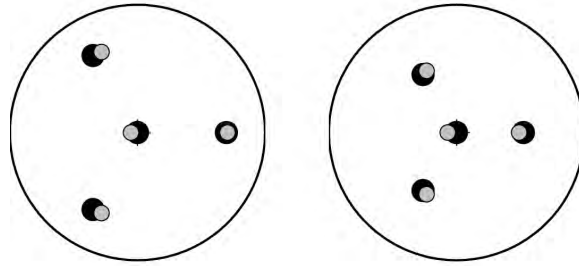


Figure 6.9: Two solutions on the sphere for $N = 8$ showing both Hemispheres separately. The black solutions is two centered equilateral triangles, whereas the embedded grey solutions is a numerical determined close solutions.

Fig. 6.5 for $N = 3$. This would never happen on the plane and seems surprising. However, it is consistent with the analytical results in [49]. The same phenomenon also happens for the case with vortices on the same latitude with a vortex at the origin, also for $N = 3, \dots, 8$, cf. Fig. 6.6 for $N = 4$. Notices that for $N = 3$ this configuration is identical to the co-linear configuration.

Finally, the constant C has been decreased, $C < 1$ to see whether the solutions approach the solutions on the plane. Computations using random initial conditions show that the solutions clearly approach the North Pole. The solutions on the plane have also been used as initial conditions in the computations, cf. Eq. (6.12). The relative difference between the planar solution and the solution on the sphere for each solution will be defined as

$$\eta_\alpha = \frac{\sum_{\beta=1}^N |z_\beta^{pl} - (x_\beta^{sp} + iy_\beta^{sp})R|}{\sum_{\beta=1}^N |z_\beta^{pl}|} \quad (6.14)$$

and averaging over the different solutions gives

$$\eta = \frac{\sum \eta_\alpha}{\#\text{solutions}}, \quad (6.15)$$

which is the variable that will be used. For $N = 2$ and $C = \frac{1}{4000}$ the relative difference between the planar solution and the solution on the sphere is $\eta = 6.2 \cdot 10^{-5}$. When C increases, η increases as well, cf. Fig. 6.10(a), where η is shown for $N = 2, \dots, 5$.

To give a more physical and intuitive measure of how close the solutions are to the pole, η has been shown with respect to the maximum vortex distance from the origin over the radius, $\max(|x_\beta^{sp} + iy_\beta^{sp}|)/R$, in Fig. 6.10(b).

When the number of vortices increases it becomes more difficult to find a converging solutions and the constant C must be increased. It is not clear why it is much more difficult to find a solution for smaller C than for $C = 1$. The figures shows, nevertheless, clearly that the solutions on the sphere approach the solutions on the plane when they approach the pole $C \rightarrow 0$, as expected. For $N = 4, 5$ the relative error becomes quite large, but it can also be seen from Fig. 6.10(b) that the configurations are not very close to the pole. The

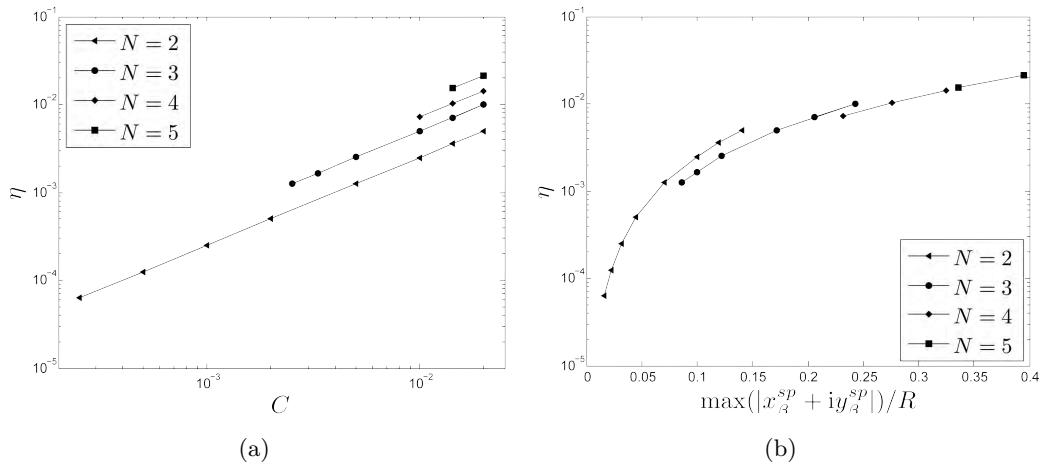


Figure 6.10: The average relative difference η between the planar solutions and the solutions on the sphere given in Eq. (6.15) vs. (a) the constant C shown on a double logarithmic scale or (b) the maximum vortex distance from the origin over the sphere radius shown on semilogarithmic scale.

qualitative similarity is, nevertheless, still pretty good, which can be seen by comparing the configurations, shown in Fig. 6.11, with the planar solutions, shown in Fig. A.7–A.11.

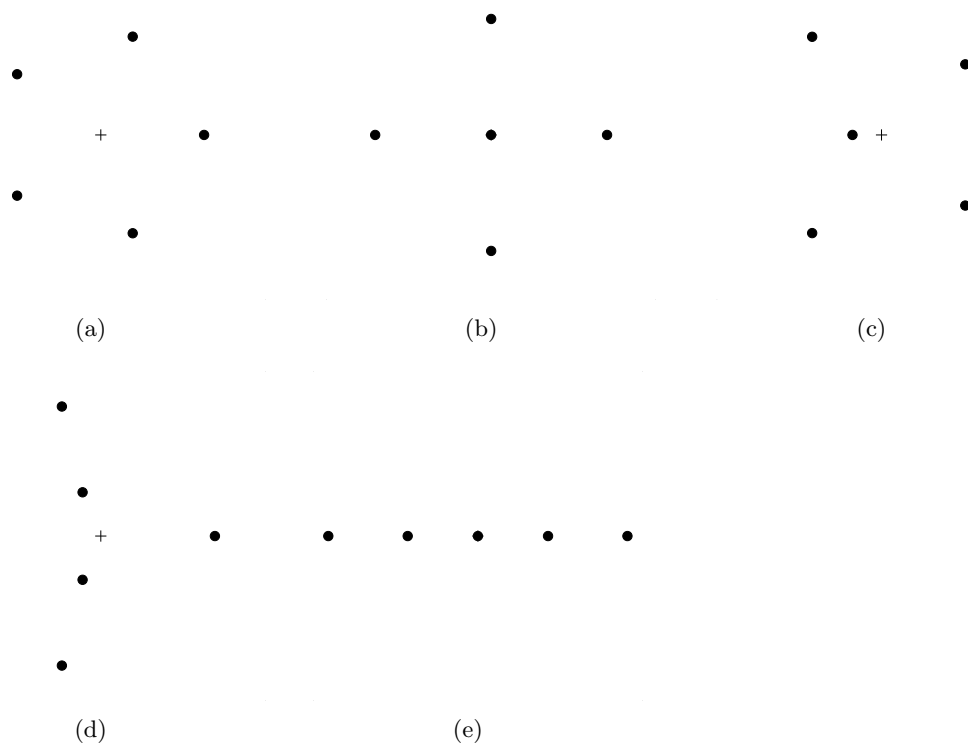


Figure 6.11: Relative equilibria on a sphere for $N = 5$ and $C = 1/70$. The configurations are seen to be similar to the planar solutions shown in Fig. A.7–A.11.

Conclusion and outlook

Conclusion

In this work relative equilibria of identical point vortices have been investigated, first on the plane and later on the sphere. The work has been motivated by several visualisations of vortex patterns in, i.a. experiments by floating magnets, experiments in superfluids and experiments by magnetic discs.

The governing equations on the plane have been derived, together with a general stability analysis for a N -vortex crystal. The governing equations have simply been solved numerically using MATLAB. Using random initial conditions all prior known solutions have been found, including the asymmetric solutions. More surprising, new solutions have been found very close to some of the prior known solutions. The first one is for $N = 7$ and extremely close to the centered nested equilateral triangles. Close solutions have also been found close to the heptagon and the centered nonagon, and close pairs exist for the configurations with more rings, as well.

The co-rotating points, that are points of relative rest, have been computed. A small circulation has now been imposed to one of these, whereupon the governing equations have been solved again. This circulation has been increased in 1000 steps until all vortices are identical, while all the intermediate steps are relative equilibria. The initial conditions for the solver are always the former solutions.

These computations have recreated all prior known solutions for $N = 2, \dots, 8$ including the first close solutions for $N = 7$ [21] and the first asymmetric solution for $N = 8$ [13]. The computations have also revealed bifurcations in the solutions paths, which is the main result of this work. The continuations can, thus, give two different solution path, where the two paths would be coinciding in the start or in the end, and, in this way, one relative equilibrium for N vortices and one co-rotating point can grow into two solutions for $N + 1$. The first bifurcation is observed going from $N = 5$ to $N = 6$. Computations have also been done in the reverse direction by decreasing the circulation of one vortex. Bifurcations in this direction have also been observed, the first one going from $N = 6$ to $N = 5$. One of the two solutions paths has always a kink or a non-differentiability for all observed cases of bifurcations.

The close pair for $N = 7$ has been shown to originate in a bifurcation. The nested equilateral triangles $N = 6$ can, namely, grow into both close solutions with the same co-rotating point. Bifurcations have been observed for the three other known close pairs for $N \leq 8$, as well. This explain, to some degree, the existence of close relative equilibria, and

it is believed that all close solutions originate in a bifurcation. Bifurcations will always generate close relative equilibria near the bifurcation point. If the bifurcation point is sufficiently close to 1, close relative equilibria of identical point vortices will exist. The problem of finding close relative equilibria will, thus, be a matter of finding bifurcations.

The first asymmetric solution for $N = 8$ has also been connected to a bifurcation, such that two relative equilibria for $N = 7$ grow into the asymmetric solution with partial coinciding paths.

The bifurcations are associated with non-differentiabilities in one of the eigenvalues at the same time the bifurcation happens. Furthermore, the symmetry decreases or breaks down after a bifurcation.

The continuation method connects relative equilibria with N vortices with ones with $N + 1$ vortices. Thus, by induction, this method has the potential of finding all relative equilibria. However, we need to make sure that all bifurcations are found. Furthermore, it must be proven that all relative equilibria for N vortices can be connected with the ones for $N - 1$ by the continuation method.

Finally, work has been done on relative equilibria of identical point vortices on the sphere. The governing equations on the sphere have been solved numerically, for $C = \frac{\Gamma}{4\pi\Omega R^2} = 1$, $N = 2, \dots, 8$, using random initial conditions. The number of solutions are larger than on the plane. For $N = 3, \dots, 8$ two different configurations exist both with vortices lying on a great circle and with vortices on the same latitude with a vortex at the origin. For $N = 7$ two configurations exist that have no symmetry axis, but a 180° rotational symmetry. For $N = 8$ the first total asymmetric solution appears, as on the plane. One close pair of relative equilibria have been found for $N = 8$. This is two nested, centered equilateral triangles, and thus, similar to the first case on the plane, however, with a vortex at both poles. Computations have also been done with, $R > 1$, which shows that the solutions approach the solutions on the plane when the radius is increased, as expected.

We have, thus, both discovered some new interesting phenomena in vortex statics, and explained some of these by our continuation method.

Outlook

Although many aspects of vortex statics have been treated, work is still to be done, and several paths can be followed.

On the plane, a more analytical approach of identifying bifurcations, is needed. Normally bifurcations can occur only when the governing system of equations becomes singular, in the sense of the Implicit function theorem [52]. Implementation of this would be of great importance to this work.

On the sphere, many different research paths can be pursued. The dependence on the constant $C = \frac{\Gamma}{4\pi\Omega R^2}$ is still unknown, and a complete continuation from the solutions on the plane $C \rightarrow 0$ to some $C \geq 1$ would be very interesting to produce. The stability of the computed relative equilibria is still undetermined, as well, and should be determined. Finally, a continuation, like the one done on the plane starting with co-rotating points, could be done, together with the accompanying investigation of possible close pairs of solutions and bifurcations.

Figures of vortex crystals

In this appendix all known relative equilibria of identical point vortices for $N = 2, \dots, 8$ are shown. The plus denotes the center of rotation.

A.1 $N = 2$



Figure A.1

A.2 $N = 3$

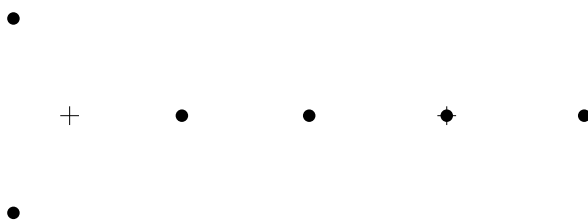


Figure A.2

Figure A.3

A.3 $N = 4$

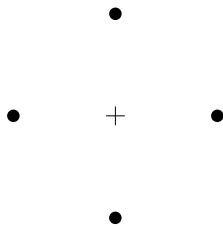


Figure A.4

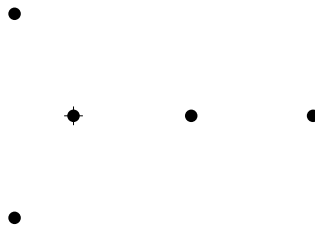


Figure A.5



Figure A.6

A.4 $N = 5$

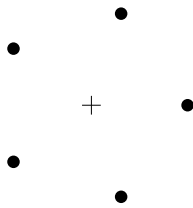


Figure A.7

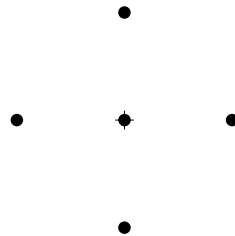


Figure A.8

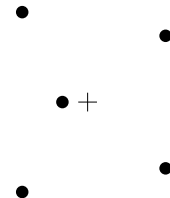


Figure A.9

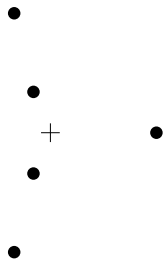


Figure A.10



Figure A.11

A.5 $N = 6$

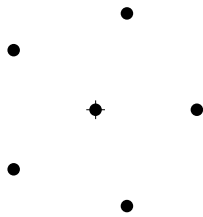


Figure A.12

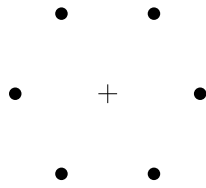


Figure A.13

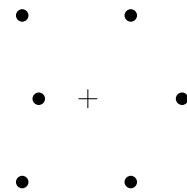


Figure A.14

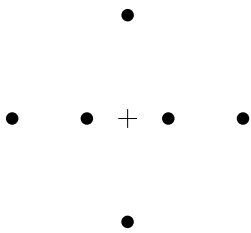


Figure A.15

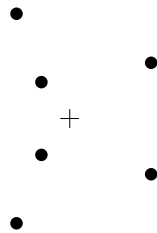


Figure A.16

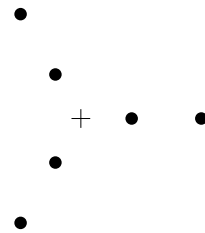


Figure A.17

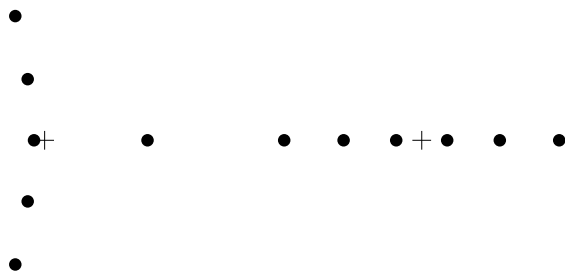


Figure A.18

Figure A.19

A.6 $N = 7$

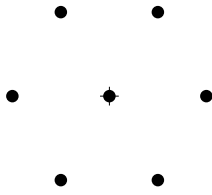


Figure A.1

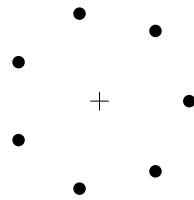


Figure A.2

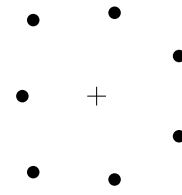


Figure A.3

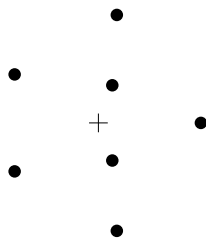


Figure A.4

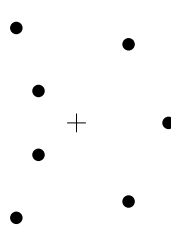


Figure A.5

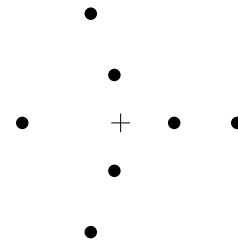


Figure A.6

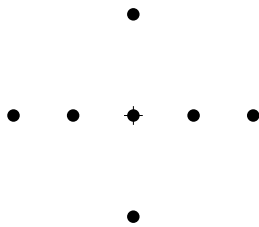


Figure A.7

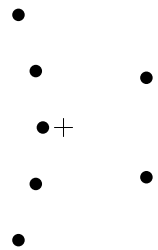


Figure A.8

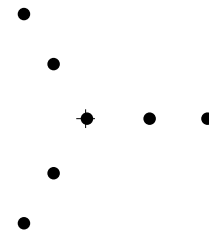


Figure A.9

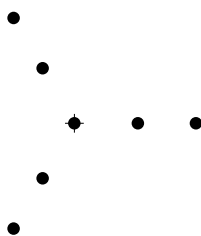


Figure A.10

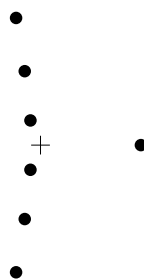


Figure A.11



Figure A.12

A.7 $N = 8$

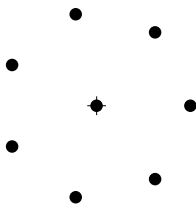


Figure A.1

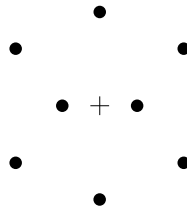


Figure A.2

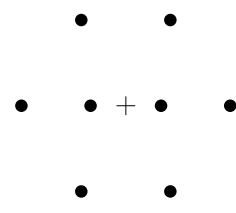


Figure A.3

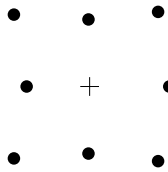


Figure A.4

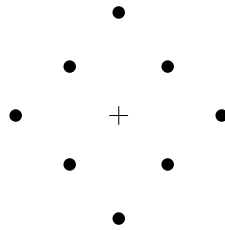


Figure A.5

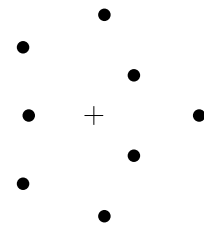


Figure A.6

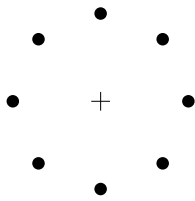


Figure A.7

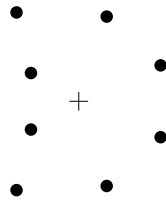


Figure A.8

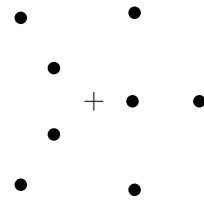


Figure A.9

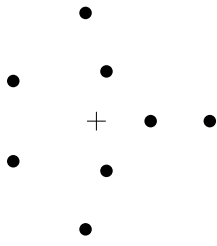


Figure A.10

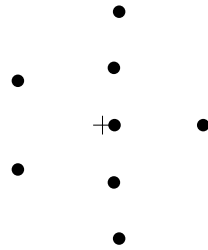


Figure A.11

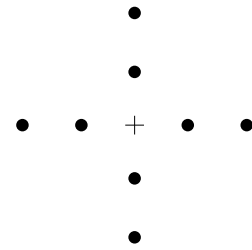


Figure A.12

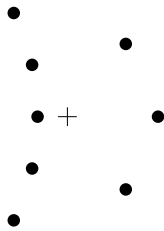


Figure A.13

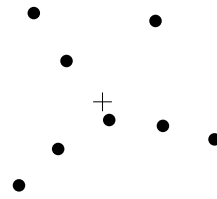


Figure A.14

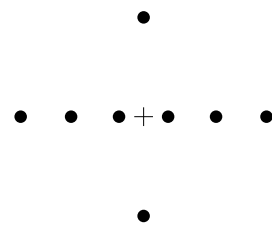


Figure A.15

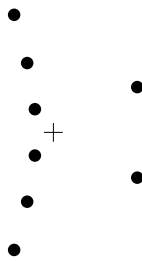


Figure A.16

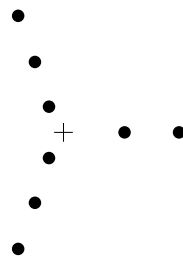


Figure A.17

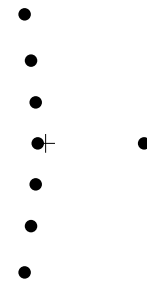


Figure A.18

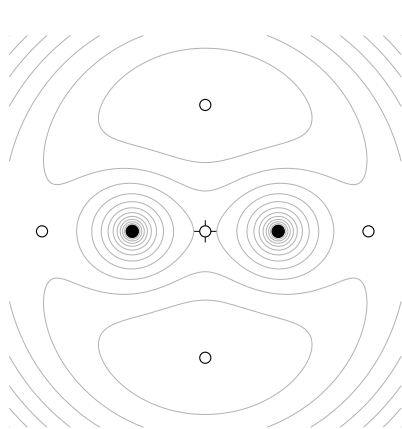


Figure A.19

Figures of co-rotating points in the plane

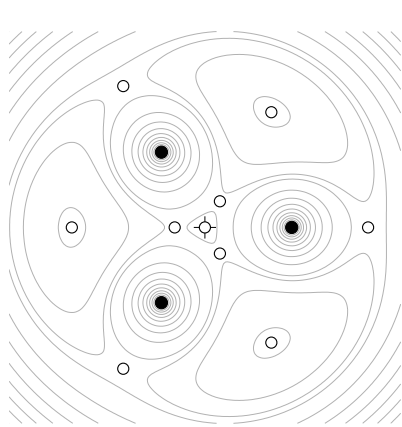
The results of the computed co-rotating points are shown in the succeeding. First, a figure is shown where the solid dots denotes the point vortices, the open circles denotes the co-rotating points and the plus denotes the origin. Furthermore, the streamlines in the rotating frame, given in Eq. (2.17), are shown. Then, the z -coordinates for the co-rotating points are given.

B.1 Co-rotating points for $N = 2$



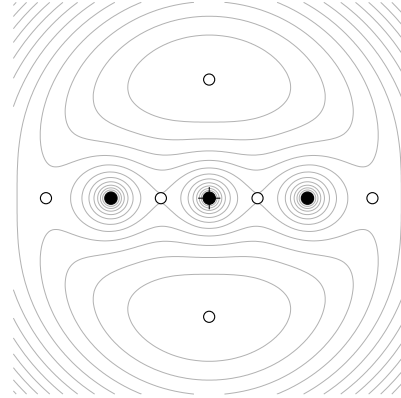
z -coordinates
0
-1.22474487139i
1.22474487139i
-1.58113883008
1.58113883008

B.2 Co-rotating points for $N = 3$



z -coordinates

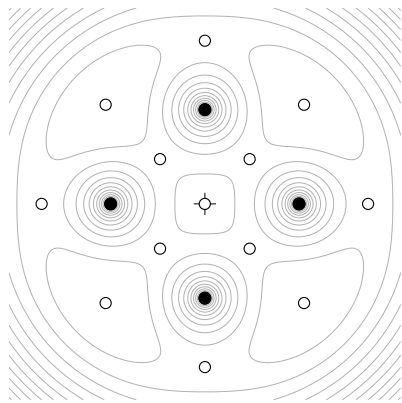
0
 -0.347296355334
 $0.173648177667 - 0.300767466361i$
 $0.173648177667 + 0.300767466361i$
 -1.53208888624
 $0.766044443119 - 1.32682789634i$
 $0.766044443119 + 1.32682789634i$
 1.87938524157
 $-0.939692620786 - 1.6275953627i$
 $-0.939692620786 + 1.6275953627i$



z -coordinates

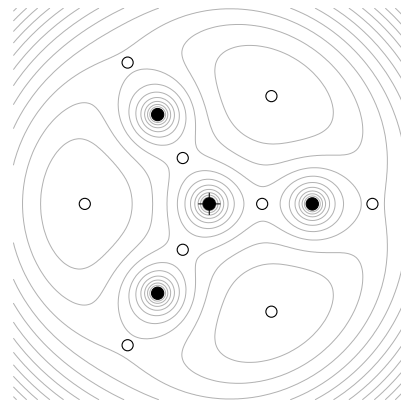
0.602114101464
 -0.602114101464
 $-1.47856033412i$
 $1.47856033412i$
 2.03407438625
 -2.03407438625

B.3 Co-rotating points for $N = 4$



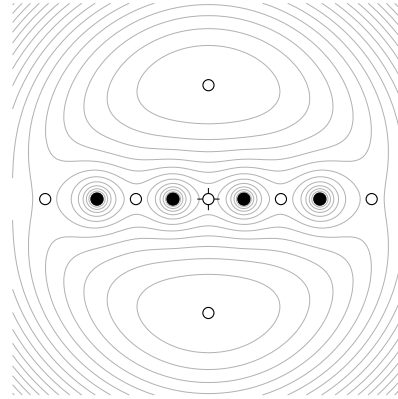
z -coordinates

0
 $0.5818609561 - 0.5818609561i$
 $-0.5818609561 - 0.5818609561i$
 $-0.5818609561 + 0.5818609561i$
 $0.5818609561 + 0.5818609561i$
 $1.28896773729 + 1.28896773729i$
 $-1.28896773729 - 1.28896773729i$
 $-1.28896773729 + 1.28896773729i$
 $1.28896773729 - 1.28896773729i$
 2.12132034356
 -2.12132034356
 $-2.12132034356i$
 $2.12132034356i$



z -coordinates

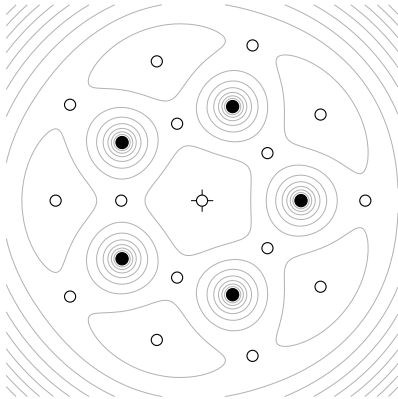
0.726960401692
 $-0.363480200846 + 0.629566175411i$
 $-0.363480200846 - 0.629566175411i$
 -1.706373209
 $0.853186604499 - 1.47776254733i$
 $0.853186604499 + 1.47776254733i$
 2.23860545044
 $-1.11930272522 - 1.93868918913i$
 $-1.11930272522 + 1.93868918913i$



z -coordinates

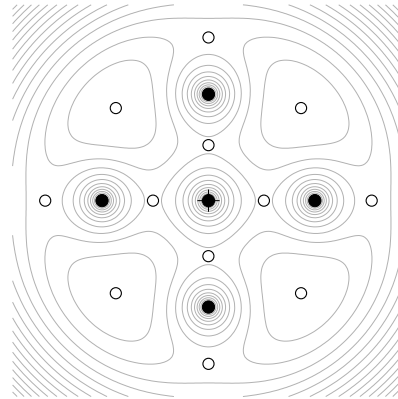
0
 1.07461254417
 -1.07461254417
 $1.68677440101i$
 $-1.68677440101i$
 -2.41768647262
 2.41768647262

B.4 Co-rotating points for $N = 5$



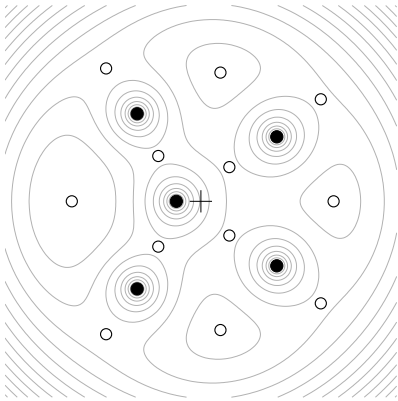
z -coordinates

0
 -1.15574899441
 $0.935020577713 + 0.679332214269i$
 $0.935020577713 - 0.679332214269i$
 $-0.357146080506 + 1.09918261234i$
 $-0.357146080506 - 1.09918261234i$
 -2.0937194618
 $1.69385462605 - 1.23065742208i$
 $1.69385462605 + 1.23065742208i$
 $-0.646994895148 + 1.99124553744i$
 $-0.646994895148 - 1.99124553744i$
 2.33349505242
 $-1.8878371537 + 1.37159397811i$
 $-1.8878371537 - 1.37159397811i$
 $0.721089627488 + 2.21928567535i$
 $0.721089627488 - 2.21928567535i$



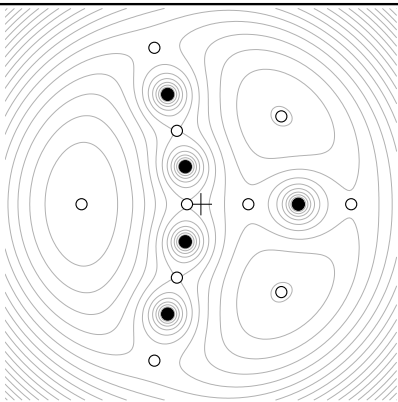
z -coordinates

0.824747546356
 -0.824747546356
 $0.824747546356i$
 $-0.824747546356i$
 $-1.37568345991 - 1.37568345991i$
 $-1.37568345991 + 1.37568345991i$
 $1.37568345991 + 1.37568345991i$
 $1.37568345991 - 1.37568345991i$
 2.42526821407
 -2.42526821407
 $-2.42526821407i$
 $2.42526821407i$



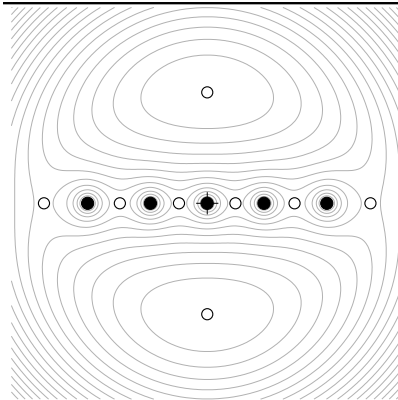
z -coordinates

$0.429630133045 + 0.516067743683i$
 $0.429630133045 - 0.516067743683i$
 $-0.641979215484 - 0.684237851783i$
 $-0.641979215484 + 0.684237851783i$
 -1.94752601345
 $0.29633061331 - 1.94260014511i$
 $0.29633061331 + 1.94260014511i$
 2.00303961986
 $1.8106617192 - 1.53904510993i$
 $1.8106617192 + 1.53904510993i$
 $-1.4297317671 + 2.00555081185i$
 $-1.4297317671 - 2.00555081185i$



z -coordinates

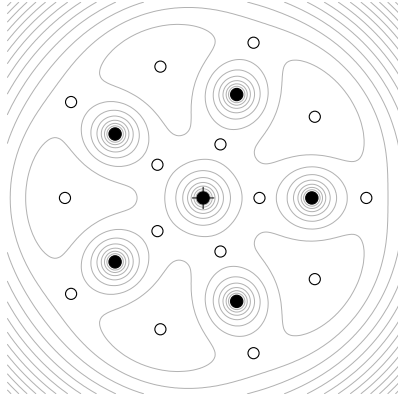
-0.221573287679
 0.75865281667
 $-0.382887594374 + 1.17276372238i$
 $-0.382887594374 - 1.17276372238i$
 $1.28640603006 - 1.40424221289i$
 $1.28640603006 + 1.40424221289i$
 -1.90737102166
 2.40315670833
 $-0.743331302571 - 2.50025011476i$
 $-0.743331302571 + 2.50025011476i$



z -coordinates

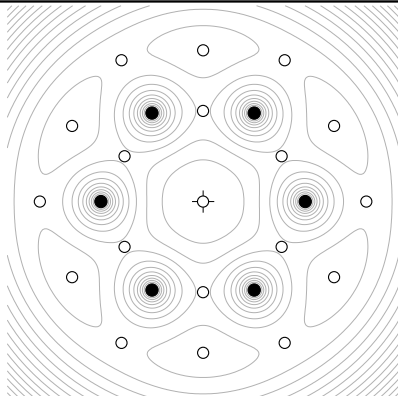
-0.47625103427
 0.47625103427
 -1.47524091772
 1.47524091772
 $1.8734365813i$
 $-1.8734365813i$
 2.75623823119
 -2.75623823119

B.5 Co-rotating points for $N = 6$



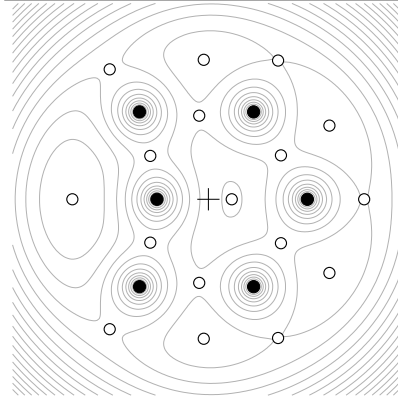
z -coordinates

0.897658149617
 $-0.726220698179 + 0.527630221945i$
 $-0.726220698179 - 0.527630221945i$
 $0.277391623371 + 0.853723632598i$
 $0.277391623371 - 0.853723632598i$
 -2.19951308502
 $1.77944346513 + 1.2928413536i$
 $1.77944346513 - 1.2928413536i$
 $-0.679686922621 + 2.09186125218i$
 $-0.679686922621 - 2.09186125218i$
 2.59928257234
 $-2.10286377421 + 1.52781996257i$
 $-2.10286377421 - 1.52781996257i$
 $0.803222488037 + 2.47206462812i$
 $0.803222488037 - 2.47206462812i$



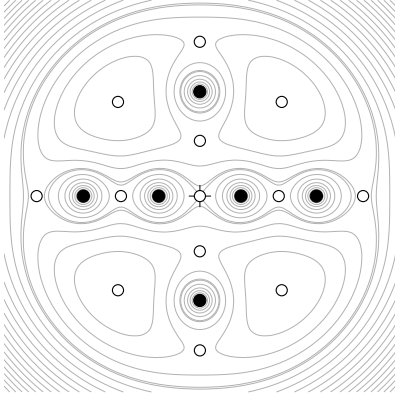
z -coordinates

0
 $1.21513809593 + 0.701560306789i$
 $-1.21513809593 + 0.701560306789i$
 $1.21513809593 - 0.701560306789i$
 $-1.21513809593 - 0.701560306789i$
 $-1.40312061358i$
 $1.40312061358i$
 $-2.0272436001 - 1.17042963823i$
 $-2.0272436001 + 1.17042963823i$
 $2.0272436001 - 1.17042963823i$
 $2.0272436001 + 1.17042963823i$
 $-2.34085927646i$
 $2.34085927646i$
 -2.52654908626
 2.52654908626
 $-1.26327454313 - 2.1880556926i$
 $1.26327454313 + 2.1880556926i$
 $1.26327454313 - 2.1880556926i$
 $-1.26327454313 + 2.1880556926i$

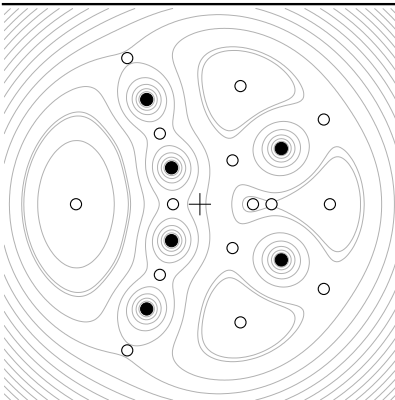


z -coordinates

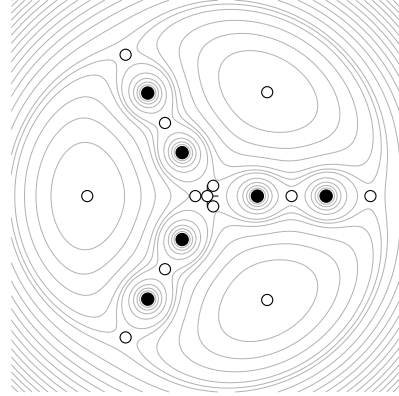
0.379876126086
 $-0.946641815063 + 0.706822401277i$
 $-0.946641815063 - 0.706822401277i$
 $-0.15017842566 + 1.36098265478i$
 $-0.15017842566 - 1.36098265478i$
 $1.18094780251 - 0.714617486388i$
 $1.18094780251 + 0.714617486388i$
 -2.2159709421
 $-0.075677490658 - 2.27181715847i$
 $-0.075677490658 + 2.27181715847i$
 $1.97078110448 - 1.19968537167i$
 $1.97078110448 + 1.19968537167i$
 $1.13350357526 - 2.25985291224i$
 $1.13350357526 + 2.25985291224i$
 2.53595748687
 $-1.6080967538 - 2.11626834069i$
 $-1.6080967538 + 2.11626834069i$

 z -coordinates

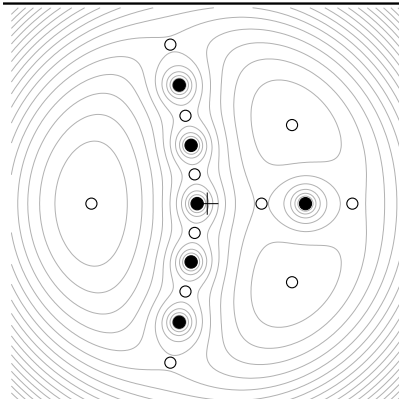
2.76345281598
 1.38631324284 - 1.59358097126i
 1.38631324284 + 1.59358097126i
 1.33550111823
 0.935372874501i
 -2.61260115972i
 2.61260115972i
 -0.935372874501i
 0
 -1.33550111823
 -1.38631324284 + 1.59358097126i
 -1.38631324284 - 1.59358097126i
 -2.76345281598

 z -coordinates

-0.458220385397
 0.907837404229
 0.558071226575 + 0.748818339723i
 0.558071226575 - 0.748818339723i
 1.22474487139
 -0.683423955777 - 1.20767041037i
 -0.683423955777 + 1.20767041037i
 -2.11777196374
 0.693910376737 + 2.0193776172i
 0.693910376737 - 2.0193776172i
 2.22297143929
 2.11917459266 + 1.44833021973i
 2.11917459266 - 1.44833021973i
 -1.24120740365 + 2.49872449968i
 -1.24120740365 - 2.49872449968i

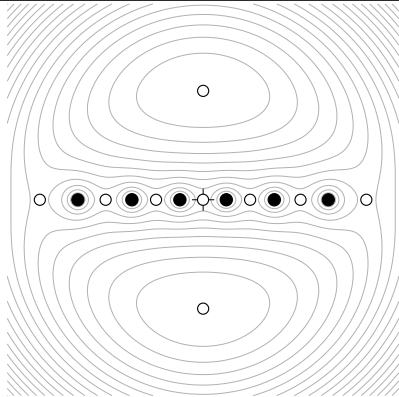
 z -coordinates

0
 -1.21513809593 + 0.701560306789i
 -1.21513809593 - 0.701560306789i
 1.21513809593 - 0.701560306789i
 1.21513809593 + 0.701560306789i
 1.40312061358i
 -1.40312061358i
 -2.0272436001 + 1.17042963823i
 -2.0272436001 - 1.17042963823i
 2.0272436001 + 1.17042963823i
 2.0272436001 - 1.17042963823i
 -2.34085927646i
 2.34085927646i
 -2.52654908626
 2.52654908626
 1.26327454313 - 2.1880556926i
 -1.26327454313 + 2.1880556926i
 -1.26327454313 - 2.1880556926i
 1.26327454313 + 2.1880556926i



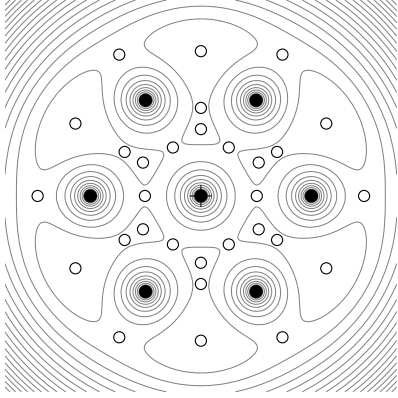
z -coordinates

$-0.224578838411 + 0.524808172961i$
 $-0.224578838411 - 0.524808172961i$
 0.974300118806
 $-0.390085772601 - 1.57365282506i$
 $-0.390085772601 + 1.57365282506i$
 $1.51925959638 + 1.40753375367i$
 $1.51925959638 - 1.40753375367i$
 -2.07404733043
 2.60048715358
 $-0.660073750921 - 2.8484548628i$
 $-0.660073750921 + 2.8484548628i$



z -coordinates

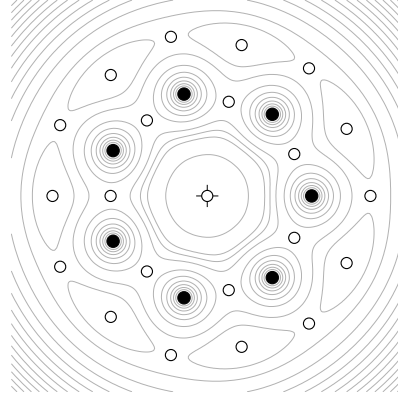
0
 -0.881604323972
 0.881604323972
 1.82861121001
 -1.82861121001
 $2.04321501933i$
 $-2.04321501933i$
 -3.06250793608
 3.06250793608

B.6 Co-rotating points for $N = 7$  z -coordinates

```

0.947206448599
-0.947206448599
0.4736032243 + 0.820304847115i
-0.4736032243 + 0.820304847115i
0.4736032243 - 0.820304847115i
-0.4736032243 - 0.820304847115i
0.979585055292 + 0.565563695367i
-0.979585055292 + 0.565563695367i
0.979585055292 - 0.565563695367i
-0.979585055292 - 0.565563695367i
0 + 1.13112739073i
0 - 1.13112739073i
1.29050886066 + 0.745075638095i
-1.29050886066 + 0.745075638095i
1.29050886066 - 0.745075638095i
-1.29050886066 - 0.745075638095i
1.49015127619i
-1.49015127619i
2.12321137292 + 1.2258366577i
-2.12321137292 + 1.2258366577i
2.12321137292 - 1.2258366577i
-2.12321137292 - 1.2258366577i
2.4516733154i
-2.4516733154i
2.76380412905
-2.76380412905
1.38190206453 + 2.39352458684i
-1.38190206453 + 2.39352458684i
1.38190206453 - 2.39352458684i
-1.38190206453 - 2.39352458684i

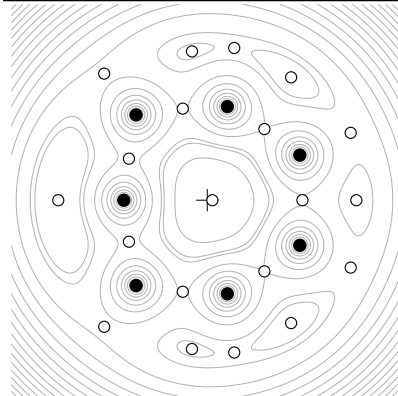
```

 z -coordinates

```

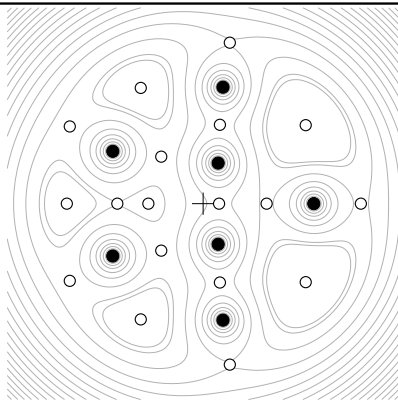
0
-1.60186149392
1.44322733671 + 0.695021654529i
1.44322733671 - 0.695021654529i
-0.998744305447 + 1.2523857465i
-0.998744305447 - 1.2523857465i
0.356447715695 + 1.56169948187i
0.356447715695 - 1.56169948187i
-2.56490154781
2.31089644381 + 1.11286907403i
2.31089644381 - 1.11286907403i
-1.59918995783 + 2.00532077951i
-1.59918995783 - 2.00532077951i
0.570744287926 + 2.50059411096i
0.570744287926 - 2.50059411096i
2.70598046563
-2.43800415668 + 1.17408092241i
-2.43800415668 - 1.17408092241i
1.68715122435 + 2.11562071897i
1.68715122435 - 2.11562071897i
-0.602137300479 + 2.63813588576i
-0.602137300479 - 2.63813588576i

```



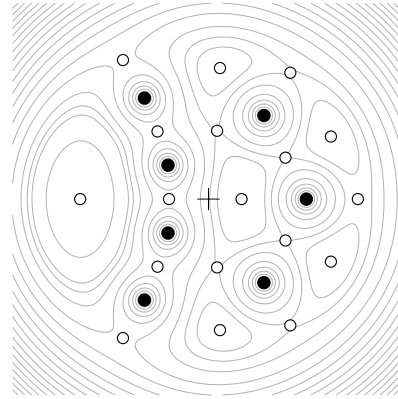
z -coordinates

0.088712037482
 -1.34350437564 + 0.712902226731i
 -1.34350437564 - 0.712902226731i
 0.982253313669 + 1.22262267656i
 0.98225331367 - 1.22262267656i
 -0.419076892193 + 1.57193675606i
 -0.419076892192 - 1.57193675606i
 1.6349323423
 1.44126879706 + 2.11076384329i
 1.44126879706 - 2.11076384329i
 -2.55904462096
 2.56093721872
 -0.262306919056 + 2.55637519817i
 -0.262306919055 - 2.55637519817i
 0.463464095798 + 2.61412169547i
 0.463464095799 - 2.61412169547i
 2.46513299259 + 1.15760866847i
 2.46513299259 - 1.15760866847i
 -1.76878317563 + 2.17441475954i
 -1.76878317563 - 2.17441475954i



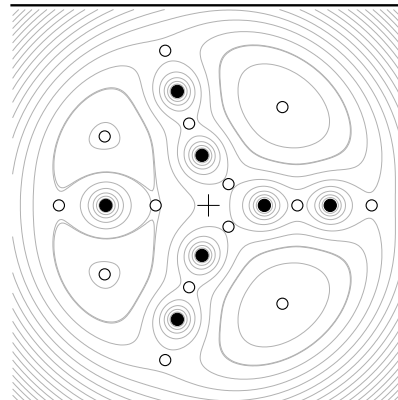
z -coordinates

0.285317526974
 -0.978818836182
 -0.74815514705 + 0.840168462659i
 -0.74815514705 - 0.840168462659i
 1.13620188618
 0.301004304856 + 1.409219944i
 0.301004304856 - 1.409219944i
 -1.5328921888
 1.83507147025 + 1.40283835553i
 1.83507147025 - 1.40283835553i
 -1.11351187486 + 2.06852740157i
 -1.11351187486 - 2.06852740157i
 -2.43615001785
 -2.3828696187 + 1.37992574773i
 -2.3828696187 - 1.37992574773i
 2.81959773978
 0.47774274125 + 2.87837016276i
 0.47774274125 - 2.87837016276i



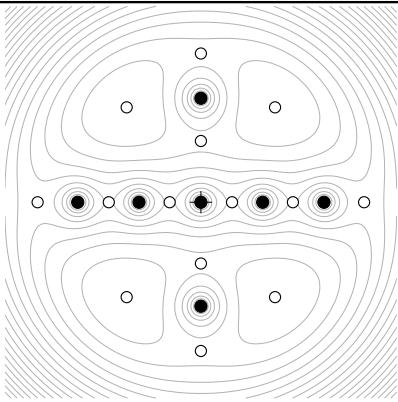
z -coordinates

0.601145477571
 -0.716006103311
 0.157329333583 + 1.23798163851i
 0.157329333583 - 1.23798163851i
 -0.924297656129 + 1.2262608591i
 -0.924297656129 - 1.2262608591i
 1.39717118408 + 0.751869052691i
 1.39717118408 - 0.751869052691i
 -2.32754914222
 0.209755847519 + 2.37746403503i
 0.209755847519 - 2.37746403503i
 2.22175102255 + 1.13447473531i
 2.22175102255 - 1.13447473531i
 2.71007814917
 1.4845360515 + 2.29136312213i
 1.4845360515 - 2.29136312213i
 -1.55060554749 + 2.52173223734i
 -1.55060554749 - 2.52173223734i

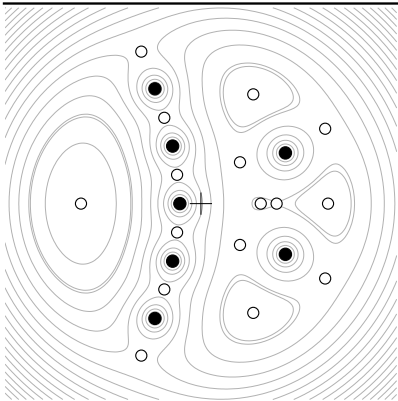


z -coordinates

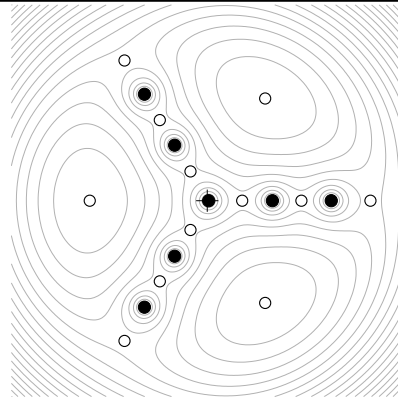
$0.370130691619 + 0.393313783486i$
 $0.370130691619 - 0.393313783486i$
 -0.975185475326
 $-0.356888451509 + 1.51174113175i$
 $-0.356888451509 - 1.51174113175i$
 1.64288712463
 $1.36776888726 + 1.81616407631i$
 $1.36776888726 - 1.81616407631i$
 $-1.91636059567 + 1.27398391917i$
 $-1.91636059567 - 1.27398391917i$
 -2.76367330347
 $-0.799073204161 + 2.85720183887i$
 $-0.799073204161 - 2.85720183887i$
 3.01592252217

 **z -coordinates**

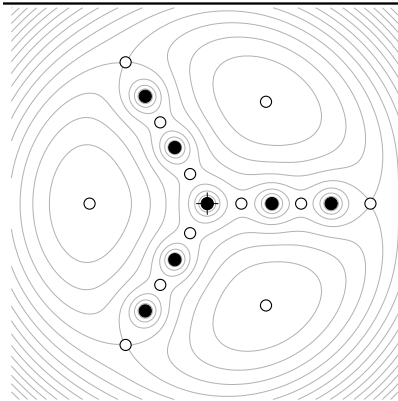
0.586184503848
 -0.586184503848
 $1.15041725318i$
 $-1.15041725318i$
 1.72828851475
 -1.72828851475
 $1.39331395156 + 1.78150967812i$
 $-1.39331395156 + 1.78150967812i$
 $1.39331395156 - 1.78150967812i$
 $-1.39331395156 - 1.78150967812i$
 $2.79311407814i$
 $-2.79311407814i$
 3.06505652595
 -3.06505652595

 **z -coordinates**

$-0.449796483003 + 0.545782008991i$
 $-0.449796483003 - 0.545782008991i$
 $0.740872744867 + 0.782045605613i$
 $0.740872744867 - 0.782045605613i$
 1.13394216385
 1.43297323091
 $-0.692034969625 + 1.62378418459i$
 $-0.692034969625 - 1.62378418459i$
 -2.26806600875
 $0.990638650451 + 2.06703799506i$
 $0.990638650451 - 2.06703799506i$
 2.40624526795
 $2.35187582821 + 1.41654199319i$
 $2.35187582821 - 1.41654199319i$
 $-1.12573419542 + 2.87538464474i$
 $-1.12573419542 - 2.87538464474i$

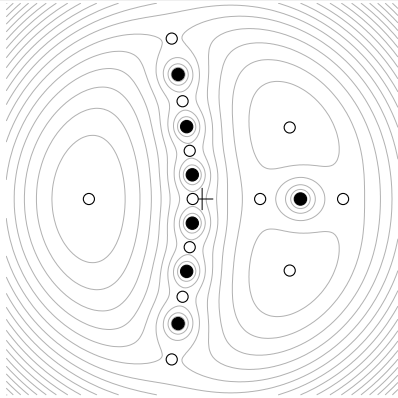
 **z -coordinates**

$-0.31686951325 + 0.554796383227i$
 $-0.31686951325 - 0.554796383227i$
 0.662129413117
 $-0.899062418588 + 1.52764753953i$
 $-0.899062418588 - 1.52764753953i$
 1.78435766995
 -2.22522710968
 $1.09833527661 + 1.93624306717i$
 $1.09833527661 - 1.93624306717i$
 $-1.56738309262 + 2.65786982194i$
 $-1.56738309262 - 2.65786982194i$
 3.09313235803



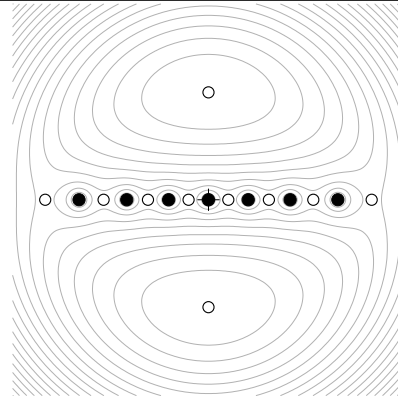
z -coordinates

0.646747064693
 $-0.323373532346 + 0.560099387847i$
 $-0.323373532346 - 0.560099387847i$
1.77654798524
 $-0.888273992619 + 1.53853568626i$
 $-0.888273992619 - 1.53853568626i$
 -2.22576006183
 $1.11288003092 + 1.92756475628i$
 $1.11288003092 - 1.92756475628i$
3.08813326995
 $-1.54406663497 + 2.67440186204i$
 $-1.54406663497 - 2.67440186204i$



z -coordinates

-0.184756527274
 $-0.244040091888 + 0.949709034482i$
 $-0.244040091888 - 0.949709034482i$
1.14354953657
 $-0.384034941573 + 1.92622123329i$
 $-0.384034941573 - 1.92622123329i$
 $1.72502669308 + 1.40810872677i$
 $1.72502669308 - 1.40810872677i$
 -2.2288632019
2.77593365871
 $-0.596963564842 + 3.15826169915i$
 $-0.596963564842 - 3.15826169915i$



z -coordinates

0.406782010086
 -0.406782010086
1.23987048181
 -1.23987048181
2.14792799503
 -2.14792799503
2.20005002618i
 $-2.20005002618i$
3.34419720004
 -3.34419720004

Figures of continuation of vortex crystals in the plane

The results by growing relative equilibria using co-rotating points, as described in Section 4.2, are given in the succeeding. The black dots denotes the point vortices at the start, whereas the red dots denotes the point vortices at the end. The open circles denotes the co-rotating point, for which the circulation is applied to, and the lines denotes the solution paths, as the circulation γ is increased. For every configuration γ is increased from 0 to 1 or 1 to 0 with 1000 steps. The plus denotes the center of rotation.

Only one example is shown when several configurations are identical by rotation or mirroring.

C.1 Continuation from $N = 2$ to $N = 3$

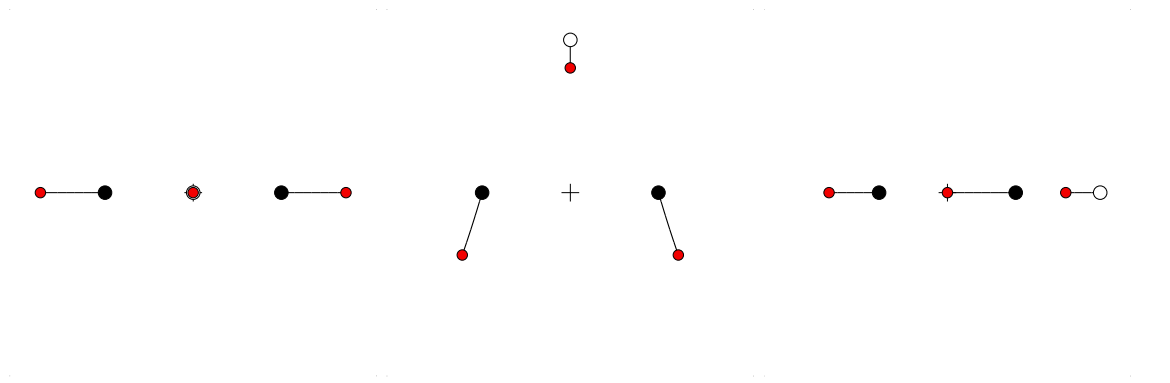


Figure C.1

Figure C.2

Figure C.3

C.2 Continuation from $N = 3$ to $N = 2$

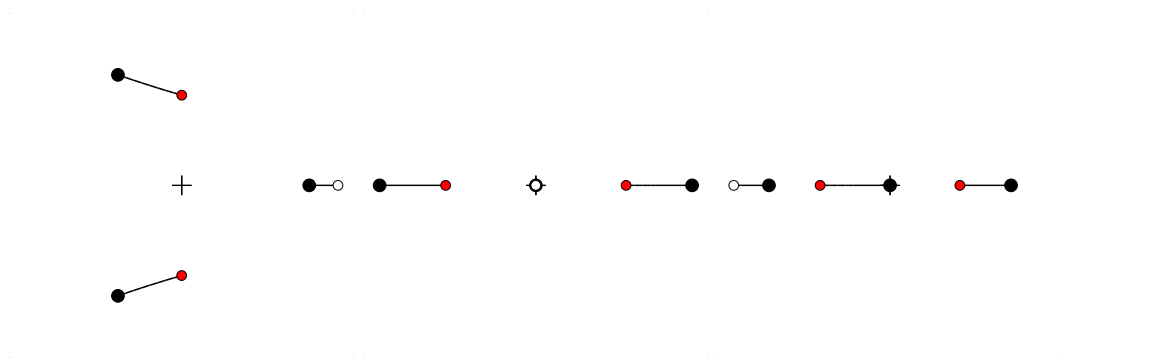


Figure C.4

Figure C.5

Figure C.6

C.3 Continuation from $N = 3$ to $N = 4$

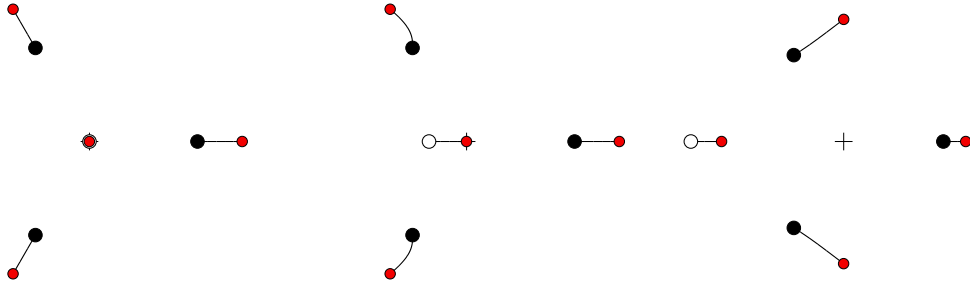


Figure C.7

Figure C.8

Figure C.9

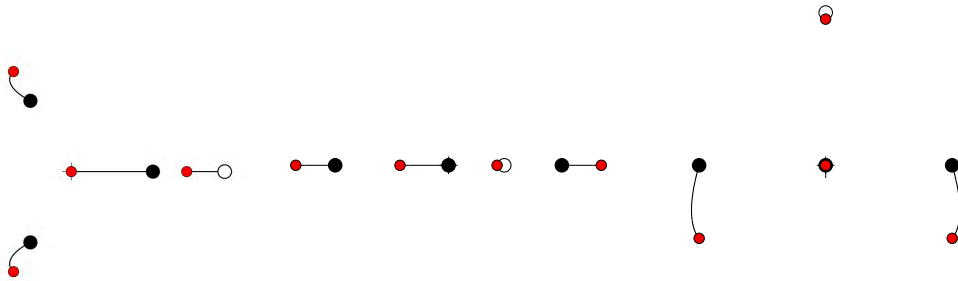


Figure C.10

Figure C.11

Figure C.12



Figure C.13

C.4 Continuation from $N = 4$ to $N = 3$

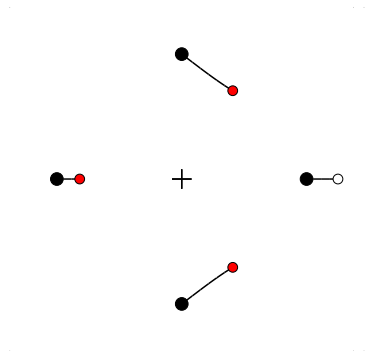


Figure C.14

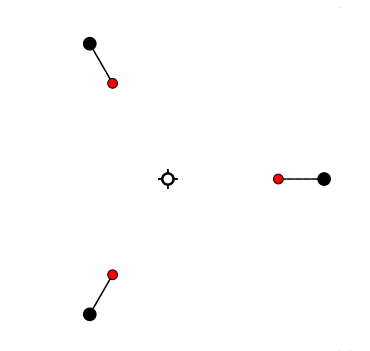


Figure C.15

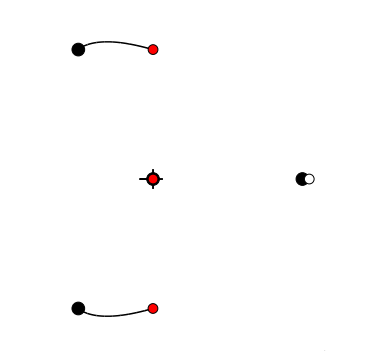


Figure C.16

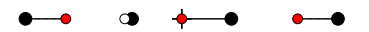


Figure C.17

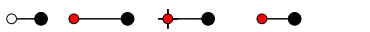


Figure C.18

C.5 Continuation from $N = 4$ to $N = 5$

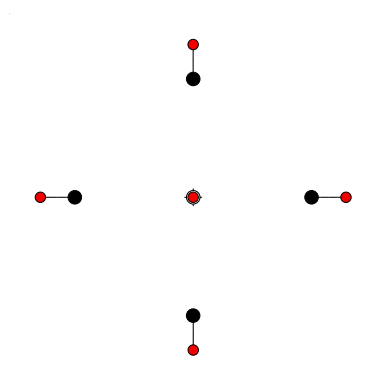


Figure C.19

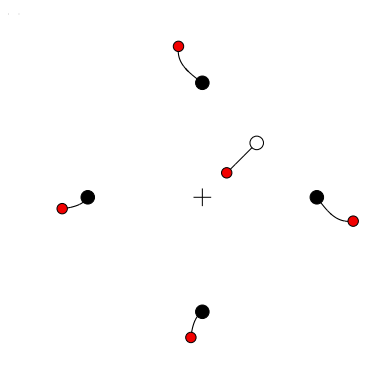


Figure C.20

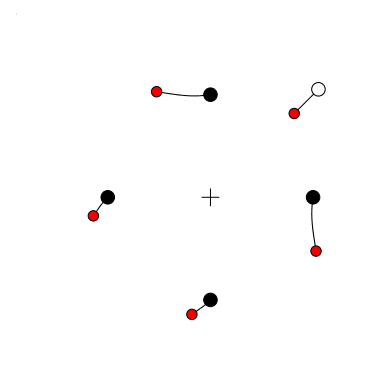


Figure C.21

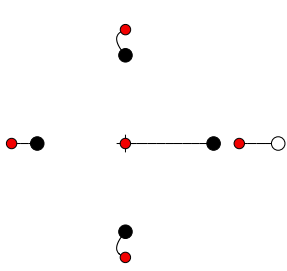


Figure C.22

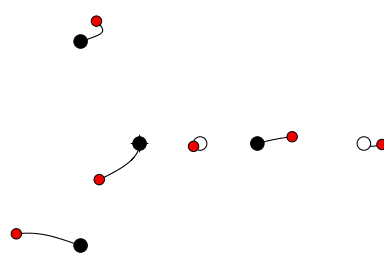


Figure C.23

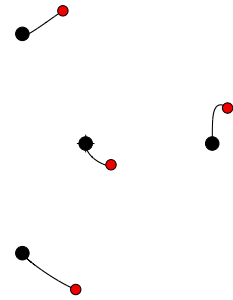


Figure C.24

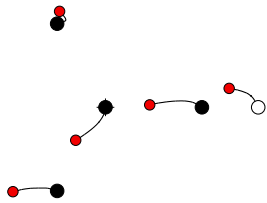


Figure C.25



Figure C.26

Figure C.27

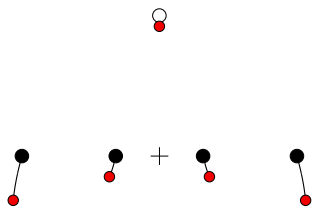


Figure C.28



Figure C.29

C.6 Continuation from $N = 5$ to $N = 4$

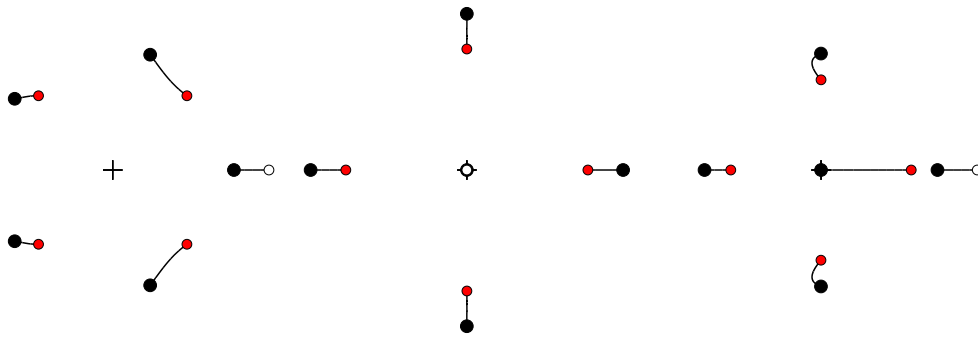


Figure C.30



Figure C.31

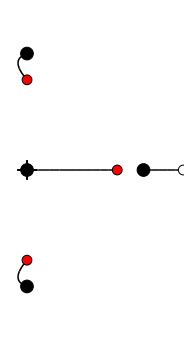


Figure C.32

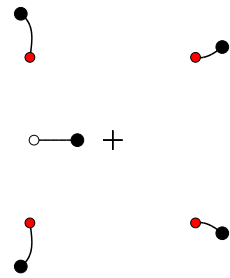


Figure C.33

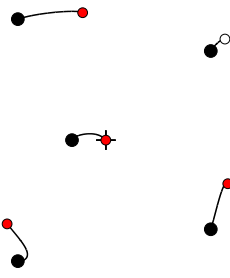


Figure C.34

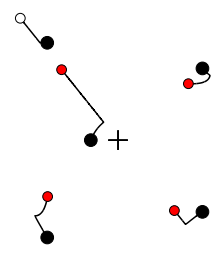


Figure C.35

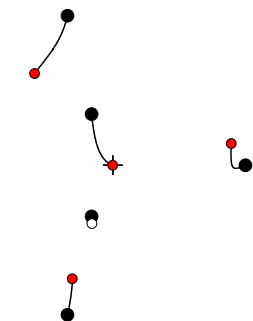


Figure C.36

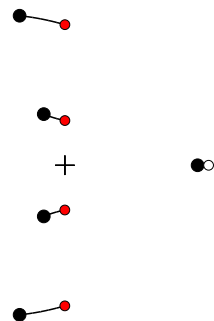


Figure C.37

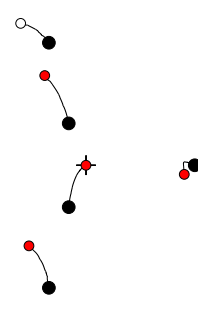


Figure C.38



Figure C.39

Figure C.40

Figure C.41

C.7 Continuation from $N = 5$ to $N = 6$

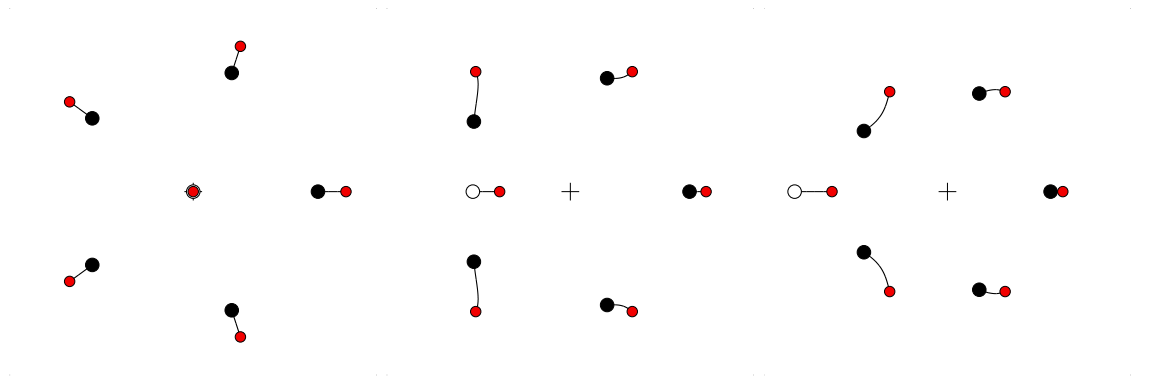


Figure C.42

Figure C.43

Figure C.44

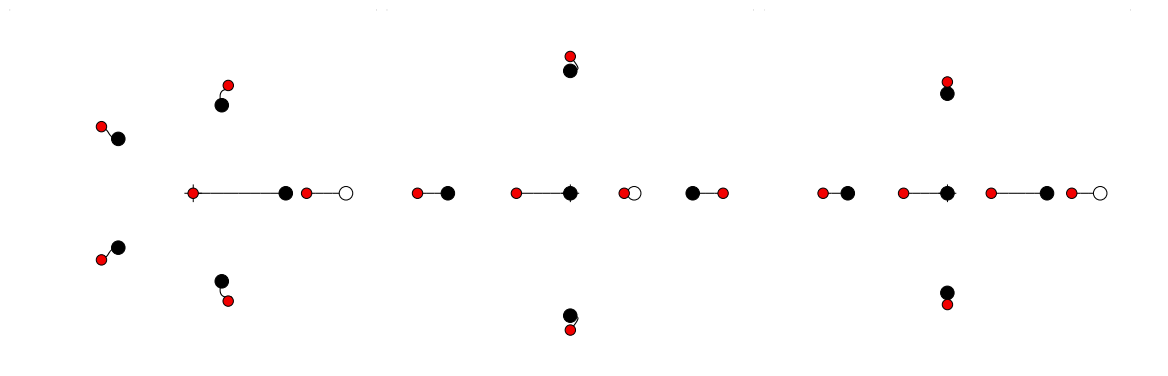


Figure C.45

Figure C.46

Figure C.47

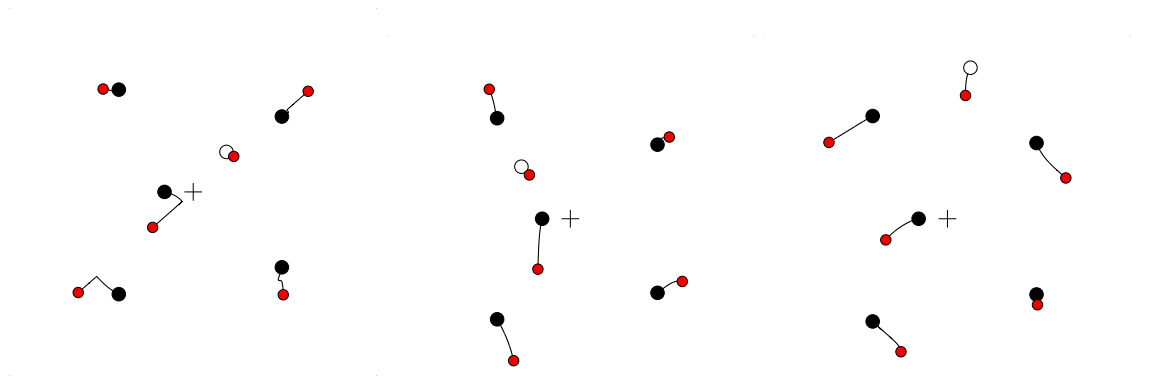


Figure C.48

Figure C.49

Figure C.50

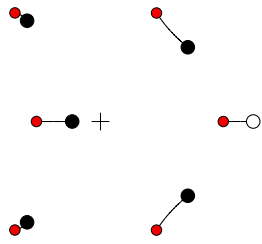


Figure C.51

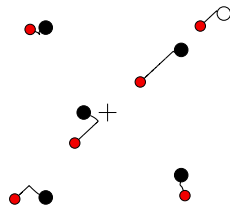


Figure C.52

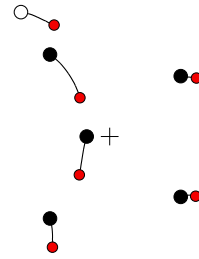


Figure C.53

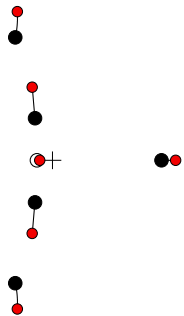


Figure C.54

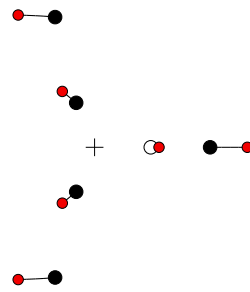


Figure C.55

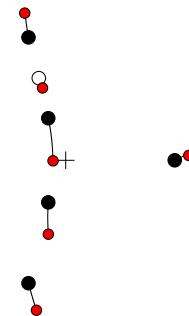


Figure C.56

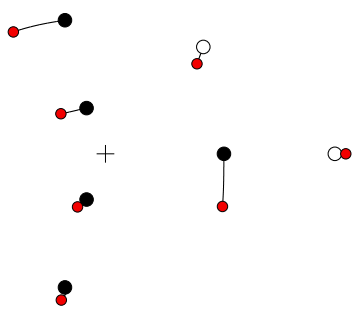


Figure C.57

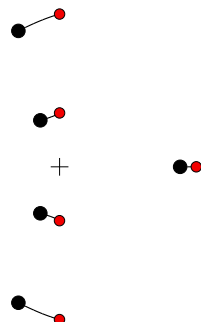


Figure C.58

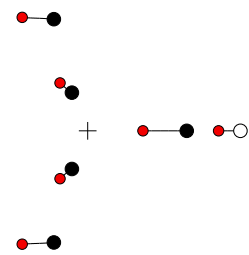


Figure C.59

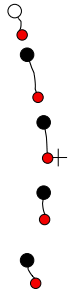


Figure C.60



Figure C.61



Figure C.62

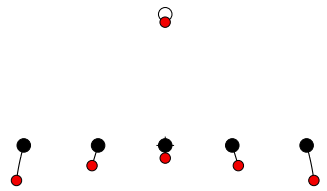


Figure C.63



Figure C.64

C.8 Continuation from $N = 6$ to $N = 5$

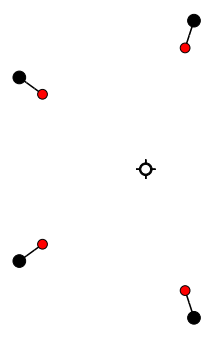


Figure C.65

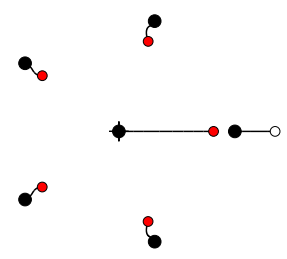


Figure C.66

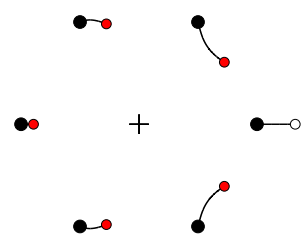


Figure C.67

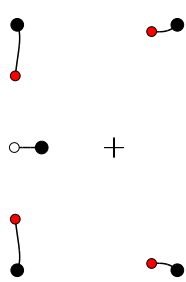


Figure C.68

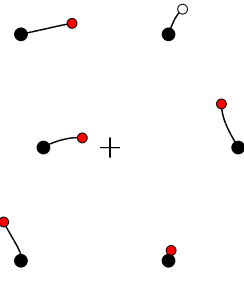


Figure C.69

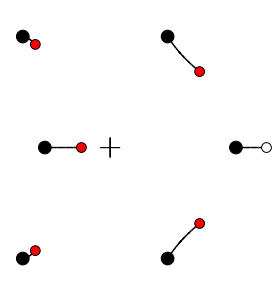


Figure C.70

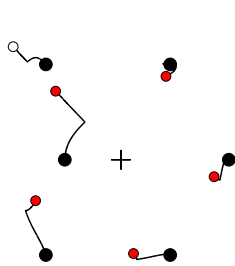


Figure C.71

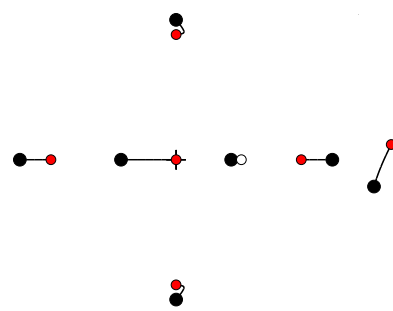


Figure C.72

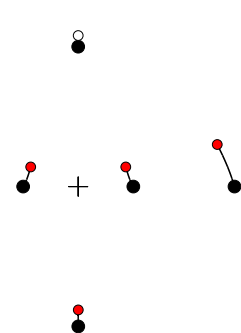


Figure C.73

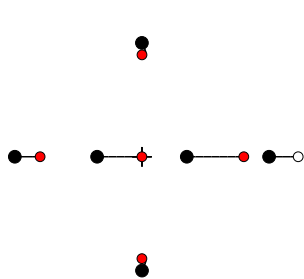


Figure C.74

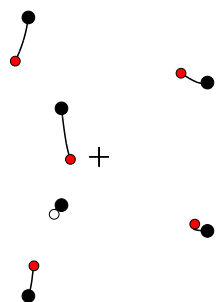


Figure C.75

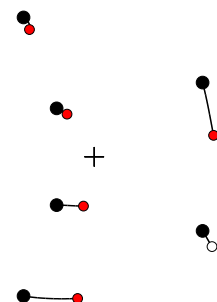


Figure C.76

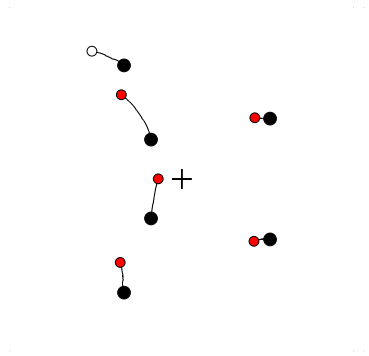


Figure C.77

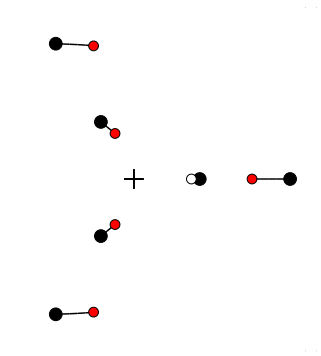


Figure C.78

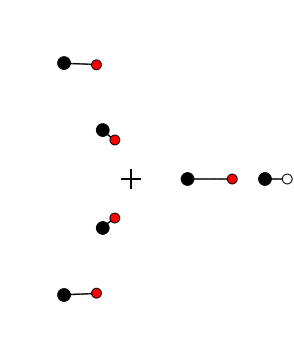


Figure C.79

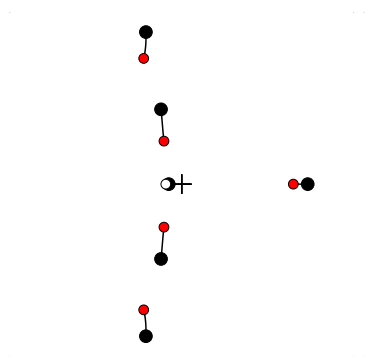


Figure C.80

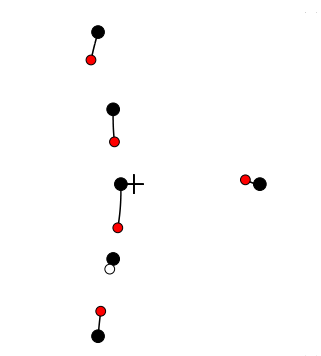


Figure C.81

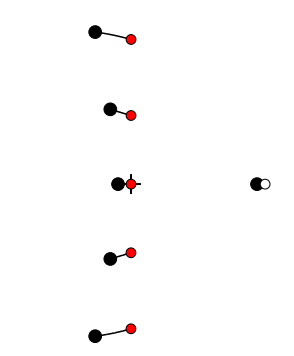


Figure C.82

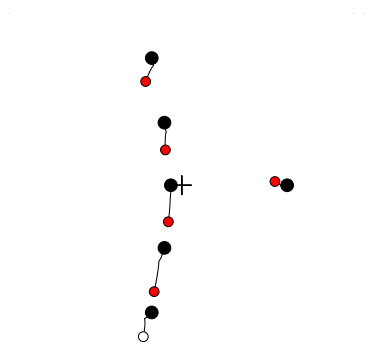


Figure C.83

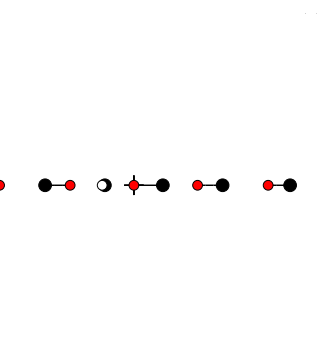


Figure C.84

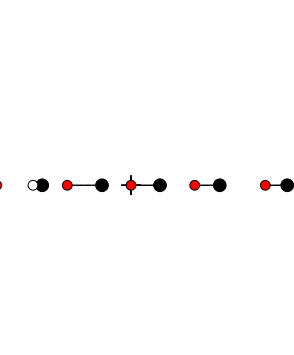


Figure C.85



Figure C.86

C.9 Continuation from $N = 6$ to $N = 7$

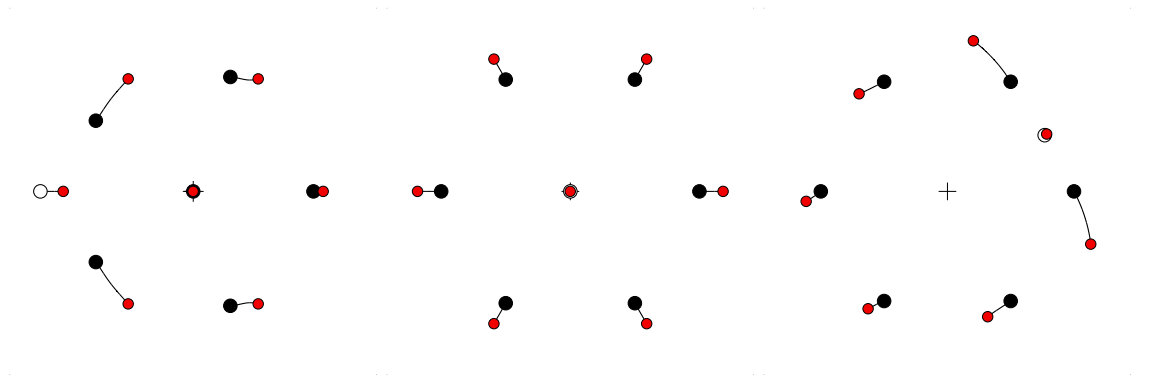


Figure C.87

Figure C.88

Figure C.89

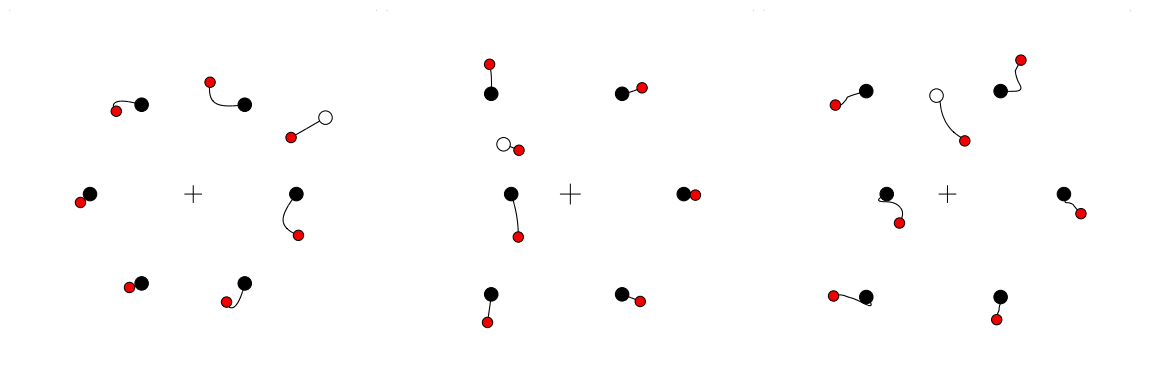


Figure C.90

Figure C.91

Figure C.92

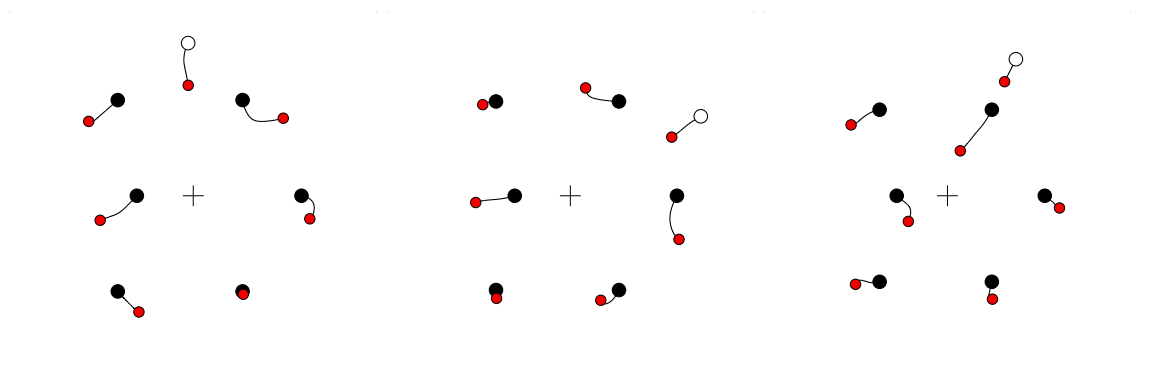


Figure C.93

Figure C.94

Figure C.95

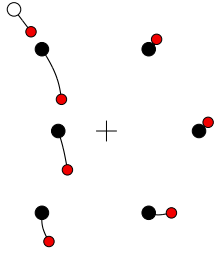


Figure C.96

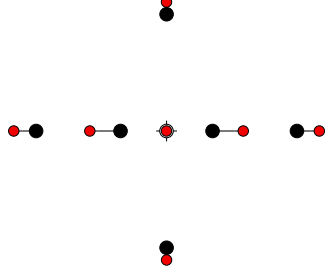


Figure C.97

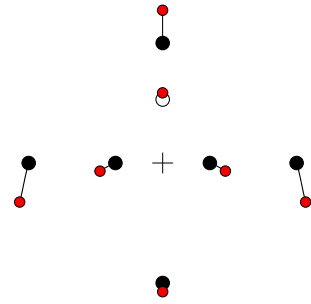


Figure C.98

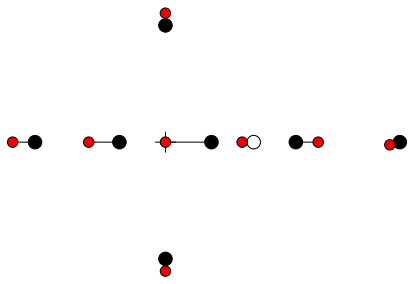


Figure C.99

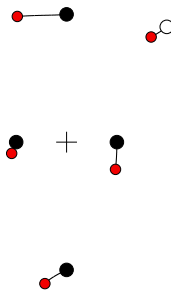


Figure C.100

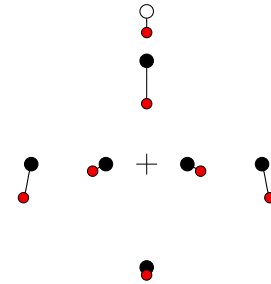


Figure C.101

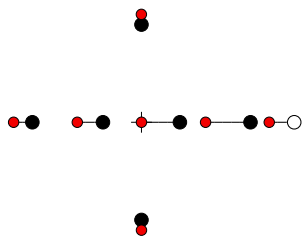


Figure C.102

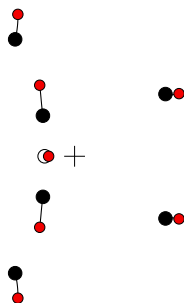


Figure C.103

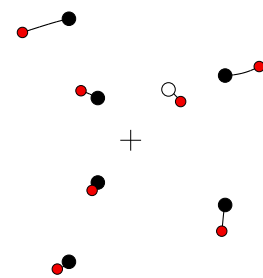


Figure C.104

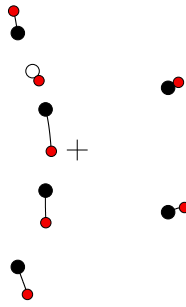


Figure C.105

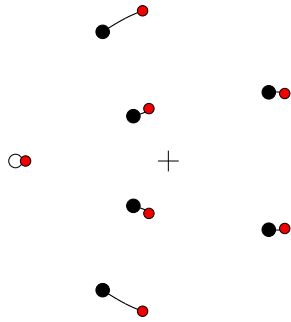


Figure C.106

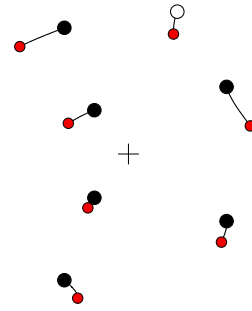


Figure C.107

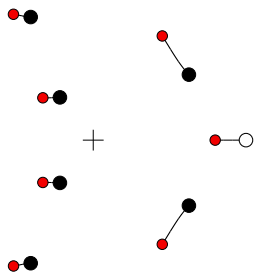


Figure C.108

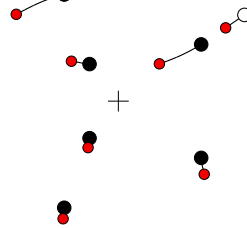


Figure C.109

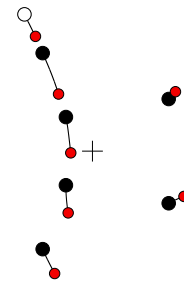


Figure C.110

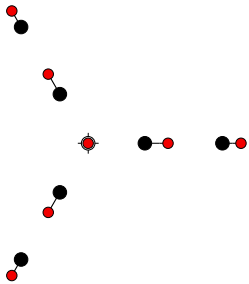


Figure C.111

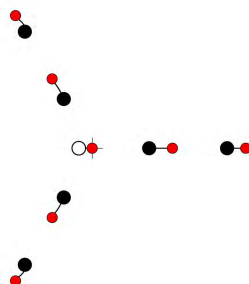


Figure C.112

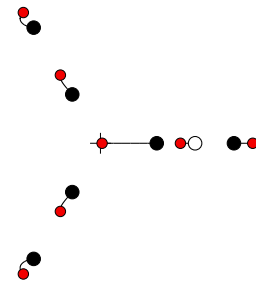


Figure C.113

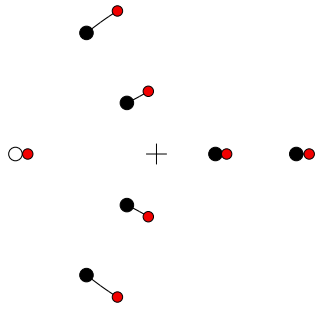


Figure C.114

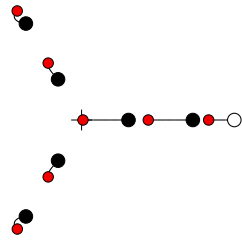


Figure C.115

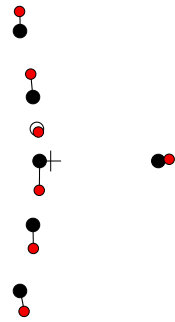


Figure C.116

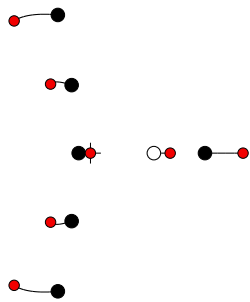


Figure C.117

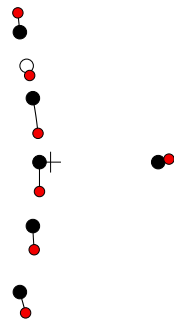


Figure C.118

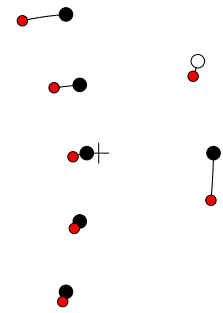


Figure C.119

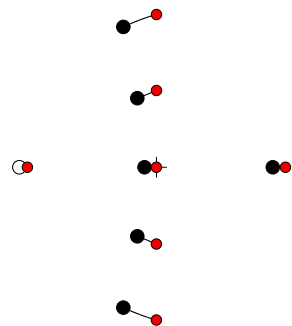


Figure C.120

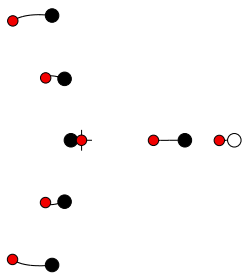


Figure C.121

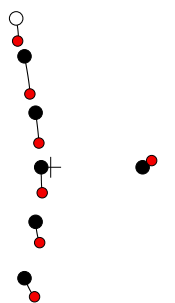


Figure C.122



Figure C.123



Figure C.124



Figure C.125

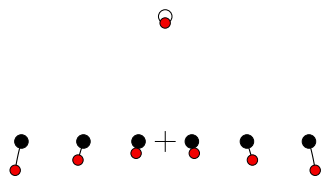


Figure C.126

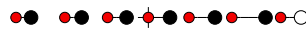


Figure C.127

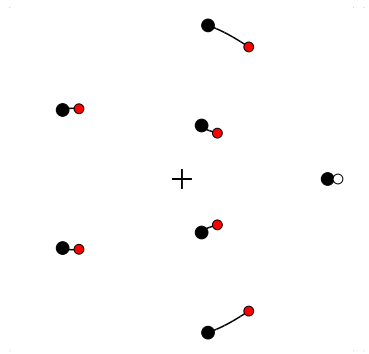


Figure C.137

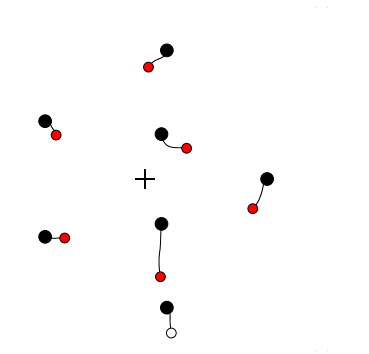


Figure C.138

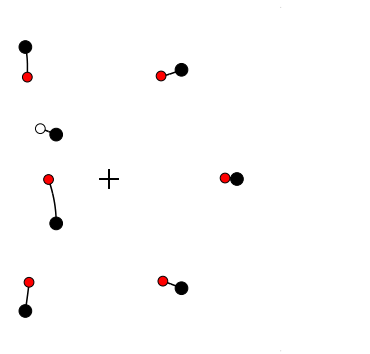


Figure C.139

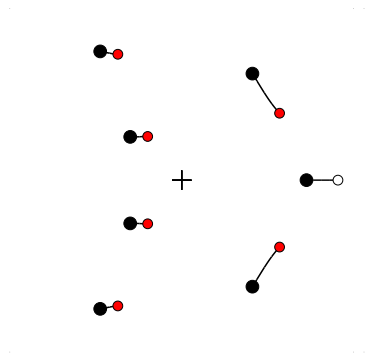


Figure C.140

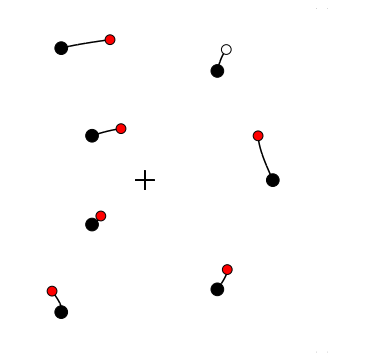


Figure C.141

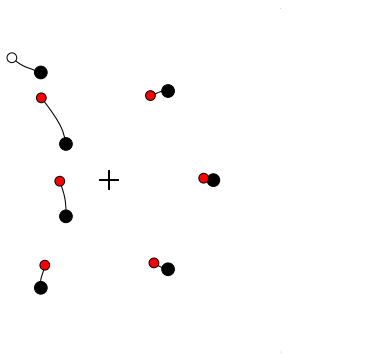


Figure C.142

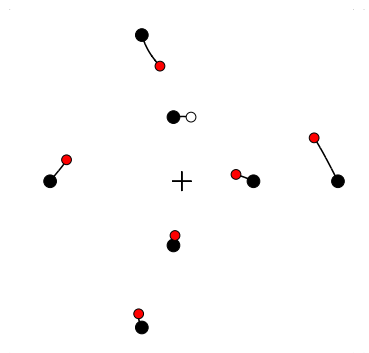


Figure C.143

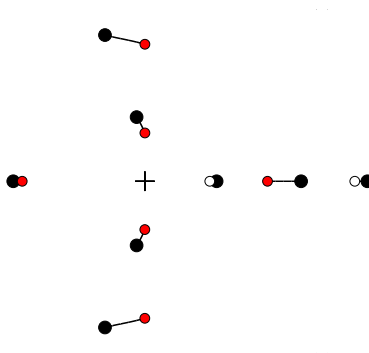


Figure C.144

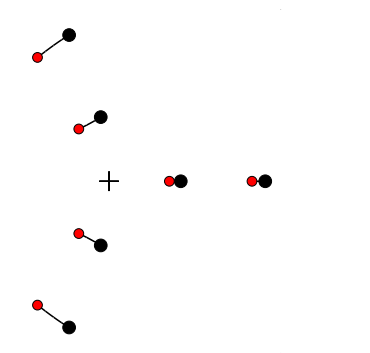


Figure C.145

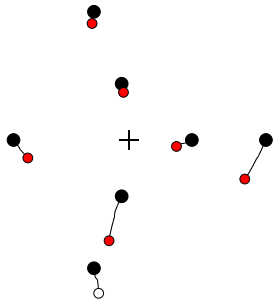


Figure C.146

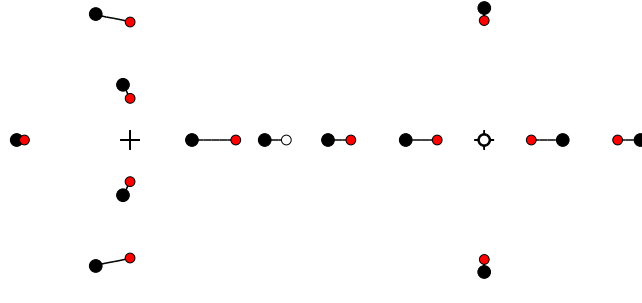


Figure C.147

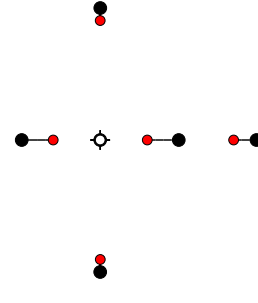


Figure C.148

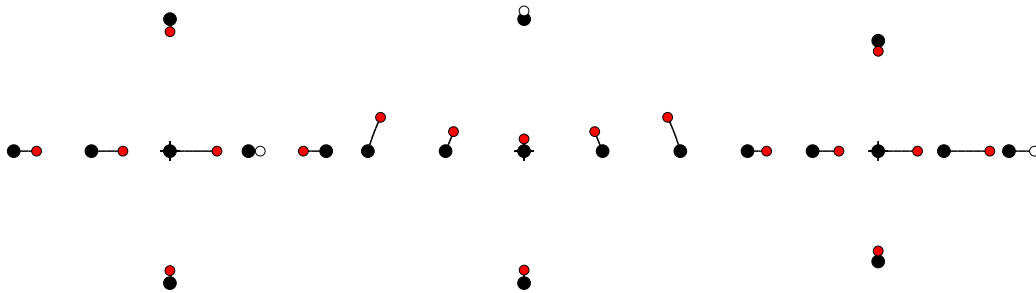


Figure C.149

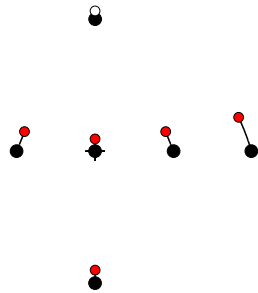


Figure C.150

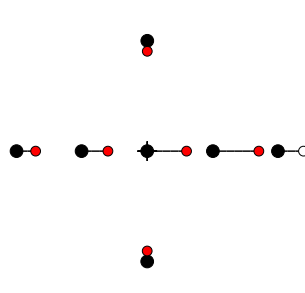


Figure C.151

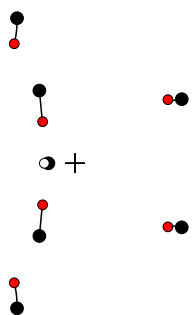


Figure C.152

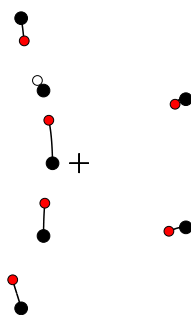


Figure C.153

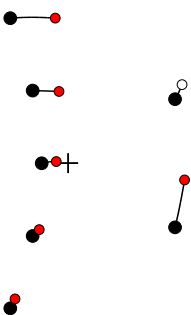


Figure C.154

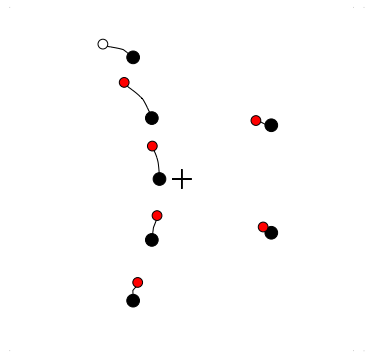


Figure C.155

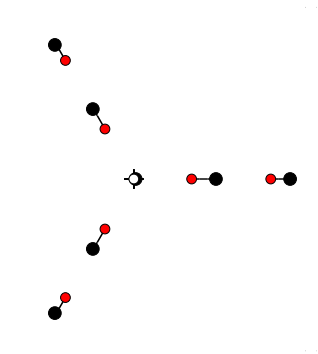


Figure C.156

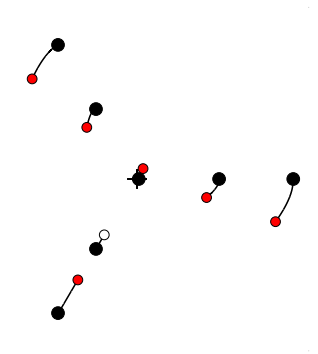


Figure C.157

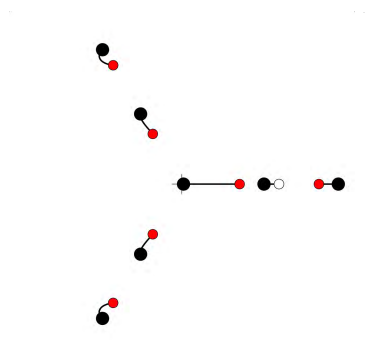


Figure C.158

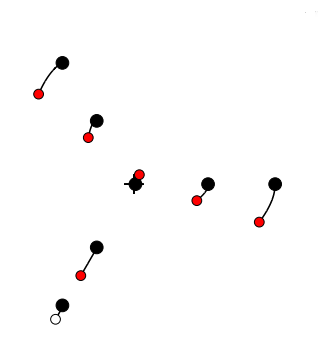


Figure C.159

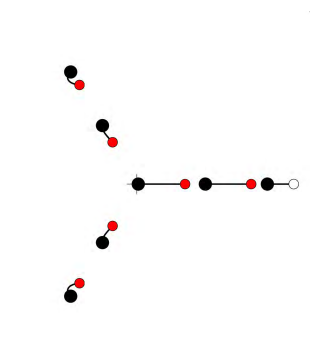


Figure C.160

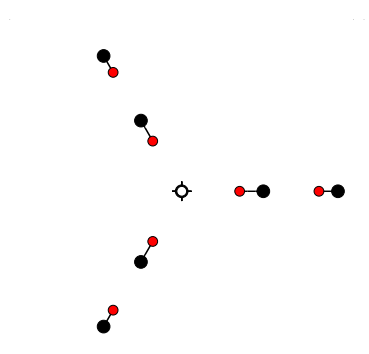


Figure C.161

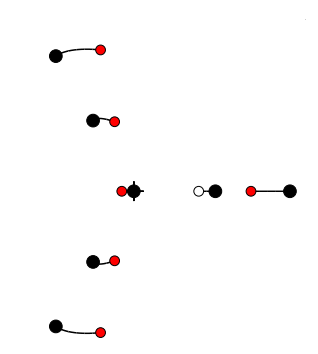


Figure C.162

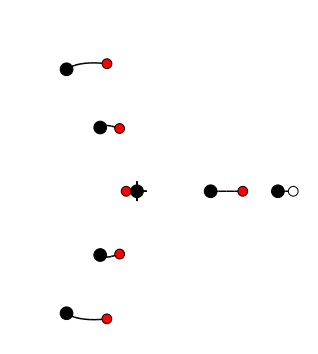


Figure C.163

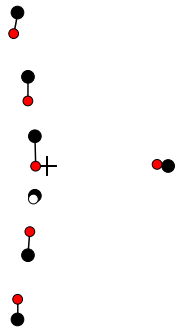


Figure C.164

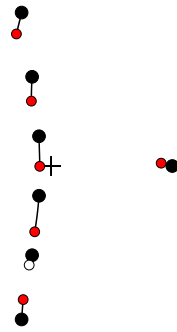


Figure C.165

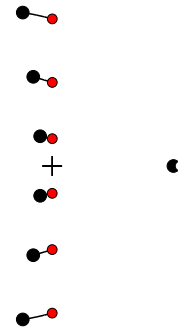


Figure C.166

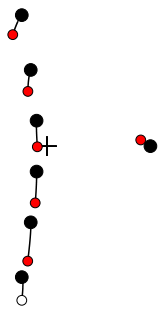


Figure C.167



Figure C.168

Figure C.169



Figure C.170

Figure C.171

C.11 Continuation from $N = 7$ to $N = 8$

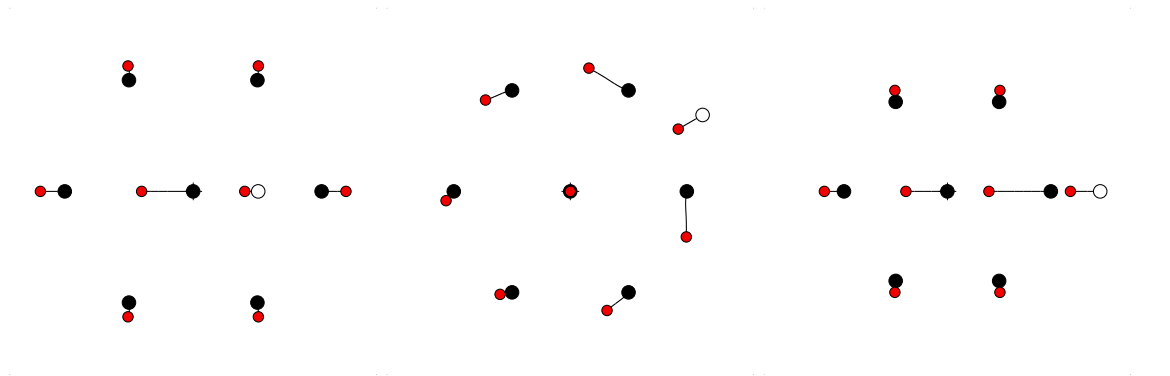


Figure C.172

Figure C.173

Figure C.174

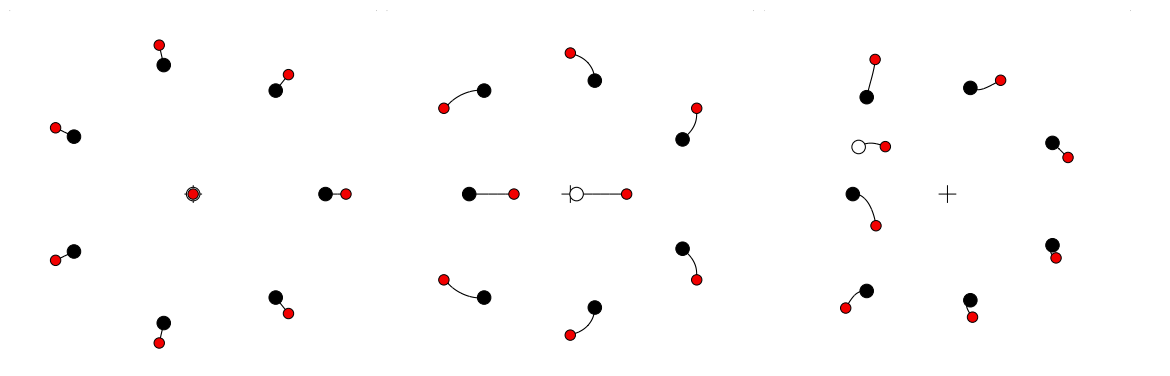


Figure C.175

Figure C.176

Figure C.177

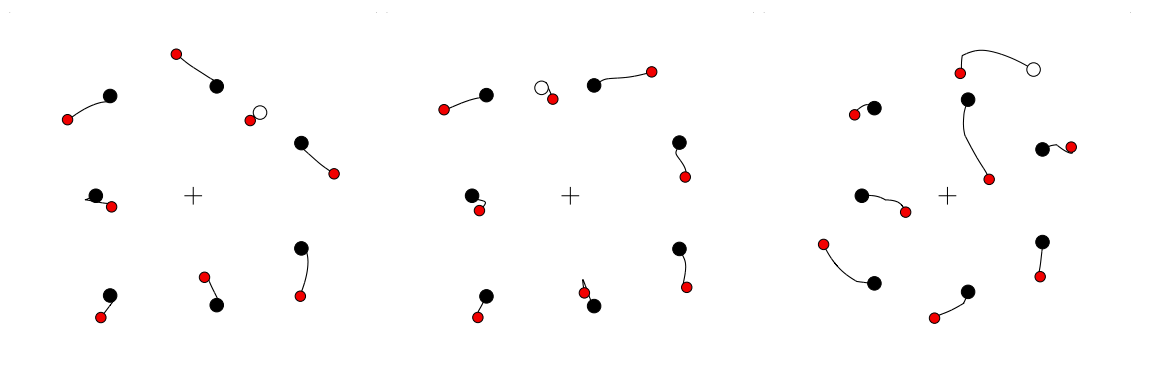


Figure C.178

Figure C.179

Figure C.180

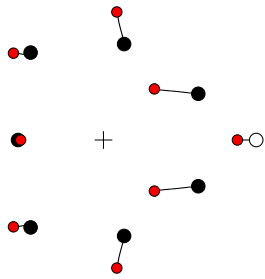


Figure C.181

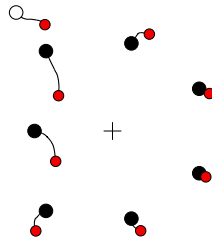


Figure C.182

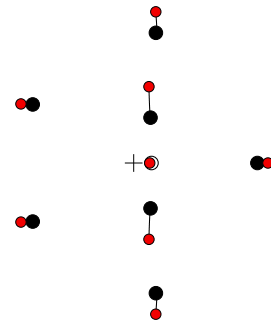


Figure C.183

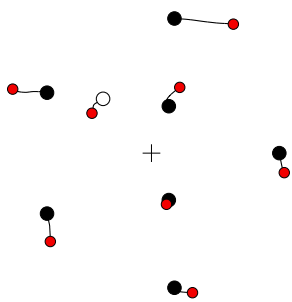


Figure C.184

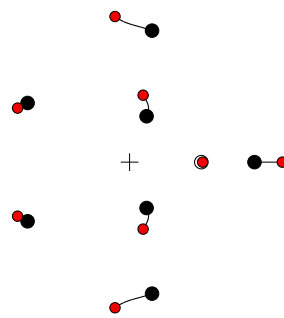


Figure C.185

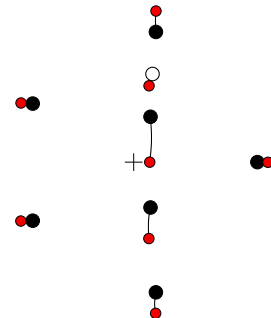


Figure C.186

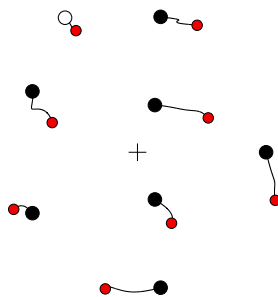


Figure C.187

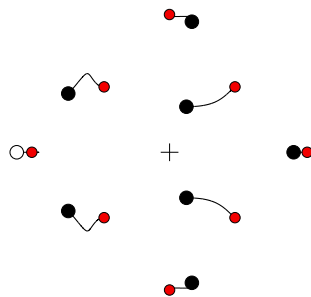


Figure C.188

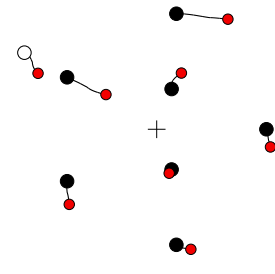


Figure C.189

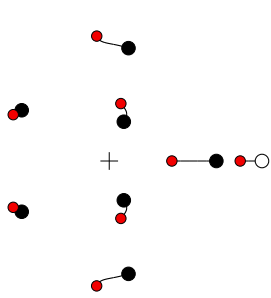


Figure C.190

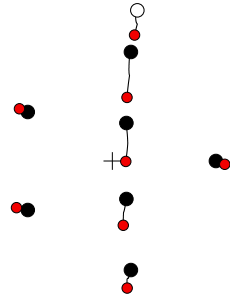


Figure C.191

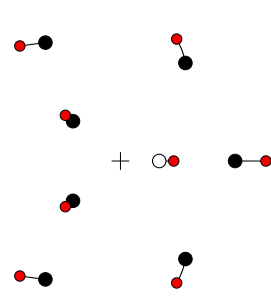


Figure C.192

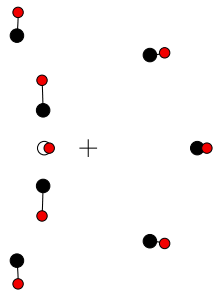


Figure C.193

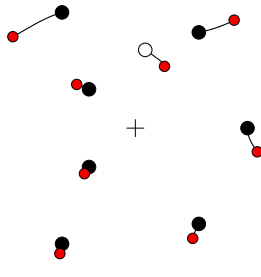


Figure C.194

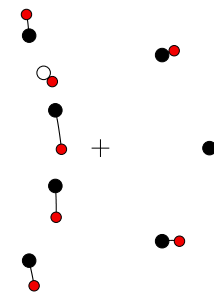


Figure C.195

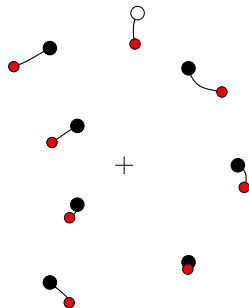


Figure C.196

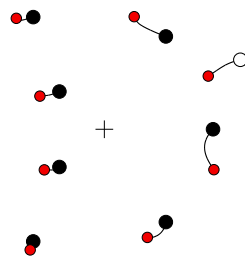


Figure C.197

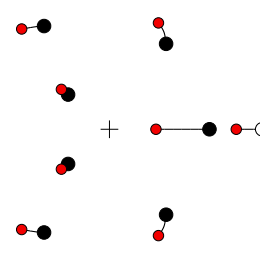


Figure C.198

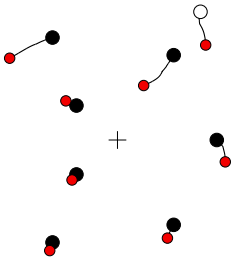


Figure C.199

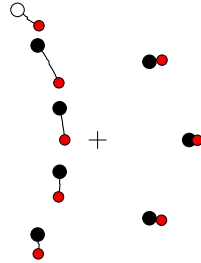


Figure C.200

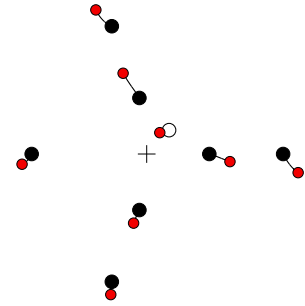


Figure C.201

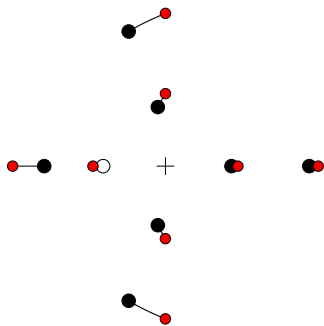


Figure C.202

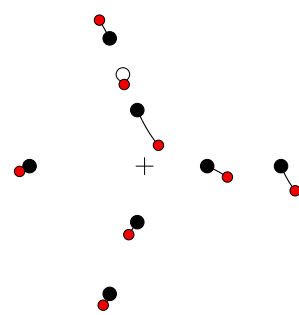


Figure C.203

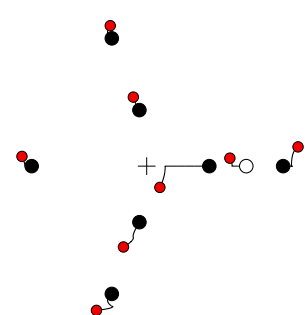


Figure C.204

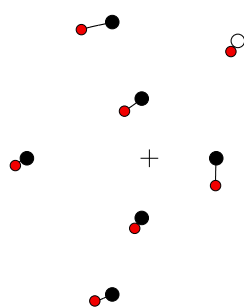


Figure C.205

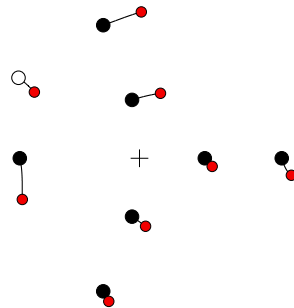


Figure C.206

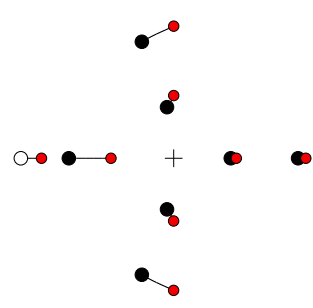


Figure C.207

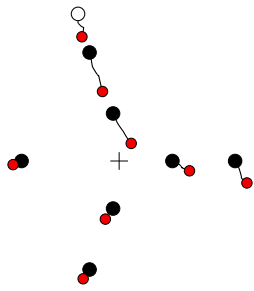


Figure C.208

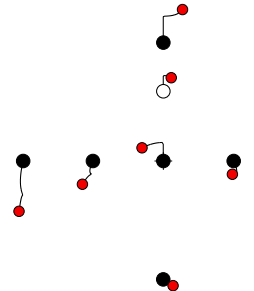


Figure C.209

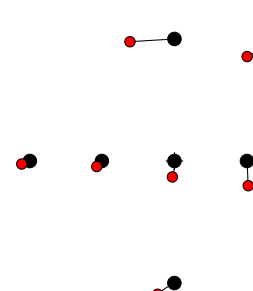


Figure C.210

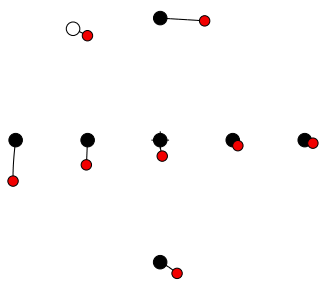


Figure C.211

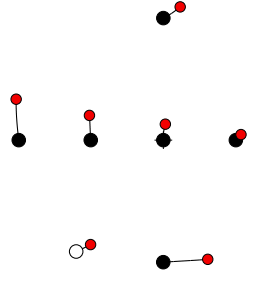


Figure C.212

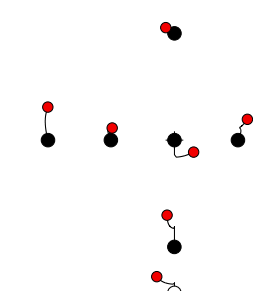


Figure C.213

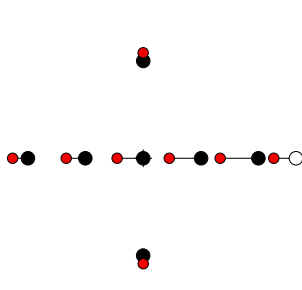


Figure C.214

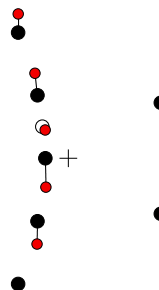


Figure C.215

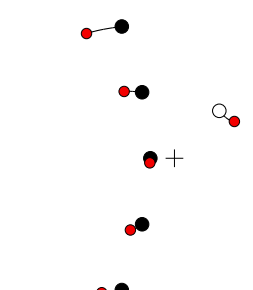


Figure C.216

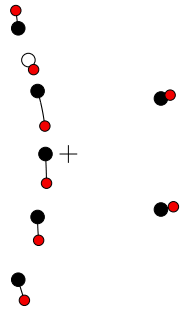


Figure C.217

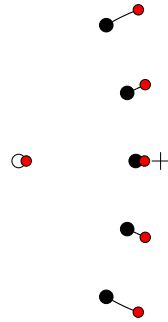


Figure C.218

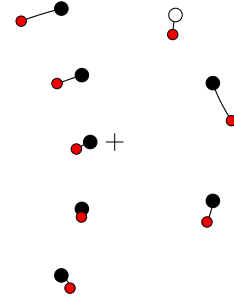


Figure C.219

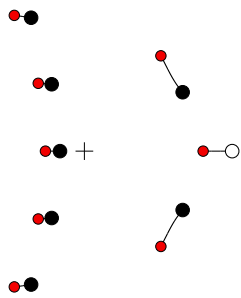


Figure C.220

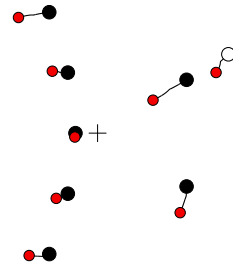


Figure C.221

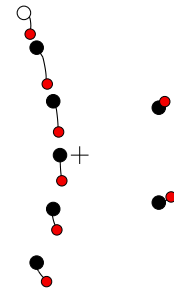


Figure C.222

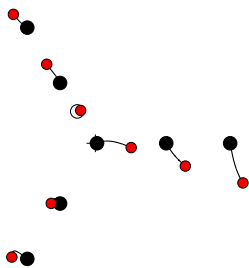


Figure C.223

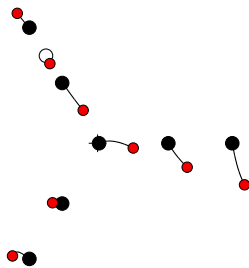


Figure C.224

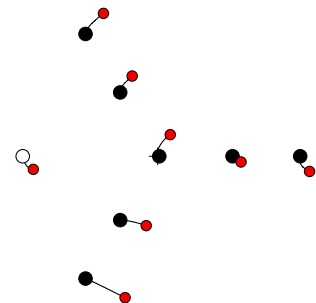


Figure C.225

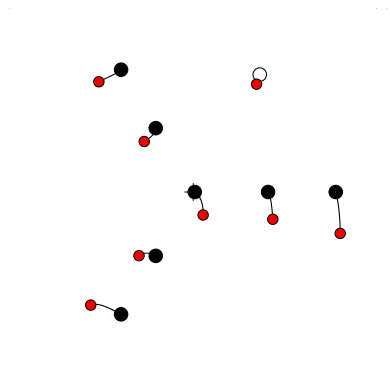


Figure C.226

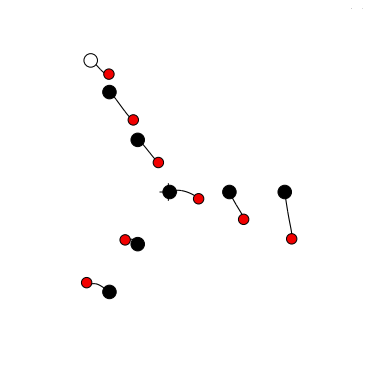


Figure C.227

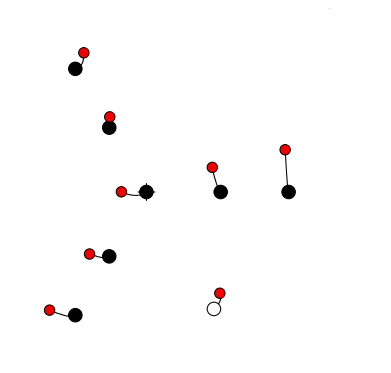


Figure C.228

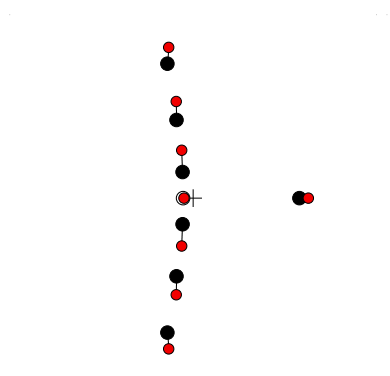


Figure C.229

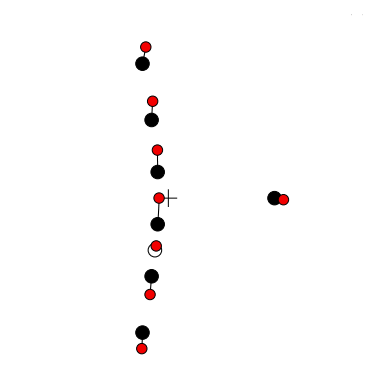


Figure C.230

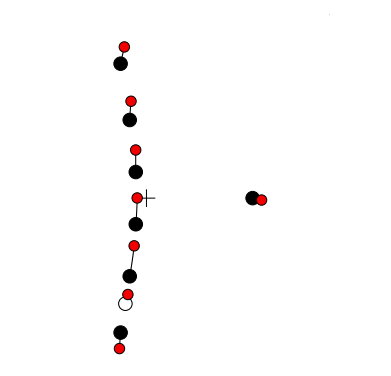


Figure C.231

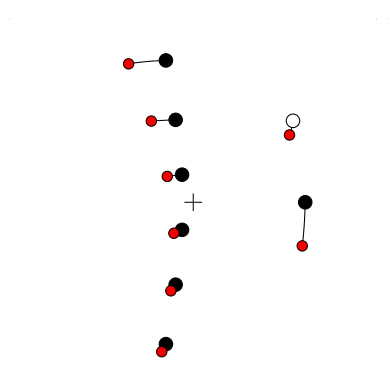


Figure C.232

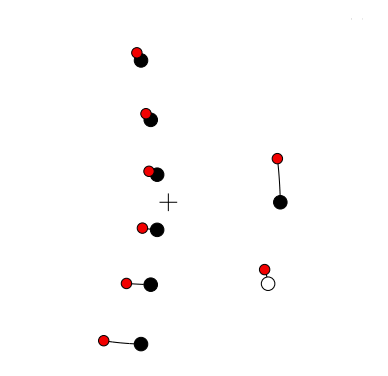


Figure C.233

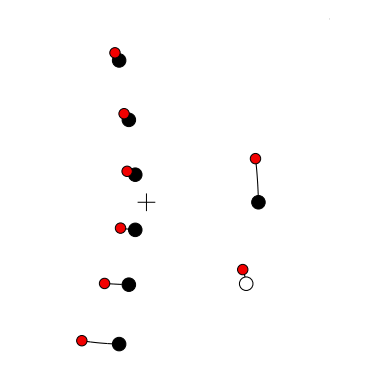


Figure C.234

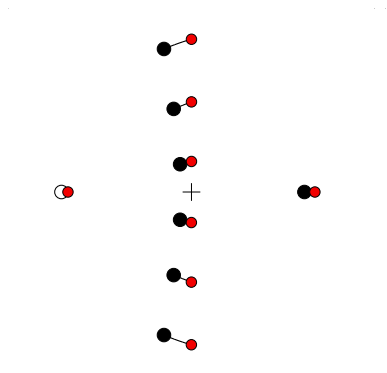


Figure C.235

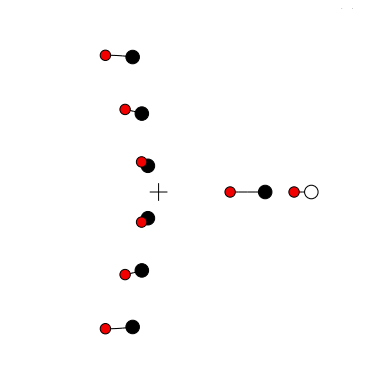


Figure C.236

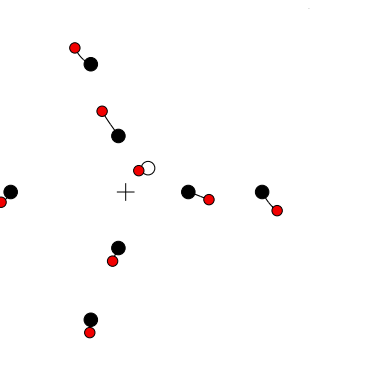


Figure C.237

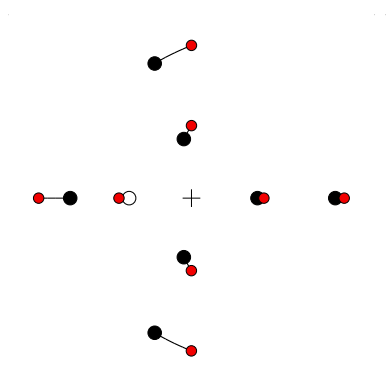


Figure C.238

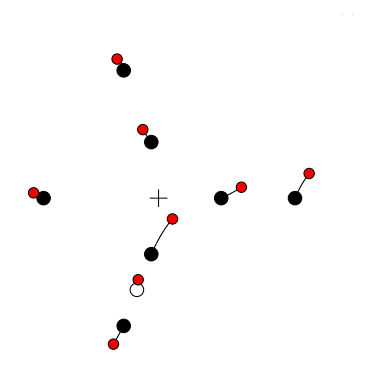


Figure C.239

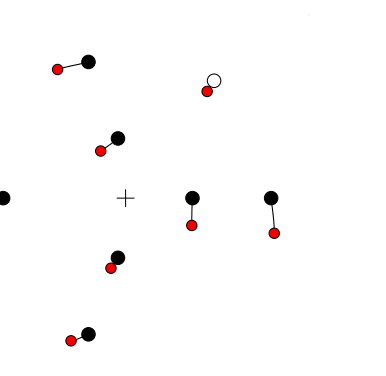


Figure C.240

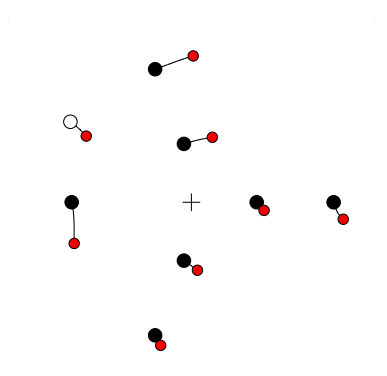


Figure C.241

C.12 Continuation from $N = 8$ to $N = 7$

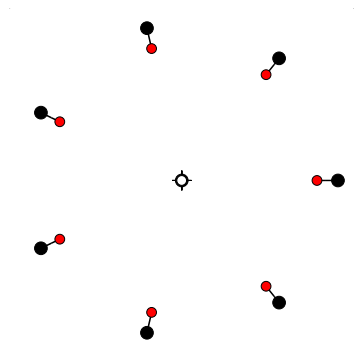


Figure C.242

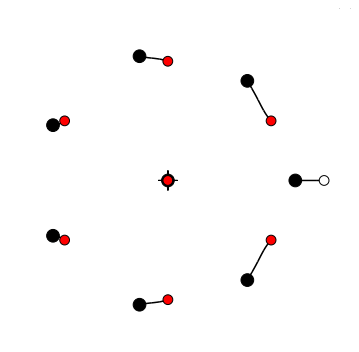


Figure C.243

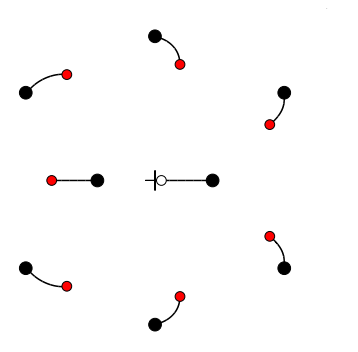


Figure C.244

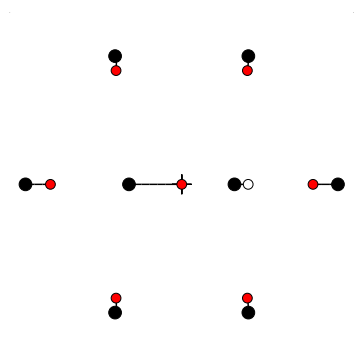


Figure C.245

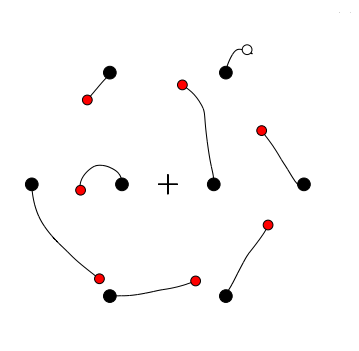


Figure C.246

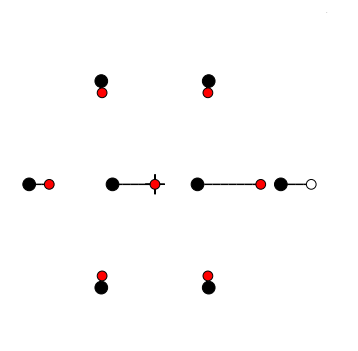


Figure C.247

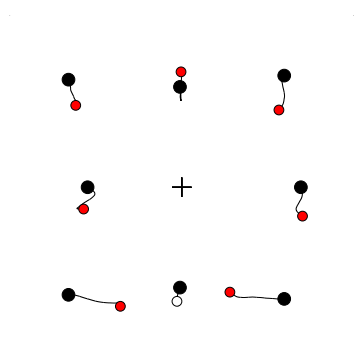


Figure C.248

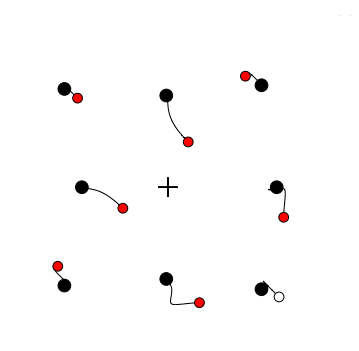


Figure C.249

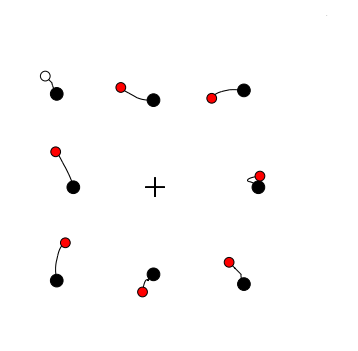


Figure C.250

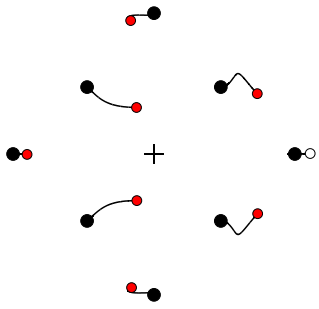


Figure C.251

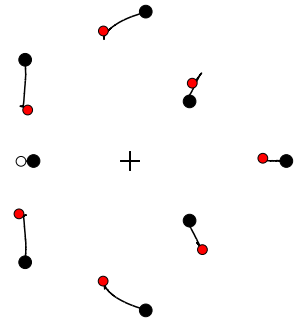


Figure C.252

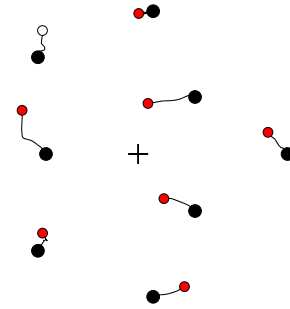


Figure C.253

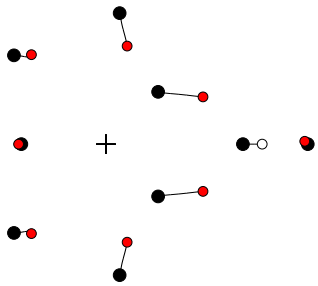


Figure C.254

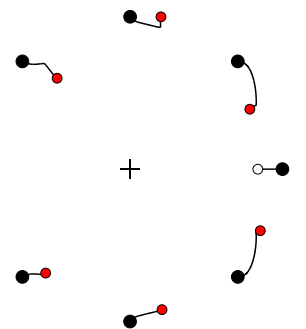


Figure C.255

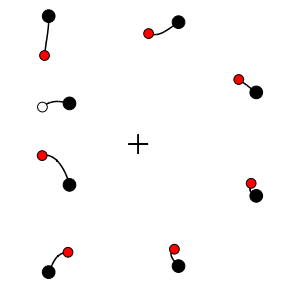


Figure C.256

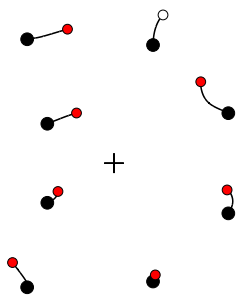


Figure C.257

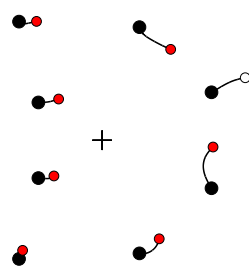


Figure C.258

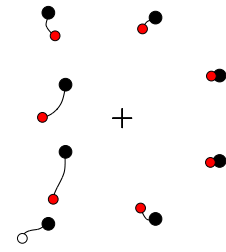


Figure C.259

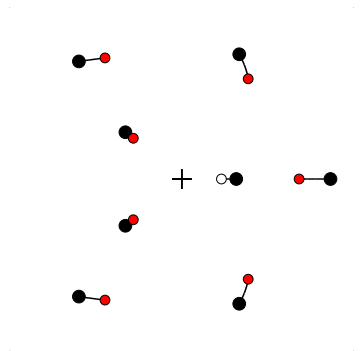


Figure C.260

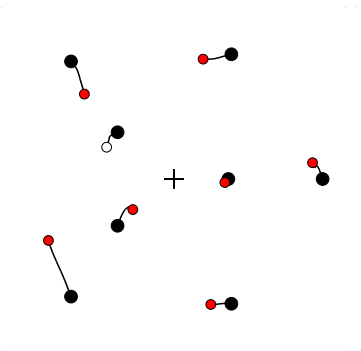


Figure C.261

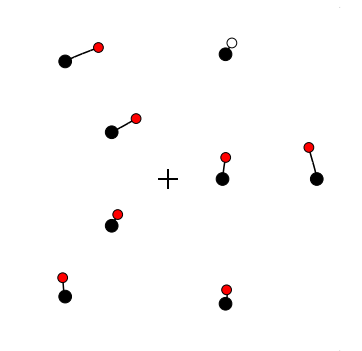


Figure C.262

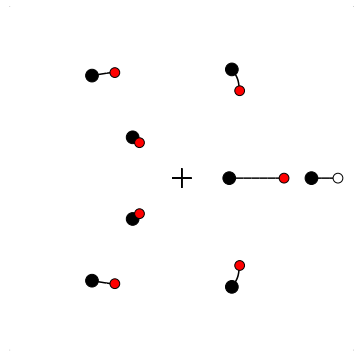


Figure C.263

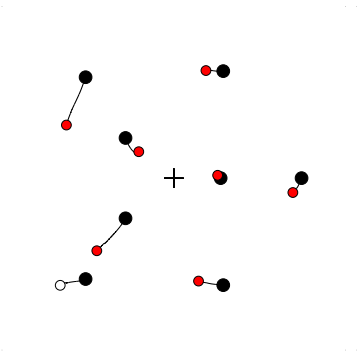


Figure C.264

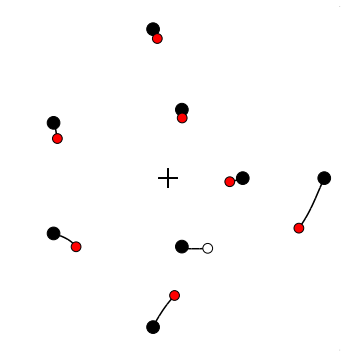


Figure C.265

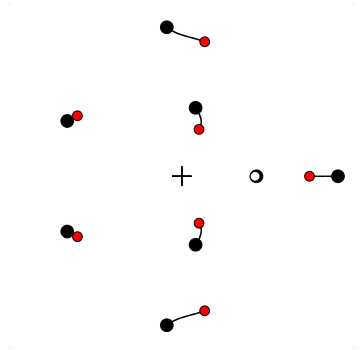


Figure C.266

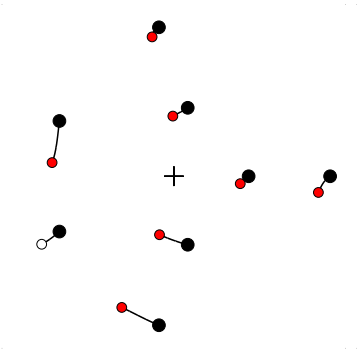


Figure C.267

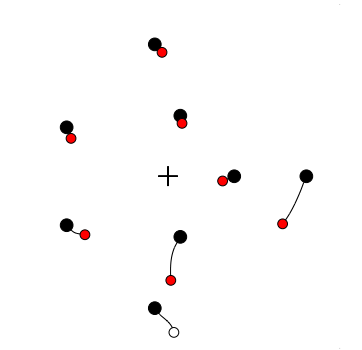


Figure C.268

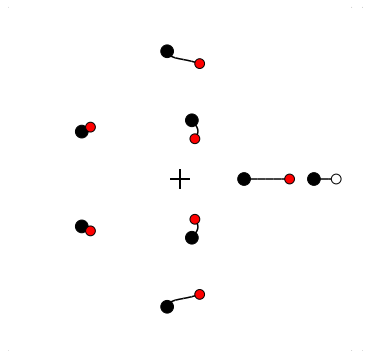


Figure C.269

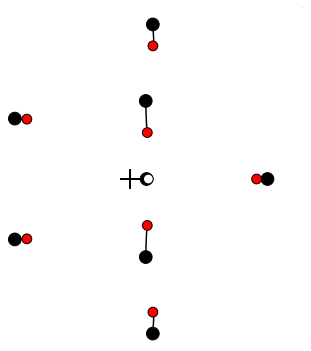


Figure C.270

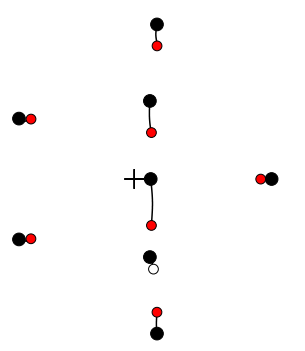


Figure C.271

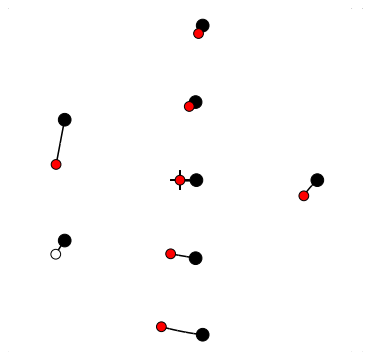


Figure C.272

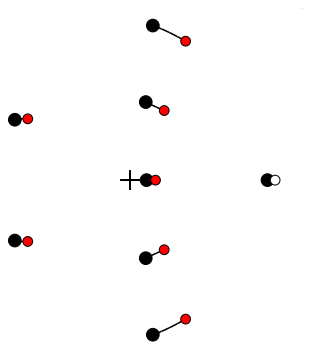


Figure C.273

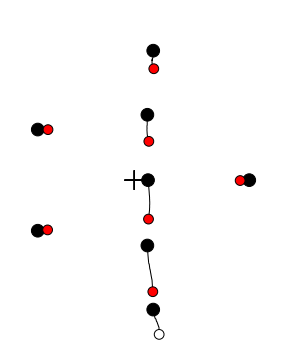


Figure C.274

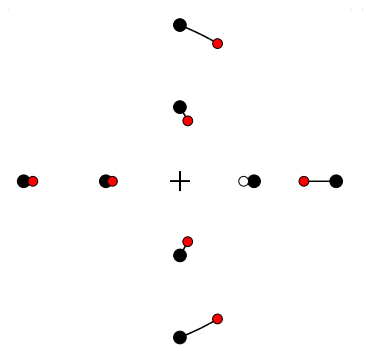


Figure C.275

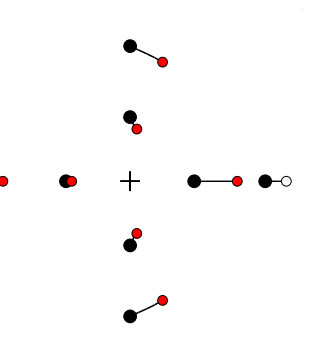


Figure C.276

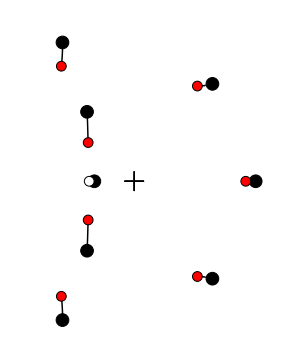


Figure C.277

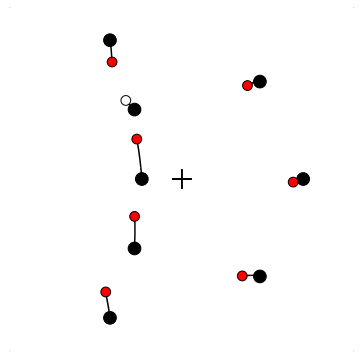


Figure C.278

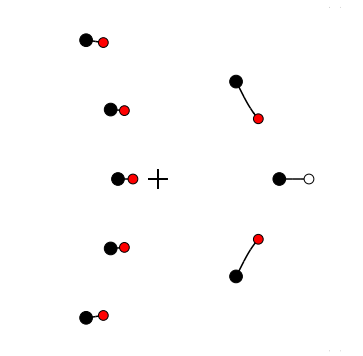


Figure C.279

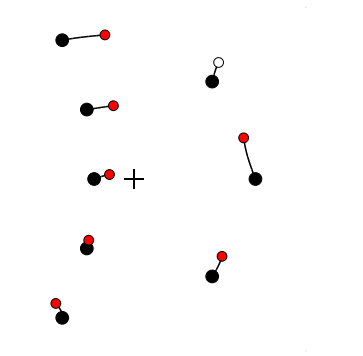


Figure C.280

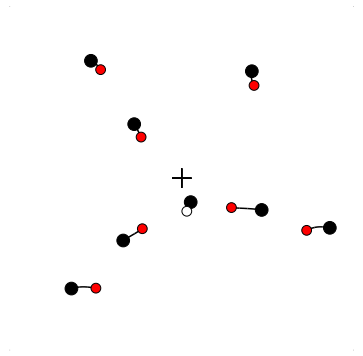


Figure C.281

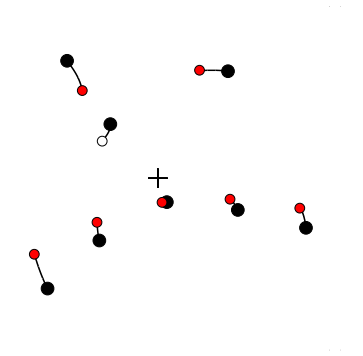


Figure C.282

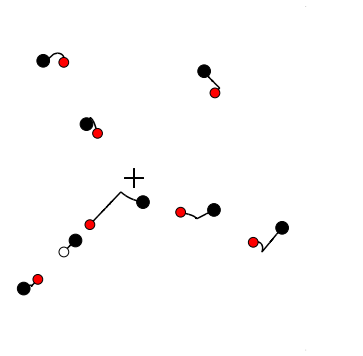


Figure C.283

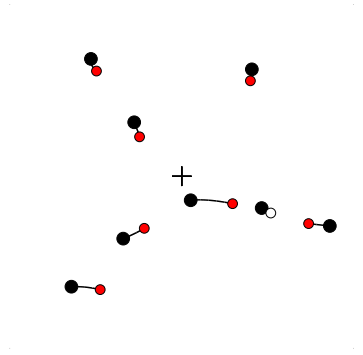


Figure C.284

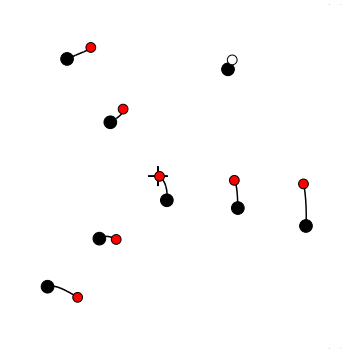


Figure C.285

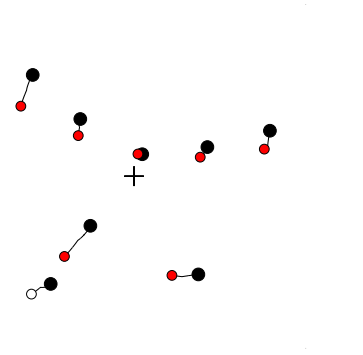


Figure C.286

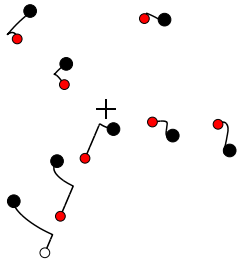


Figure C.287

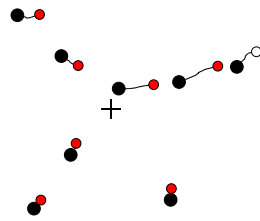


Figure C.288

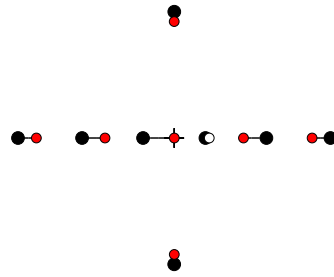


Figure C.289

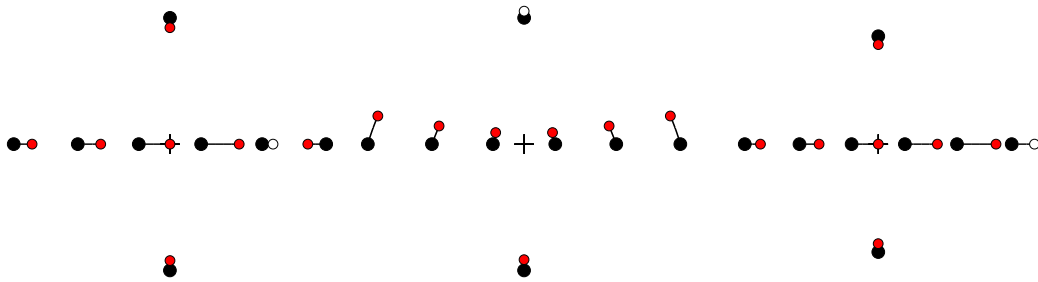


Figure C.290

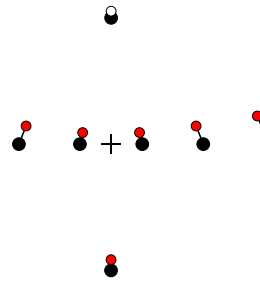


Figure C.291

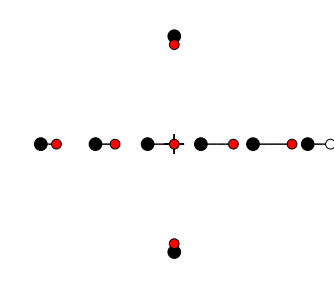


Figure C.292

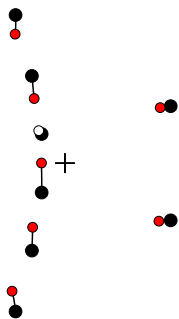


Figure C.293

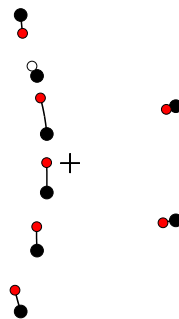


Figure C.294

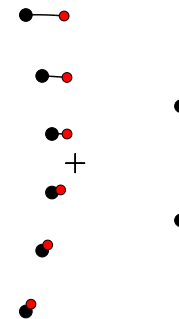


Figure C.295

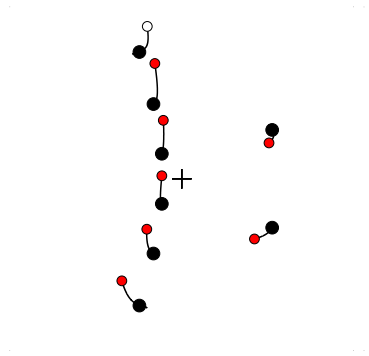


Figure C.296

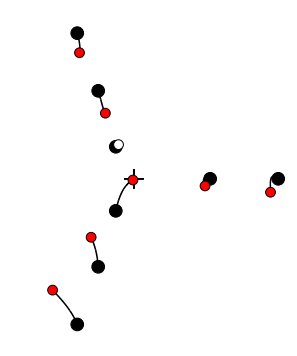


Figure C.297

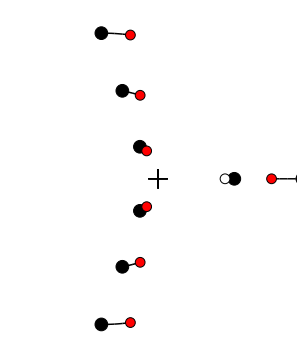


Figure C.298

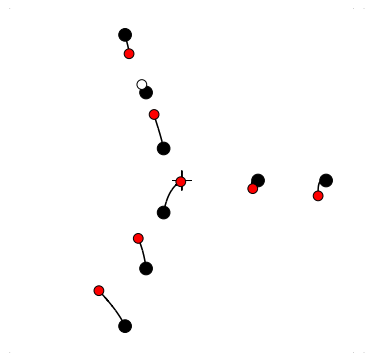


Figure C.299

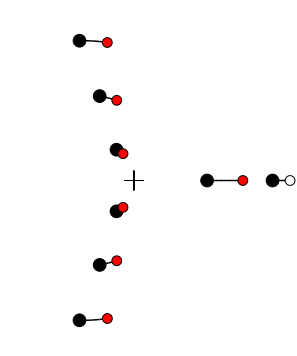


Figure C.300

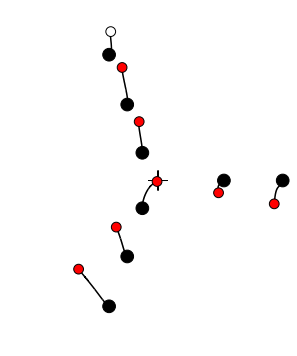


Figure C.301

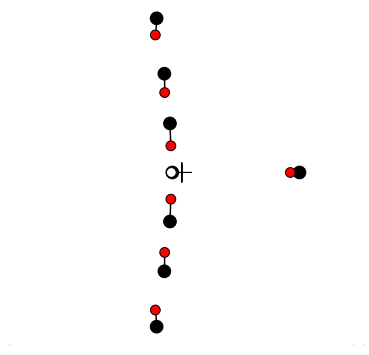


Figure C.302

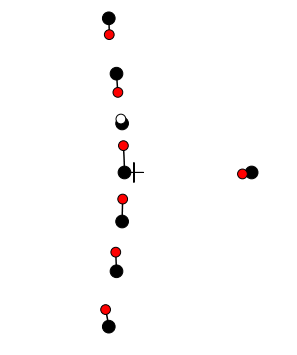


Figure C.303

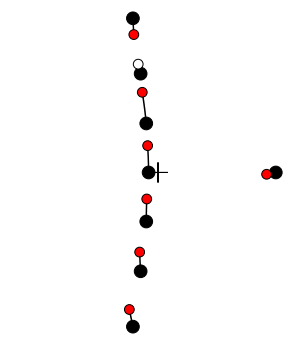


Figure C.304

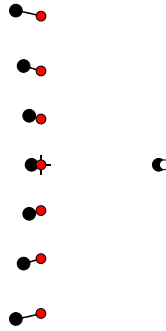


Figure C.305

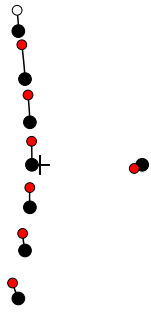


Figure C.306

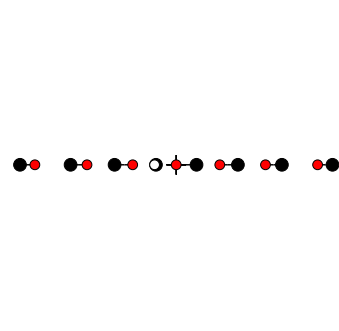


Figure C.307

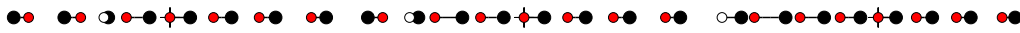


Figure C.308

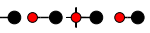


Figure C.309



Figure C.310

Relative equilibria on a sphere

The relative equilibria on the sphere for $C = \frac{\Gamma}{4\pi\Omega R^2} = 1$, as described in Chapter 6, are shown in the succeeding. The solid dots denotes, as always, the vortices and the circle denotes equator. The configurations are either shown on the plane by a stereographic projection, or on two planes mapping each hemispheres separately.

D.1 Relative equilibria for $N = 2$

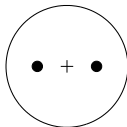


Figure D.1

D.2 Relative equilibria for $N = 3$

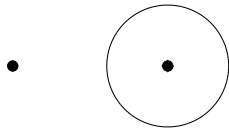


Figure D.2

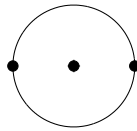


Figure D.3

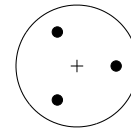


Figure D.4

D.3 Relative equilibria for $N = 4$

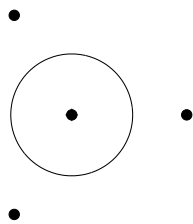


Figure D.5

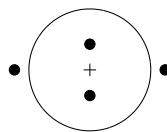


Figure D.6

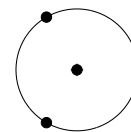


Figure D.7

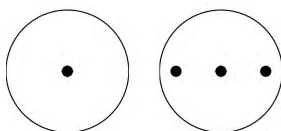


Figure D.8

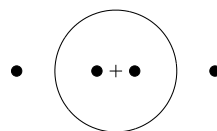


Figure D.9

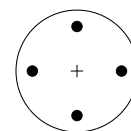


Figure D.10

D.4 Relative equilibria for $N = 5$

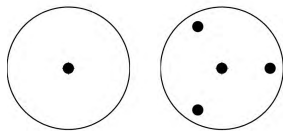


Figure D.11

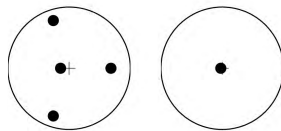


Figure D.12

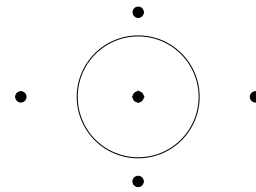


Figure D.13

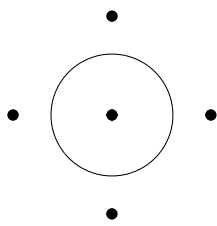


Figure D.14

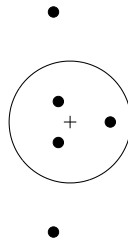


Figure D.15

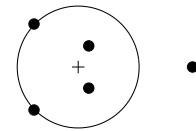


Figure D.16

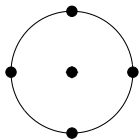


Figure D.17

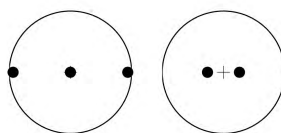


Figure D.18

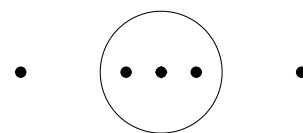


Figure D.19

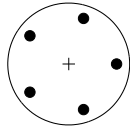


Figure D.20

D.5 Relative equilibria for $N = 6$

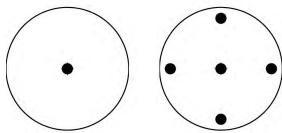


Figure D.21

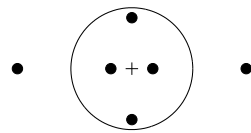


Figure D.22

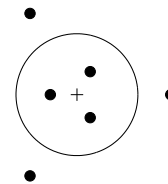


Figure D.23

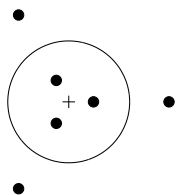


Figure D.24

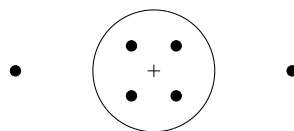


Figure D.25

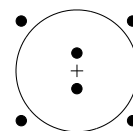


Figure D.26

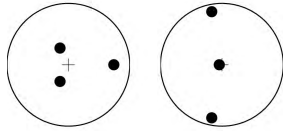


Figure D.27

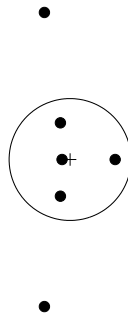


Figure D.28

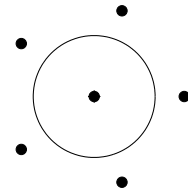


Figure D.29

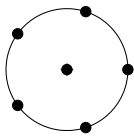


Figure D.30

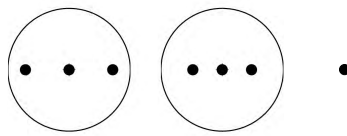


Figure D.31

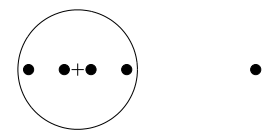


Figure D.32

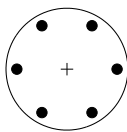


Figure D.33

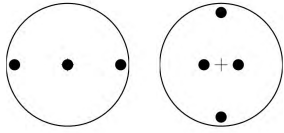


Figure D.34

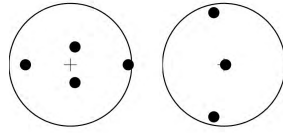


Figure D.35

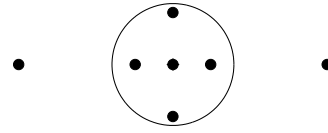


Figure D.36

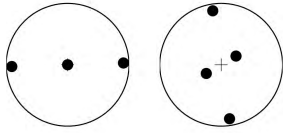


Figure D.37

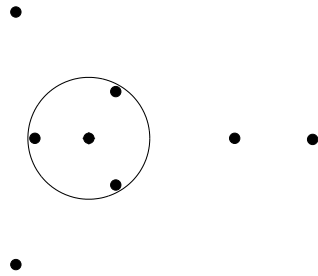


Figure D.38

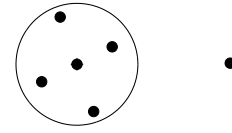


Figure D.39

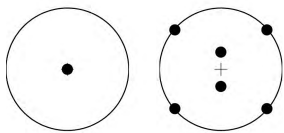


Figure D.40

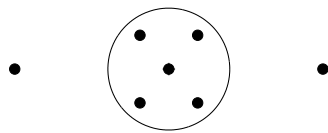


Figure D.41

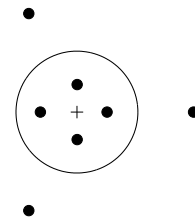


Figure D.42

D.6 Relative equilibria for $N = 7$

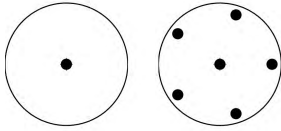


Figure D.43

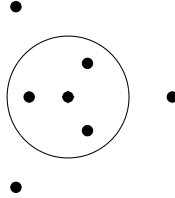


Figure D.44

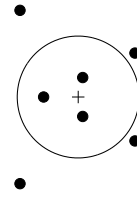


Figure D.45

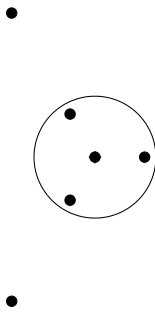


Figure D.46

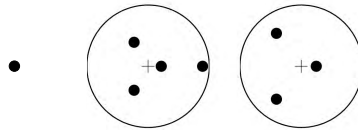


Figure D.47

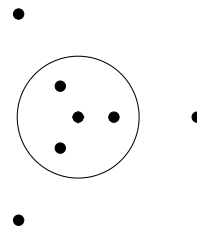


Figure D.48

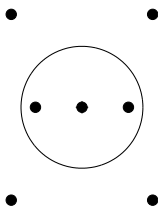


Figure D.49

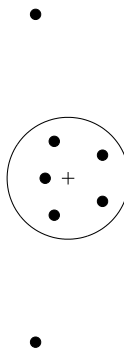


Figure D.50

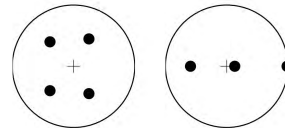


Figure D.51

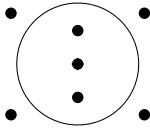


Figure D.52

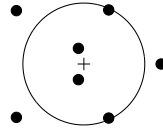


Figure D.53

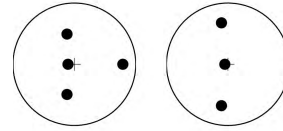


Figure D.54

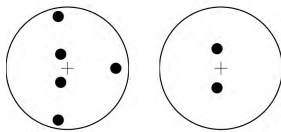


Figure D.55

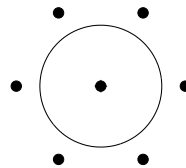


Figure D.56

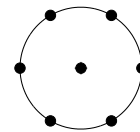


Figure D.57

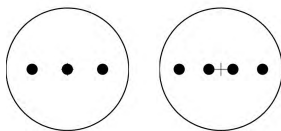


Figure D.58

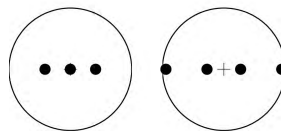


Figure D.59

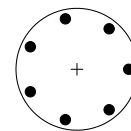


Figure D.60

D.7 Relative equilibria for $N = 8$

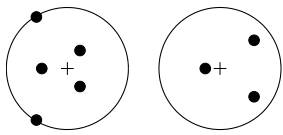


Figure D.61

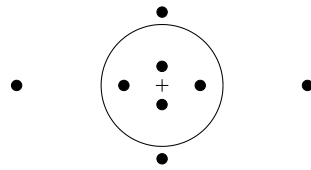


Figure D.62

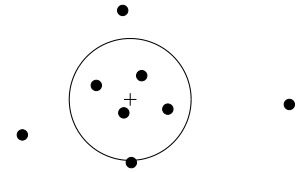


Figure D.63

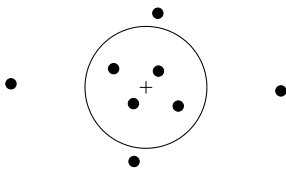


Figure D.64

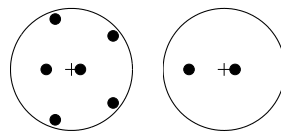


Figure D.65

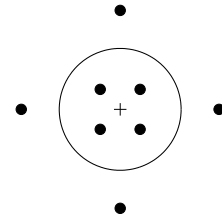


Figure D.66

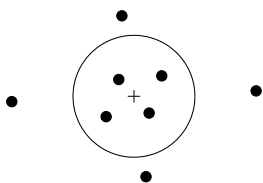


Figure D.67

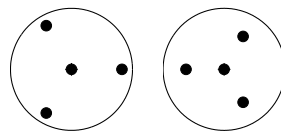


Figure D.68

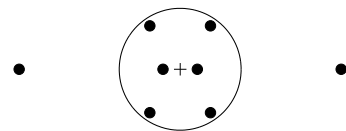


Figure D.69

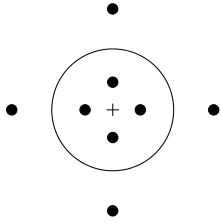


Figure D.70

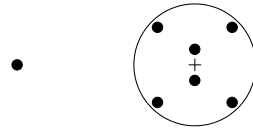


Figure D.71

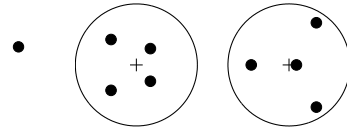


Figure D.72

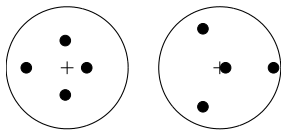


Figure D.73

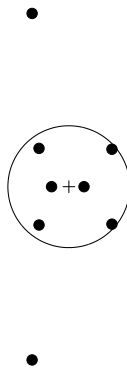


Figure D.74

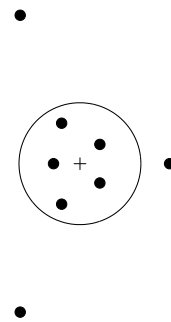


Figure D.75

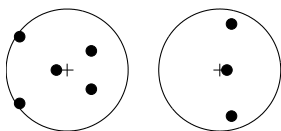


Figure D.76

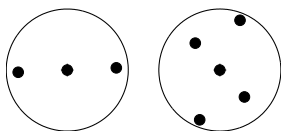


Figure D.77

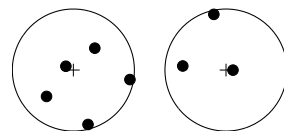


Figure D.78

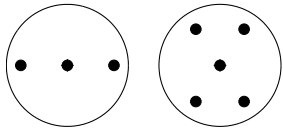


Figure D.79

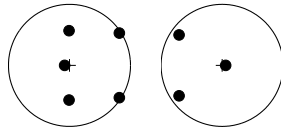


Figure D.80

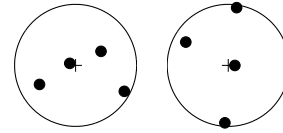


Figure D.81

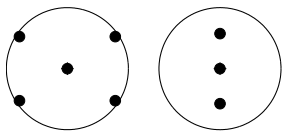


Figure D.82

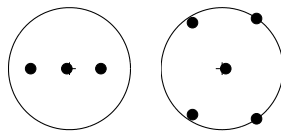


Figure D.83

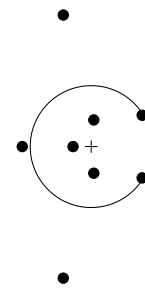


Figure D.84

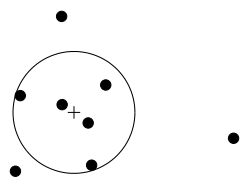


Figure D.85

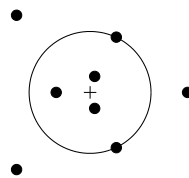


Figure D.86

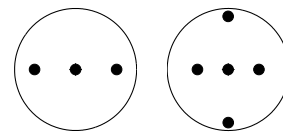


Figure D.87

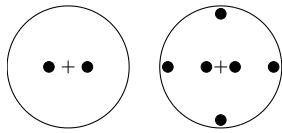


Figure D.88

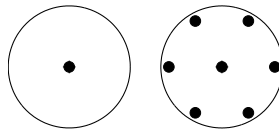


Figure D.89

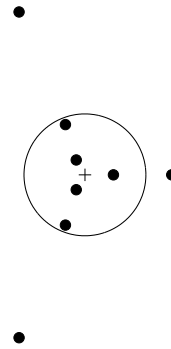


Figure D.90

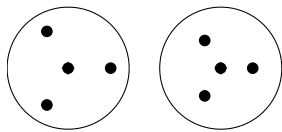


Figure D.91

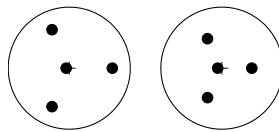


Figure D.92

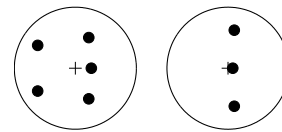


Figure D.93

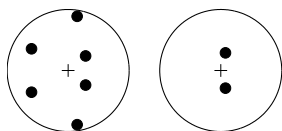


Figure D.94

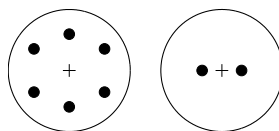


Figure D.95

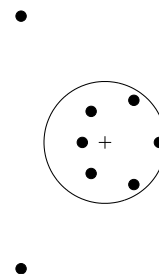


Figure D.96

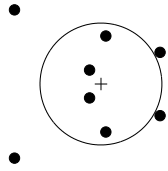


Figure D.97

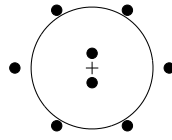


Figure D.98

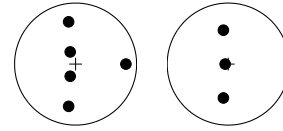


Figure D.99

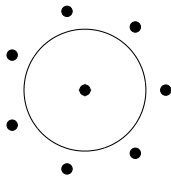


Figure D.100

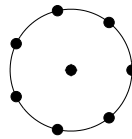


Figure D.101

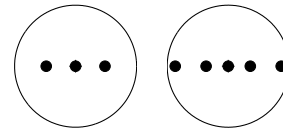


Figure D.102

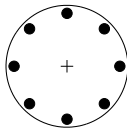


Figure D.103

Letter published in Physics of Fluid

Close pairs of relative equilibria for identical point vortices

Tobias Dirksen^{1,a)} and Hassan Aref^{2,3,b)}

¹*Department of Physics, Technical University of Denmark, Lyngby, Denmark*

²*Center for Fluid Dynamics, Technical University of Denmark, Lyngby, Denmark*

³*Engineering Science and Mechanics, Virginia Tech, Blacksburg, Virginia 24061, USA*

(Received 16 March 2011; accepted 20 April 2011; published online 23 May 2011)

Numerical solution of the classical problem of relative equilibria for identical point vortices on the unbounded plane reveals configurations that are very close to the analytically known, centered, symmetrically arranged, nested equilateral triangles. New numerical solutions of this kind are found for $3n + 1$ vortices, where $n = 2, 3, \dots, 30$. A sufficient, although apparently not necessary, condition for this phenomenon of close solutions is that the “core” of the configuration is marginally stable, as occurs for a central vortex surrounded by an equilateral triangle. The open, regular heptagon also has this property, and new relative equilibria close to the nested, symmetrically arranged, regular heptagons have been found. The centered regular nonagon is also marginally stable. Again, a new family of close relative equilibria has been found. The closest relative equilibrium pairs occur, however, for symmetrically nested equilateral triangles. © 2011 American Institute of Physics. [doi:10.1063/1.3590740]

The problem of relative equilibria of identical point vortices goes back to work by Mayer, W. Thomson (the later Lord Kelvin), and J. J. Thomson in the 1870s.¹ This problem, and closely related problems, arise in a variety of contexts.²

The equations to be solved are as follows: Let the vortex positions be given as N points in the complex plane, z_1, \dots, z_N . To find all solutions of the system¹

$$\bar{z}_\alpha = \sum_{\beta=1}^N \prime \frac{1}{z_\alpha - z_\beta}, \quad \alpha = 1, \dots, N. \quad (1)$$

The overbar on the left signifies complex conjugation, the prime on the summation sign that $\beta \neq \alpha$.

Several numerical explorations have been undertaken, the most comprehensive being the *Los Alamos Catalog* compiled in the late 1970s, henceforth referred to simply as the Catalog.³ It was unfortunately never published in the archival literature although many of the results may be found in a companion paper.⁴ The Catalog was inspired by the first visualizations⁵ of relative equilibria in He II, and so emphasized linearly stable configurations. When one expands the search to all relative equilibria, a large number of unstable configurations are found. Thus, for $N = 4$, there is just one entry in the Catalog, a square of vortices. Two additional configurations are known: the marginally stable, centered, equilateral triangle, and an unstable, collinear configuration with the vortex positions at the roots of the Hermite polynomial H_4 . A configuration close to the centered equilateral triangle, known for the 4-body problem of celestial mechanics,⁶ appears not to arise for point vortices. For $N = 5$, both the regular pentagon and the centered square are linearly stable (and in the Catalog), but there are three additional unstable relative equilibria. For $N = 6$, eight relative equi-

libria are known of which six are unstable. The regular hexagon and the centered, regular pentagon are the only two stable configurations – and the only two reported in the Catalog.

For $N = 7$, we know 11 relative equilibria, although just one of these, the centered, regular hexagon is linearly stable. Here, we report an additional configuration, found numerically, the smallest of a family of relative equilibria that are extremely close to the analytically known centered, symmetric, nested equilateral triangle configurations. All 12 relative equilibria are shown in Fig. 1 arranged by decreasing values of

$$\theta = \frac{2}{N(N-1)} \sum_{\alpha,\beta=1}^N \prime \log |z_\alpha - z_\beta|. \quad (2)$$

(The kinetic energy of interaction of the vortices is proportional to $-\theta$.) Some of these configurations are known analytically, such as the centered hexagon, Fig. 1(a), and the marginally stable, regular heptagon, Fig. 1(b), both included in the Catalog. Of the remaining configurations, the centered, triple digon,⁷ Fig. 1(g), the centered, symmetric double-ring,⁸ Fig. 1(j), and the collinear configuration with vortices at the zeros of H_7 , Fig. 1(l), are known analytically.

We have computed these states using MATLAB to solve Eq. (1) in double precision (of which ten digits are given in the results reported). Once a solution is obtained, we check that it verifies the convergence criterion

$$\frac{1}{N} \sum_{\alpha=1}^N \left| \bar{z}_\alpha - \sum_{\beta=1}^N \prime \frac{1}{z_\alpha - z_\beta} \right| < \varepsilon, \quad (3)$$

where ε is a convergence parameter that we typically set to 10^{-13} . For $N = 7$, the computations revealed a new configuration, Fig. 1(i). To the naked eye, this new configuration is identical to the centered, symmetric double-ring, Fig. 1(j), with vortex positions

^{a)}Electronic mail: tobiasdirksen@gmail.com.

^{b)}Electronic mail: haref@vt.edu.

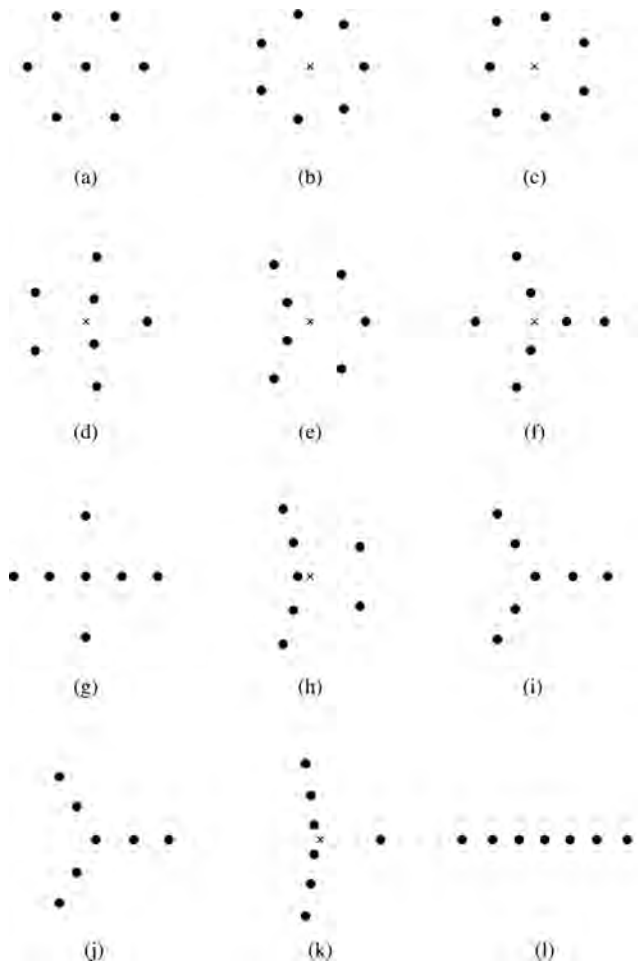


FIG. 1. Numerically determined relative equilibria of seven vortices. Centers of rotation indicated by small crosses (when not coincident with a vortex).

$$\begin{aligned} 1.2251565538, & \quad -0.6125782769 \pm 1.0610166992i, \\ 2.3449928398, & \quad -1.1724964199 \pm 2.0308233710i, \end{aligned}$$

and 0. These coordinates are just $R_1, R_1 e^{\pm i2\pi/3}$, and $R_2, R_2 e^{\pm i2\pi/3}$ (and 0), where R_1 and R_2 satisfy^{7,8}

$$R_1^2 + R_2^2 = 7, \quad R_1^5 + R_2^5 = 5(R_1^3 + R_2^3). \quad (4)$$

The value of θ , Eq. (2), for this configuration is 1.6035139510... in agreement with analysis.⁹ For the new solution, Fig. 1(i), the computed vortex positions are

$$\begin{aligned} 1.2350850139 & \quad -0.6172513235 \pm 1.0524323669i, \\ 2.3511504807 & \quad -1.1891361698 \pm 2.0175029435i, \\ 0.0265394920. & \end{aligned}$$

The value of θ , Eq. (2), is 1.6035146448... In a numerical exploration where the existence of relative equilibria different from those seen previously is assessed visually from a plot of vortex positions, or even from a calculation of an energy measure equivalent to θ in Eq. (2) but only to accuracy 10^{-6} , one could easily mistake the new configuration for the known, centered double-ring.

Initially, we were suspicious that the new configuration was a numerical artifact even though the stringent check (3) had been applied. Hence, we also checked the calculations to accuracy 10^{-300} using *Maple* and found both solutions to be present. These checks confirm the existence of two very close relative equilibria.

Another argument in favor of the existence of the new configuration is that a similar pair occurs close to the centered, symmetric triple-ring configuration 1-3-3-3, which is again known analytically.⁷ The configuration consists of a central vortex and three concentric, symmetrically placed, equilateral triangles of vortices. The vortex coordinates in this relative equilibrium are

$$\begin{aligned} 1.1257068936, & \quad -0.5628534468 \pm 0.9748907671i, \\ 2.0668001012, & \quad -1.0334000506 \pm 1.7899013922i, \\ 3.0758935826, & \quad -1.5379467913 \pm 2.6638019818i, \end{aligned}$$

and 0. These coordinates are $R_p e^{i2\pi\alpha/3}$, $p = 1, 2, 3$, and $\alpha = 1, 2, 3$, where R_1, R_2 , and R_3 satisfy the equations⁷

$$\begin{aligned} R_1^2 + R_2^2 + R_3^2 &= 15, \\ R_1^5 + R_2^5 + R_3^5 &= 8(R_1^3 + R_2^3 + R_3^3), \\ \frac{R_1^2 - 2}{R_1^3} + \frac{R_2^2 - 2}{R_2^3} + \frac{R_3^2 - 2}{R_3^3} &= 0. \end{aligned} \quad (5)$$

The value of θ , Eq. (2), is 1.8554011511... The coordinates in the new relative equilibrium are

$$\begin{aligned} 1.1430054923, & \quad -0.5635151208 \pm 0.9642351902i, \\ 2.0782582001, & \quad -1.0475637987 \pm 1.7748721082i, \\ 3.0842676267, & \quad -1.5635635748 \pm 2.6439155247i, \\ 0.0437536693. & \end{aligned}$$

For this configuration, we find $\theta = 1.8554026277...$

We found other instances of close relative equilibria for ten vortices, although none as close as the pair just given. The two similar configuration pairs in Figs. 2(a)–2(d) can be distinguished by careful visual inspection. Relative

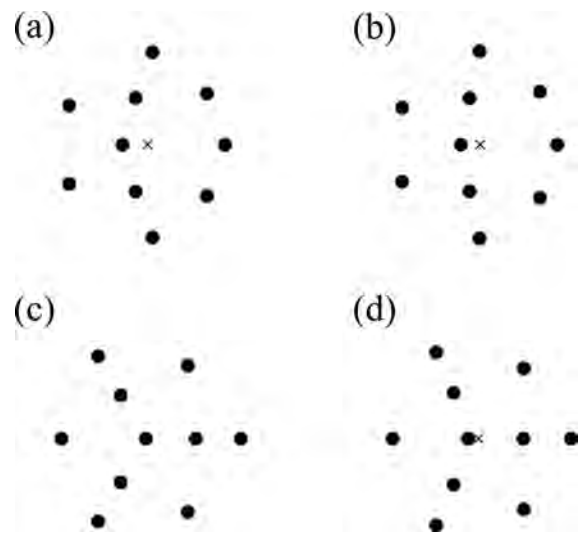


FIG. 2. Two examples, (a), (b) and (c), (d), of pairs of close relative equilibria for ten vortices.

differences in individual coordinates are larger than in the previous examples. The values of θ for the two configurations in each pair in Fig. 2 agree to accuracy 10^{-3} . The pair in Figs. 2(c) and 2(d) is the most interesting for the present discussion since Fig. 2(c) is a centered, staggered configuration of nested equilateral triangles in the nomenclature of Ref. 7.

There appear to be centered, symmetric configurations of arbitrarily many nested, similar, regular polygons. For n nested regular s -gons, we find the following system of equations for the radii R_1, \dots, R_n :

$$\frac{2R_p^2 - s - 1}{R_p^s} = 2s \sum_{q=1}^n \prime \frac{1}{R_p^s - R_q^s}, \quad p = 1, \dots, n. \quad (6)$$

The prime on the summation sign means $q \neq p$. The vortex positions in such a relative equilibrium are $R_p e^{i2\pi\alpha/s}$, $p = 1, \dots, n$, $\alpha = 1, \dots, s$, and 0. Equations (4) and (5) are reduced versions of Eqs. (6) for $s=3$ and $n=2$ and 3, respectively. For $s=2$, Eqs. (6) are satisfied by the zeros of the Hermite polynomial of degree $2n+1$. We shall not pause to derive Eq. (6) here. A derivation can be based on the generating polynomial approach explained in Ref. 11, in particular, Eq. (2.6).

For $s=3$, we have found solutions to Eq. (6) for n up to 30 numerically. We assume there are solutions for all natural numbers n . These describe configurations of $3n+1$ vortices arranged on n symmetrically nested, equilateral triangles with a vortex at the center. Based on the results for $n=2, 3$, we expect that close to each of these symmetric relative equilibria there is a second relative equilibrium with lower symmetry. We have checked this conjecture for $n=4, \dots, 30$. In each case, we find a new, close relative equilibrium that is indistinguishable from the symmetric configuration to the naked eye. The left panel of Fig. 3 provides an example for $n=10$. The vortices in the analytically known configuration are shown as black dots centered on the vortex positions. The new, close configuration is shown by superimposed white dots centered on the new vortex positions. All dots of the new configuration are seen to fall inside the black dots representing the analytically known configuration.

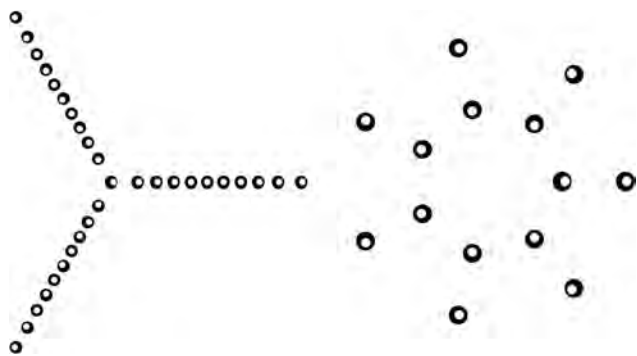


FIG. 3. Close relative equilibria for 31 (left) and 14 (right) vortices. The analytical, symmetrically-nested, regular-polygon solution is shown as black dots, the close, new, numerically determined solution is shown as superimposed white dots. These results have been checked to accuracy 10^{-300} using Maple.

With the new seven-vortex configuration added to the list, the number of known relative equilibria of seven identical vortices stands at 12. There are 19 known eight-vortex relative equilibria. The total could also be stated as 20 since for $N=8$, we encounter the smallest asymmetric relative equilibrium.¹⁰ A reflection of this configuration in a line through its centroid is again a relative equilibrium and not one that can be obtained by rotation from the original configuration.

For nine vortices, we found a total of 35 relative equilibria. Four of these are asymmetric so one could count each of them as two different configurations for a total of 39. For ten vortices, we found 59 relative equilibria of which 13 are asymmetric. We have not yet done a systematic count for larger values of N . For $N=13$, where we were interested in whether there was another relative equilibrium close to the symmetric 1-3-3-3-3 configuration, we found at least 275 relative equilibria. The total number of relative equilibria appears to grow rapidly with N , and the number of asymmetric configurations among them also grows.

Let $z_\alpha^{(0)}$ and z_α be two close relative equilibria. To linear order in $\delta z_\alpha = z_\alpha - z_\alpha^{(0)}$, we have

$$\overline{\delta z_\alpha} = \sum_{\beta=1}^N A_{\alpha\beta} \delta z_\beta, \quad (7a)$$

where the matrix $A_{\alpha\beta}$ is the matrix that arises in the linear stability theory for the configuration $z_\alpha^{(0)}$

$$A_{\alpha\beta} = \sum_{\gamma=1}^N \prime \frac{\delta_{\alpha\beta}}{(z_\alpha^{(0)} - z_\gamma^{(0)})^2} - \frac{1 - \delta_{\alpha\beta}}{(z_\alpha^{(0)} - z_\beta^{(0)})^2}. \quad (7b)$$

We write Eq. (7a) in an easily understood vector-matrix notation

$$\overline{\delta z} = A \delta z, \quad \delta z = \overline{AA} \delta z. \quad (8)$$

Since A is symmetric, \overline{AA} is Hermitian. Furthermore, because of the form of this matrix, all its eigenvalues are non-negative. The existence of a close relative equilibrium suggests that the matrix \overline{AA} must have an eigenvector with eigenvalue 1. Now, $z^{(0)}$ is always a “trivial” eigenvector of \overline{AA} with eigenvalue 1 (cf. Ref. 12 where the analogous result for $N=3$ and arbitrary vortex strengths is given). Thus, we expect that a close pair of relative equilibria will manifest itself by the matrix \overline{AA} having a close degeneracy of the eigenvalue 1.

We have computed the eigenvalues of \overline{AA} for each of the configurations found. The eigenvalue spectra for close configurations are, of course, also close. For example, in the case of Figs. 1(i) and 1(j), the eigenvalue spectrum of the analytically known configuration is 0.0000, 1.0000, 1.0456 (multiplicity 2), 5.5157 (multiplicity 2), and 6.1539. The eigenvalues of the new configuration are 0.0000, 0.9555, 1.0000, 1.1396, 5.3727, 5.6504, and 6.1674. (The eigenvalue 0 is also always present, cf. Ref. 12.) The pattern of the less symmetrical configuration having a stable mode with eigenvalue less than but somewhat close to 1 recurs for the other close pairs.

A related observation is that the eigenvalue spectrum of the centered, equilateral triangle is 0, 1 (with multiplicity 3). This suggests a very “flat” energy surface around this state. As further equilateral triangles are added, this degeneracy in the stability matrix for the “core” of the configuration may be the main feature that allows a close relative equilibrium to exist.

Among the open and centered regular polygons, the open heptagon and centered nonagon are both marginally stable in linear theory, i.e., the eigenvalue 1 of \overline{AA} is the largest and is degenerate. Hence, one suspects that close to the heptagon double-ring, there would be another close relative equilibrium of lower symmetry. We have checked this conjecture and, indeed, such a configuration is found numerically. It is shown in the right panel in Fig. 3, where the analytically known double ring^{7,8} is plotted using black dots, the new numerically determined, close, 14-vortex relative equilibrium using superimposed white dots. The two configurations are obviously very close, although not quite as close as in the case of the nested equilateral triangles. Further, close relative equilibrium pairs exist as more heptagonal rings are added. The ring radii in the analytical solutions satisfy equations similar to Eq. (6) but with $-s + 1$ in the numerator instead of $-s - 1$ (and for heptagons $s = 7$). Similarly, for the centered, regular nonagons we have found relative equilibria that are close to the centered double- and triple-rings but, again, not as close as in the case of the equilateral triangles. The centered equilateral triangle is unique in that *all* infinitesimal perturbations with fixed centroid have eigenvalue 1. The open regular heptagon and centered regular nonagon also have linearly stable modes.

We do not have a full understanding of why the phenomenon of close pairs of solutions to Eq. (1) arises. The closest solutions appear in the vicinity of the centered, symmetric, nested equilateral triangle configurations. Close solutions also occur in other cases when the “core” of the configuration is marginally stable and the eigenvalue 1 has multiplicity larger than 1. However, quite close solutions, such as Figs. 2(a) and 2(b), arise in cases where this mechanism of a marginally stable “core” does not seem to be applicable. The phenomenon of close relative equilibria was a surprise to us. We have since learned of similar situations in other problems of this kind.^{6,13,14} For relative equilibria with

vortices of both positive and negative circulations examples of continua of solutions are known, e.g., for the stationary relative equilibria¹⁵ and for a certain five-vortex example.¹⁶ However, the expectation is that when all vortices are of one sign, in particular, for identical vortices, “finiteness” of solutions prevails. Implicit in this expectation was that the different relative equilibria would be easily distinguishable.

We thank B. Eckhardt, R. Hansen, K. O’Neil, and D. Vainchtein for discussions and comments. This work was supported in part by a Niels Bohr Visiting Professorship at the Technical University of Denmark sponsored by the Danish National Research Foundation.

¹H. Aref, P. K. Newton, M. A. Stremler, T. Tokieda, and D. L. Vainchtein, “Vortex crystals,” *Adv. Appl. Mech.* **39**, 1 (2003).

²P. K. Newton and G. Chamoun, “Vortex lattice theory: A particle interaction perspective,” *SIAM Rev.* **51**, 501 (2009).

³L. J. Campbell and R. M. Ziff, “A catalog of two-dimensional vortex patterns,” *Rev. Informal Report LA-7384-MS*, Los Alamos National Laboratory, 1978, pp.1–40.

⁴L. J. Campbell and R. M. Ziff, “Vortex patterns and energies in a rotating superfluid,” *Phys. Rev. B* **20**, 1886 (1979).

⁵E. J. Yarmchuk, M. J. V. Gordon, and R. E. Packard, “Observation of stationary vortex arrays in rotating superfluid Helium,” *Phys. Rev. Lett.* **43**, 214 (1979).

⁶K. Glass, “Equilibrium configurations for a system of N particles in the plane,” *Phys. Lett. A* **235**, 591 (1997).

⁷H. Aref and M. van Buren, “Vortex triple rings,” *Phys. Fluids* **17**, 057104, (2005).

⁸T. H. Havelock, “Stability of motion of rectilinear vortices in ring formation,” *Philos. Mag.* **11**, 617 (1931).

⁹H. Aref, “A note on the energy of relative equilibria of point vortices,” *Phys. Fluids* **19**, 103603 (2007).

¹⁰H. Aref and D. L. Vainchtein, “Asymmetric equilibrium patterns of point vortices,” *Nature* **392**, 769 (1998).

¹¹H. Aref, “Relative equilibria of point vortices and the fundamental theorem of algebra,” *Proc. R. Soc. London, Ser. A* (in press).

¹²H. Aref, “Stability of relative equilibria of three vortices,” *Phys. Fluids* **21**, 094101 (2009).

¹³K. Sacha and B. Eckhardt, “Pathways to non-sequential multiple ionization in strong laser fields,” *J. Phys. B* **36**, 3293 (2003).

¹⁴K. A. O’Neil, “Central configurations of identical masses lying along curves,” *Phys. Rev. E* **79**, 066601 (2009).

¹⁵A. B. Bartman, “A new interpretation of the Adler-Moser KdV polynomials: Interaction of vortices,” in *Nonlinear and Turbulent Processes in Physics*, edited by R. Z. Sagdeev (Harwood Academic, Newark, NJ, 1984), Vol. 3, pp. 1175–1181.

¹⁶G. E. Roberts, “A continuum of relative equilibria in the five-body problem,” *Physica D* **127**, 141 (1999).

Bibliography

- [1] J. R. Abo-Shaer, C. Raman, J. M. Vogels, and W. Ketterle, “Observation of vortex lattices in bose- einstein condensates,” *Science*, vol. 292, 2001.
- [2] D. J. Acheson, *Elementary Fluid Dynamics*. Oxford University Press, 1990.
- [3] H. Aref, P. K. Newton, M. A. Stremler, T. Tokieda, and D. L. Vainchtein, “Vortex crystals,” *Advances in Applied Mechanics*, vol. 39, pp. 1–79, 2003.
- [4] H. Aref, “Motion of three vortices,” *Physics of Fluid*, vol. 22, pp. 393–400, 1979.
- [5] —, “Integrable, chaotic, and turbulent vortex motion in two-dimensional flows,” *Annual Review of Fluid Mechanics*, vol. 15, pp. 345–389, 1983.
- [6] —, “A note on the energy of relative equilibria of point vortices,” *Physics of Fluids*, vol. 19, p. 103603, 2007.
- [7] —, “Point vortex dynamics: A classical mathematical playground,” *Journal of Mathematical Physics*, vol. 48, p. 065401, 2007.
- [8] —, “Vortices and polynomials,” *Fluid Dynamics Research*, vol. 39, pp. 5–23, 2007.
- [9] —, “Stability of relative equilibria of three vortices,” *Physics of Fluid*, vol. 21, p. 094101, 2009.
- [10] —, “Relative equilibria of point vortices and the fundamental theorem of algebra,” *Proceedings of the Royal Society A*, vol. 467, pp. 2168–2184, 2011.
- [11] H. Aref, P. Beelen, and M. Brøns, “Bilinear relative equilibria of identical point vortices,” *sub judice in Journal of Nonlinear Science*, 2011.
- [12] H. Aref and M. Brøns, “On stagnation points and streamline topology in vortex flows,” *Journal of Fluid Mechanics*, vol. 370, pp. 1–27, 1998.
- [13] H. Aref and D. L. Vainchtein, “Point vortices exhibit asymmetric equilibria,” *Nature*, vol. 392, pp. 769–770, 1998.
- [14] H. Aref and M. van Buren, “Vortex triple rings,” *Physics of fluids*, vol. 17, pp. 1–21, 2005.

- [15] G. B. Arfken and H. J. Weber, *Mathematical methods for physicists*. Elsevier Academic Press, 2005.
- [16] V. Bogomolov, “Dynamics of vorticity at a sphere,” *Fluid Dynamics*, vol. 12, pp. 863–870, 1977.
- [17] —, “Two-dimensional fluid dynamics on a sphere,” *Izvestiya Atmospheric and Oceanic Physics*, vol. 15, pp. 18–22, 1979.
- [18] L. J. Campbell and R. M. Ziff, “A catalog of two-dimensional vortex patterns,” 1978, Los Alamos Scientific Laboratory Report No. LA-7384-MS, pp.1-40.
- [19] P. A. Clarkson, “Vortices and polynomials,” *Studies in Applied Mathematics*, vol. 123, no. 1, pp. 37–62, 2009.
- [20] T. Dirksen, “Computation of vortex patterns,” 2010, project report.
- [21] T. Dirksen and H. Aref, “Close pairs of relative equilibria for identical point vortices,” vol. 23, no. 5, p. 051706, 2011.
- [22] D. Durkin and J. Fajans, “Experimental dynamics of a vortex within a vortex,” *Phys. Rev. Lett.*, vol. 85, pp. 4052–4055, 2000.
- [23] —, “Experiments on two-dimensional vortex patterns,” *Physics of Fluids*, vol. 12, p. 289, 2000.
- [24] T. Erber and G. M. Hockney, “Equilibrium configurations of N equal charges on a sphere,” *Journal of Physics A: Mathematical and General*, vol. 24, p. L1369, 1991.
- [25] W. Gröbli, “Spezielle probleme über die bewegung geradliniger paralleler wirbelfäden,,” *Vierteljschr. Naturf. Ges. Zürich*, vol. 22, pp. 37–82, 129–168, 1877.
- [26] I. S. Gromeka, “On vortex motions of liquid on a sphere,” *Uchenye Zapiski Imperatorskogo Kazanskogo Universiteta [Scientific Notes of the Imperial Kazan University]*, vol. 3, pp. 202–236, 1885, in Russian.
- [27] B. A. Grzybowski, H. A. Stone, and G. M. Whitesides, “Dynamic self-assembly of magnetized, millimetre-sized objects rotating at a liquid-air interface,” *Nature*, vol. 405, pp. 1033–1036, 2000.
- [28] S. Gueron and I. Shafir, “On a discrete variational problem involving interacting particles,” *SIAM Journal on Applied Mathematics*, vol. 60, 1999.
- [29] T. Havelock, “The stability of motion of rectilinear vortices in ring formation,” *Philosophical Magazine*, vol. 11, pp. 617–633, 1931.
- [30] M. I. Jamaloodeen and P. K. Newton, “The n-vortex problem on a rotating sphere. ii. Heterogeneous Platonic solid equilibria,” *Proceedings of the Royal Society A*, vol. 462, pp. 3277–3299, 2006.
- [31] D. Khavinson and G. Neumann, “From the fundamental theorem of algebra to astrophysics: A ”harmonious path”,,” *Notices of the American Mathematical Society*, vol. 55, pp. 666–675, 2008.

- [32] L. G. Khazin, “Regular polygons of point vortices and resonance instability of steady states,” *Soviet Phys. Dokl.*, vol. 21, pp. 567–569, 1976.
- [33] R. Kidambi and P. K. Newton, “Motion of three point vortices on a sphere,” *Physica D: Nonlinear Phenomena*, vol. 116, pp. 143–175, 1998.
- [34] Y. Kimura and H. Okamoto, “Vortex motion on a sphere,” *Journal of Physical Society of Japan*, vol. 56, pp. 4203–4206, 1987.
- [35] F. Laurent-Polz, “Point vortices on the sphere: a case with opposite vorticities,” *Nonlinearity*, vol. 15, pp. 143–171, 2002.
- [36] ———, “Relative periodic orbits in point vortex systems,” *Nonlinearity*, vol. 17, pp. 1989–2013, 2004.
- [37] ———, “Point vortices on a rotating sphere,” *Regular and chaotic dynamics*, vol. 10, pp. 39–58, 2005.
- [38] F. Laurent-Polz, J. Montaldi, and M. Roberts, “Point vortices on the sphere: stability of relative equilibria,” *Dynamical Systems (math.DS)*, 2011.
- [39] C. Lim, J. Montaldi, and M. Roberts, “Relative equilibria of point vortices on the sphere,” *Physica D*, vol. 148, pp. 97–135, 2001.
- [40] C. C. Lim, “Relative equilibria of symmetric n-body problems on a sphere: Inverse and direct results,” *Communications on Pure and Applied Mathematics*, vol. 51, no. 4, pp. 341–371, 1998.
- [41] P. Luzzatto-Fegiz and C. H. K. Williamson, “Stability of conservative flows and new steady fluid solutions from bifurcation diagrams exploiting a variational argument,” *Physical Review Letters*, vol. 104, p. 044504, 2010.
- [42] ———, “An efficient and general numerical method to compute steady uniform vortices,” *Journal of Computational Physics*, vol. 230, pp. 6495–6511, 2011.
- [43] V. Meleshko and H. Aref, “A bibliography of vortex dynamics 1858-1956,” *Advances in Applied Mechanics*, vol. 41, no. 197, pp. 197–292, 2007.
- [44] G. J. Mertz, “Stability of body-centered polygonal configurations of ideal vortices,” *Phys. Fluids*, vol. 21, pp. 1092–1095, 1978.
- [45] W. B. Morton, “On some permanent arrangements of parallel vortices and their points of relative rest,” *Proceedings of the Royal Irish Academy A*, vol. 41, pp. 94–101, 1933.
- [46] P. K. Newton, *The N-Vortex Problem - Analytical Techniques*, 1st ed. Springer-Verlag, 2001.
- [47] ———, “The n-vortex problem on a sphere: geophysical mechanisms that break integrability,” *Theor. Comput. Fluid Dyn.*, vol. 24, pp. 137–149, 2010.
- [48] P. K. Newton and G. Chamoun, “Vortex lattice theory: A particle interaction perspective,” *SIAM Review*, vol. 51, p. 501, 2009.

- [49] K. O’Neil, “Relative equilibria of point vortices that lie on a great circle of a sphere,” *Nonlinearity*, vol. 21, pp. 2043–2051, 2008.
- [50] K. A. O’Neil, “Stationary configurations of point vortices,” *Transactions of the American Mathematical Society*, vol. 302, pp. 383–425, 1987.
- [51] ———, “Central configurations of identical masses lying along curves,” *Physical Review E*, vol. 79, p. 066601, 2001.
- [52] ———, Personal communication, 2011.
- [53] S. Pekarsky and J. E. Marsden, “Point vortices on a sphere: Stability of relative equilibria,” *Journal of Mathematical Physics*, vol. 39.
- [54] L. Perko, *Differential Equations and Dynamical Systems*, 3rd ed. Springer-Verlag, 2001.
- [55] H. Snelders, “A. m. mayer’s experiments with floating magnets and their use in the atomic theories of matter,” *Annals of Science*, vol. 33, pp. 67–80, 1976.
- [56] S. H. Strogatz, *Nonlinear Dynamics and Chaos*. Westview Press, 1994.
- [57] J. Thomson, *A Treatise on the Motion of Vortex Rings: An Essay to which the Adams Prize was Adjusted in 1882*. University of Cambridge, Macmillan, London, 1883.
- [58] ———, “On the structure of the atom: an investigation of the stability and periods of oscillation of a number of corpuscles arranged at equal intervals around the circumference of a circle; with application of the results to the theory of atomic structure,” *The London, Edinburgh and Dublin philosophical magazine and journal of science*, vol. 7, pp. 237–265, 1904.
- [59] W. Thomson, “Floating magnets,” *Nature*, pp. 13–14, 1878.
- [60] W. Thomson (Lord Kelvin), “Vortex statics,” *Proceedings of the Royal Society of Edinburgh*, vol. 9, pp. 59–73, 1875.
- [61] E. J. Yarmchuk, M. J. V. Gordon, and R. E. Packard, “Observation of stationary vortex arrays in rotating superfluid helium,” *Physical Review Letters*, vol. 43, p. 214, 1979.